EXAMINING AND IMPROVING THE CHEMOPREVENTIVE EFFICACY OF CURCUMIN

DISSERTATION

SUBMITTED TO THE FACULTY OF

UNIVERSITY OF MINNESOTA

BY

ALEXANDER E GRILL

IN PARTIAL FULFILLMENT OF THE REQUIREMENTS

FOR THE DEGREE OF

DOCTOR OF PHILOSOPHY

ADVISER: DR. JAYANTH PANYAM

SEPTEMBER 2012

DEDICATION

To my grandmother Lois, my mother Donna, my sister Michelle and my wife Julia

ACKNOWLEDGEMENTS

I would first like to extend my deepest thanks my advisor Dr. Jayanth Panyam for his wisdom and guidance in my research and my life for the last several years. His motivation and brilliance made me a better scientist. Thank you for always listening to my concerns and pushing me to be my best.

I would like to thank my committee members, Dr. Cheryl Zimmeraman, Dr. Timothy Wiedmann, and Dr. Kaylee Schwertfeger for their feedback and suggestions.

Many studies in this thesis could not have been possible without the help of several other researchers at the University of Minnesota. I would like to thank Jim Fisher for his assistance in LC-MS/MS assay development and studies. Thank you to Dr. Gerry O'Sullivan and Josh Parker and everyone at the Comparative Pathology Shared Resource for their extensive assistance with histology and immunohistochemistry. A very special thank you needs to be paid to all of Research Animal Resources but especially Brenda Koniar, who tirelessly assisted me with animal studies. Special thanks to go Dr. Ron Siegel and IPRIME who helped fund a portion of this work. Thanks also to Ramola Sane who graciously assisted with the SMEDDS formulation. I'd like to thank Aaron Tietelbaum for his help with microsomal assays and HPLC development and for being a good friend.

My thanks go to Candy McDermott and Erica Stapic, who have always been kind and helpful with anything I've needed.

The support of my fellow lab members has been invaluable. The support provided by Tanmoy, Suresh, Ameya, Lin, Steve, Marina, Garvey and Udaya cannot be measured. A very special acknowledgment must be made to Dr. Komal Shahani, from

whom I inherited a passion for curcumin. Thank you to my friends Sunny and Jing, who always offered support.

Lastly, to my family, my mother, father, step-father, sister, grandmother, my wife's family and especially my wife: thank you for all of your support and love during this journey. You gave me constant inspiration and support throughout my life and brought me to this day.

ABSTRACT

Curcumin, a polyphenol extracted from turmeric, has shown chemopreventive and chemotherapeutic effects against cancer. However, curcumin suffers from poor bioavailability, which limits its clinical use. We hypothesized that *using novel microparticle and SMEDDS formulations will improve the pharmacokinetics and therapeutic efficacy of curcumin.*

Initial studies examined the anticancer efficacy of curcumin loaded poly(lactide-*co*-glycolic acid) (PLGA) microparticles in a transgenic mouse model of human epidermal growth factor receptor-2 (HER-2) cancer, Balb-neuT. HER-2 is overexpressed in 30% of breast cancer cases and is associated with poor prognosis and high incidence of metastasis. Curcumin microparticles delayed tumor appearance by 2-3 weeks and were associated with a decrease in VEGF protein levels and CD-31+ microvasculature compared to empty microparticles. However, when compared to saline controls, blank microparticles appeared to accelerate tumorigenesis. Blank PLGA microparticles were shown to activate NF-κB signaling, indicating systemic inflammation after injection. The delay in tumorigenesis with curcumin-loaded microparticles was likely attributed to the anti-inflammatory effects of curcumin. Future studies will examine the systemic effects of blank PLGA microparticles as well as explore other polymers for curcumin microparticle delivery.

A self microemulsifying drug delivery system (SMEDDS) was examined for oral delivery of curcumin. The SMEDDS formulation solubilized curcumin at high concentrations (~45 mg/mL). However, administering curcumin in the SMEDDS

formulation did not increase curcumin bioavailability but increased gut absorption, evident by increased plasma curcumin glucuronide levels. We hypothesized that oral bioavailability of curcumin could be enhanced by increasing its absorption and decreasing metabolic clearance simultaneously. Microsomal studies showed that silibinin and quercetin inhibited curcumin glucuronidation in vitro. Piperine, which was shown to improve curcumin bioavailability previously, silibinin and quercetin were administered with curcumin in vivo. Coadministration of curcumin and piperine showed high variability after dosing. Addition of silibinin significantly improved curcumin bioavailability (3.5 fold) compared to curcumin alone. Future studies should examine the chemopreventive potential of curcumin and silibinin for HER-2+ breast cancer.

TABLE OF CONTENTS

LIST OF FIGURES

LIST OF TABLES

LIST OF ABBREVIATIONS

ACN	Acetonitrile
Akt	Protein kinase B
ANOVA	Analysis of variance
AP-1	Activated protein-1
ATZ	Atazanavir
AUC	Area under the curve
Bax	Bcl2-associated X protein
Bad	Bcl2-accociated agonist of cell death
Bcl-2	B-cell lymphoma 2
Bcl_{XL}	B-cell lymphoma XL
bFGF	Basic fibroblast growth factor
BITC	Benzyl isothiocyanate
Blank MP	Empty PLGA microparticles
Cdk	Cyclin dependant kinase
CL	Clearance
COX-2	Cyclooxygenase-2
CsA	Cyclosporin A
C_{ss}	Steady state concentration
CUR	Curcumin
Curcumin MP	Curcumin loaded PLGA microparticles
CYP	Cytochrome
DMSO	Dimethyl sulfoxide

EGCG	Epigallocatechin gallate
EGF	Epidermal growth factor
EGFR	Epidermal growth factor receptor
EMT	Epidermal to mesenchymal transition
ER	Estrogen receptor
FDA	Food and Drug Administration
g	gram
GFP	Green fluorescent protein
GM-CSF	Granulocyte macrophage-colony stimulating factor
GSH	Glutathione
GST	Glutathione-s-transferase
H&E	Hematoxylin and eosin
HER-2	Human epidermal growth factor receptor-2
HER-2+	Overexression of HER-2
HLB	Hydrophilic-lipophilic balance
HPLC	High performance liquid chromatography
hr	Hour
HRP	Horseradish peroxidase
ICAM-1	Intercellular adhesion molecule
i.d.	Internal diameter
IKK	IκB kinase
IL	Interleukin
iNOS	Inducable nitric oxide synthase

I.P.	Intraperitoneal
JNK	c-Jun N-terminal kinase
kDa	Kilodaltons
kg	Kilogram
Ki-67	Cellular marker for proliferation
K_m	Michaelis constant
L	Length
LC-MS/MS	Liquid chromatography-mass spectroscopy/mass spectroscopy
M	Molar
MAPK	Mitogen activated protein kinase
mg	Milligram
min	Minute
mL	Milliliter
μL	Microliter
mM	Millimolar
μM	Micromolar
mm	Millimeter
μm	Micrometer
MMP-9	Matrix metalloproteinase-9
MMTV-LTR	Mouse mammary tumor virus-long terminal repeat
MP	Microparticles
MW	Molecular weight

NF-κB	Nuclear factor-kappa B
ng	Nanogram
nM	Nanomolar
nm	nanometer
NSAID	Non-steroidal anti-inflammatory
p53	Tumor suppressor protein
P_{app}	Apparent permeability
PCL	Poly(ε-caprolactone)
PEG	Poly(ethylene glycol)
PEO	Poly(ethylene-oxide)
PGA	Poly(glycolic acid)
PIP	Piperine
pmol	picomol
PLA	Poly(D-L-lactic acid)
PLGA	Poly(D-L-lactide-co-glycolic acid)
PR	Progesterone receptor
PVA	Poly(vinyl alcohol)
QUE	Quercetin
R_o	Rate of drug release
RNS	Reactive nitrogen species
ROS	Reactive oxygen species
rpm	Rotations per minute
SA	Salicylic acid

S.C.	Subcutaneous
SD	Standard deviation
SEM	Standard error of mean
SIL	Silibinin
SMEDDS	Self microemulsifying drug delivery system
STAT	Signal transducer and activator of transcription
SULT	Sulfotransferase
$t_{1/2}$	Half-life
TAN	Tangeretin
T_g	Glass transition temperature
TNF-α	Tumor necrosis factor-α
UDPGA	Uridine 5'-diphospho-glucuronic acid
UGT	UDP-glucuronosyltransferase
VCAM-1	Vascular cell adhesion molecule-1
VEGF	Vascular endothelial growth factor
V_{max}	Maximum reaction velocity
WAP	Whey acidic protein
w/v	weight by volume
w/w	weight by weight

CHAPTER 1

INTRODUCTION

1.1 Curcumin - general molecular mechanisms

Curcumin (diferuloylmethane) is a polyphenol extracted from the root, *Curcuma longa*, commonly known as turmeric. Curcumin makes up between 3-6% w/w of turmeric and is widely used in South Asian cuisine and as a food coloring agent. Curcumin has long been used in traditional Indian Ayurvedic medicine to treat various ailments ranging from abdominal pain to anorexia to inflammation (1). Preclinical and clinical research has revealed curcumin's effects on a wide variety of cellular pathways, resulting in therapeutic activity against a number of diseases (2, 3). Curcumin affects a number of molecular targets including kinases, metabolic enzymes, transporters, adhesion molecules and inflammation pathways such as NF-κB (4). These effects, combined with little to no side effects at high oral doses (12 g/day) (5), make curcumin a promising chemopreventive compound.

1.2 Curcumin and cancer

It is believed that tumorigenesis occurs through multiple steps (6). During initiation, reactive oxygen or nitrogen species (ROS or NOS, respectively) cause genetic alterations that affect normal cellular pathway(s) (7). During proliferation, tumor cells gain the ability to produce their own growth factors and evade apoptosis. This leads to uncontrolled cell division and tumor growth (6). During invasion, tumor cells gain the

ability to intravasate into the blood stream by losing adhesion properties and eventually seed distant tissues (8). Curcumin has beneficial effects on each of these stages.

1.2.1 Curcumin inhibits initiation

Cancer arises from genetic mutations caused by several factors. These include stray free radicals (ROS and RNS), generated from normal cellular processes as well as in pathological states, such as inflammation, and environmental carcinogens. Curcumin is a potent antioxidant (9-11). In vitro, curcumin is able to scavenge superoxide and hydroxyl radicals at low IC_{50} values (6.25 and 2.3 μg/mL, respectively) (10). Nitric oxide has been implicated as a signaling molecule during inflammation (12), and tissue nitric oxide level has been used as a diagnostic biomarker, since the level correlates with tumor progression (13). Hepatic mRNA levels of inducible nitric oxide synthase (iNOS), a producer of nitric oxide, were diminished 50-70% in mice receiving curcumin orally (14). Curcumin has also been shown to upregulate the Nrf2 pathway in ischemic brains after intraperitoneal (I.P.) administration (15). Nrf2 stimulates expression of endogenous antioxidants such as heme oxygenase-1 and glutathione (GSH). Curcumin was also shown to stimulate GSH production in lung cancer cells (A549) in vitro (16) and GSH-S-transferase (GST) in vivo in rats (17). GSH is an intracellular antioxidant and is a conjugate for Phase II metabolism. GSH conjugation to a xenobiotic (such as a carcinogen) by GST assists in clearance from the cell via cell membrane transporters, thus preventing genetic alterations (18).

1.2.2 Curcumin decreases cell proliferation

Cellular proliferation is regulated by many different yet redundant pathways. Oncogene addiction theory posits that once the main oncogenic (or tumor suppressor) pathway is returned to basal levels, the tumor cell will die (19, 20). Therefore, despite cellular signaling redundancies, targeting one key pathway is a viable option for killing a tumor cell. However, tumors are notoriously heterogeneous and patient-to-patient variability is high (21, 22). Compounds such as curcumin, which target many different pathways, are ideal for chemoprevention across diverse populations and disease states.

Curcumin has shown modulatory effects on several proliferative pathways important for cancer. A large number of the effects of curcumin stem from its ability to inhibit NF-κB activation (23). NF-κB is comprised of three subunits: IκB, which acts as an intracellular sequestering protein, and two nuclear factors (selected from p55, p65, p105 and p115) (24). Phosphorylation of IκB results in ubiquitination of IκB and the release of the sequestered nuclear factors. The nuclear factors translocate to the nucleus and activate transcription. NF-κB signaling is involved in several different inflammatory and cell proliferative pathways including epidermal growth factor receptor (EGFR) family pathways (25), transforming growth factor receptor (TGFR), tumor necrosis factor receptor (TNFR) (26) and interleukin (IL) signaling (27). Curcumin prevents phosphorylation of IκB by IκB kinase (IκBK), thus blocking the release of nuclear factors (23). Inhibition of NF-κB by curcumin has been shown to decrease cyclooxygenase-2 (COX-2) expression, a contributor to inflammation, in lung and colon cancer cells in vitro (28, 29).

Curcumin has been shown to downregulate other pro-survival pathways and upregulate pro-apoptotic pathways to induce cell death. Signal transduction from cellular receptors through kinases to stimulate transcription factors is the basis for cellular signaling. Curcumin interferes with each of these steps. Curcumin degrades and inhibits the activation of EGFR in gefitinib-resistant A549 cells (30). In this study, curcumin improved the efficacy of gefitinib in vivo and was associated with decreased tumor growth. Curcumin inhibits NF-κB induced MAPK and JNK (31, 32) activation, resulting in reduced activation of AP-1 leading to decreased transcription of proteins involved in proliferation and invasion. In T-cell leukemia, curcumin suppresses the activation of transcription factors STAT3 and STAT5 (33), which have been shown to be overexpressed in several cancers and are important for cell proliferation and differentiation (34, 35). Curcumin was also shown to degrade histone acetylatransferease p300 and inhibit its function through covalent binding, resulting in reduced cellular transcription (36).

Curcumin induces apoptosis by modulating several proteins. Curcumin downregulates Bcl-2 and Bcl_{XL} (anti-apoptotic factors) while upregulating Bax and Bad and activating caspase-3 in vivo in a peritoneal model of Dalton's lymphoma (37, 38). Angiogenesis, the formation of new blood vessels from existing ones, is necessary for tumor growth and metastasis. The expression of growth factors such as VEGF, bFGF and EGF results in angiogenesis (39, 40). Curcumin has been shown to decrease the expression of these growth factors in both a xenograft model of hepatocellular carcinoma and in a transgenic mouse model overexpessing VEGF (40-42), leading to decreased tumor growth and delayed tumorigenesis.

1.2.2.1 Effect of curcumin on HER-2

Human epidermal growth factor receptor (HER-2) is overexpressed in 30% of breast cancer cases (43, 44). The biological importance of HER-2 in breast cancer will be discussed in detail in section 1.6. Similar to its effect on EGFR, curcumin has been shown to decrease both the phosphorylation and the total protein levels of HER-2 in the AU565 (HER-2+) breast cancer cell line (45). This effect was observed to be time and concentration dependant. IC_{50} values for phosphorylation decreased by six fold while the concentration required for HER-2 depletion fell by five fold when incubation was increased by twelve hours. Further, breast cancer cell lines overexpressing HER-2 were shown to be more sensitive to curcumin treatment than other cell lines tested.

The mechanism of HER-2 depletion for curcumin is bimodal. Curcumin increases the interaction between HER-2 and CHIP, a E3 ubiquitin ligase that causes ubiquitination (46). This interaction is chaperone (Hsp70 or Hsp90) dependent. Additionally, the double bonds present on the alkyl chain of curcumin (see Table 1) can act as Michael reaction acceptors to covalently bind to HER-2. Tetrahydrocurcumin, which lacks double bonds, was unable to deplete HER-2 even at very high concentrations. This suggests that the covalent binding of curcumin to HER-2 leads to ubiquitination and subsequently degradation of HER-2. An in vivo study showed that intraperitoneally (I.P.) injected curcumin (45 mg/kg, twice a week) was able to decrease tumor growth in a BT-474 (HER-2 overexpressing) xenograft model (47). This result was comparable to Herceptin® treatment (4 mg/kg loading dose, then 2 mg/kg once a week), supporting the use of curcumin as a potential alternative.

1.2.3 Curcumin blocks invasion

Metastasis is a multistep process, beginning in the tumor where cells undergo epithelial to mesenchymal transition (EMT), which results in a loss of adhesion properties (8, 48). This allows the tumor cell to intravasate into the blood stream, followed by extravasation out of the blood vessels to colonize a distant organ. During EMT, the levels of adhesion proteins such as E-cadherin are typically reduced while matrix metalloproteinases (MMPs) are increased. MMPs degrade the tumor matrix to allow for cell migration. Curcumin has been shown to upregulate E-cadherin and inhibit EMT (49, 50). In the hepatoma cellular carcinoma cell line Hca-F, curcumin was shown to inhibit tumor cell migration by decreasing caveolin-1 protein levels and EGFR activity (51). Modulation of these proteins led to a reduction in MMP-9 and MAPK and reduced migration. Curcumin has also been shown to decrease MMP-9 expression through inhibition of NF-κB activation in vitro in astroglioma cells (32). In vivo, curcumin treatment decreased NF-κB activation and inhibited lung metastasis in a xenograft MDA-MB-231 model (52). Moreover, curcumin decreased MMP-9 levels in A549 (non-small cell lung cancer), which lead to decreased cell migration in an in vitro scratch model (53). In vivo, curcumin formulated with phosphatidylcholine was able to decrease lung metastasis in a xenograft breast cancer model and was again associated with decreased MMP-9 levels (54). Lastly, curcumin decreased the expression of VCAM-1 and ICAM-1, believed to be involved in EMT and extravasation into tissue, via NF-κB inhibition in an in vitro model of pancreatic cancer (55).

Curcumin

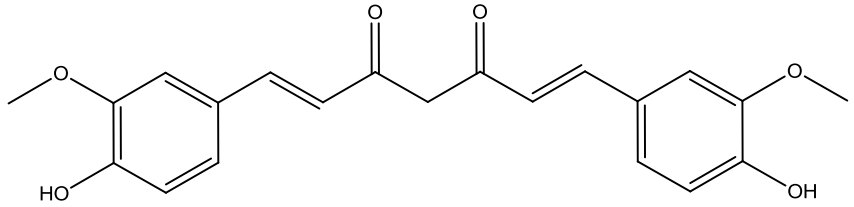

$C_{21}H_{20}O_6$

Chemical name: 1,6-heptadiene-3,5-dione-1,7-bis[4-hydroxy-3-methoxyphenyl-[1E,6E] or diferuloylmethane

Molucular weight :	368.37 g/mol
Melting point :	183˚ C
Aqueous solubility :	Practically insoluble
Organic solubility :	Soluble in methanol, ethanol, DMSO
LogP :	3.62 (predicted)
UV λ_{max} :	430 nm
Flourescent Emission :	470 nm (64)
Flourescent Excitation :	420 nm
Aqueous half life pH 5 :	199 min (57)
pH 6 :	195 min
pH 6.8 :	39 min
pH 7.2 :	9 min
pH 8 :	1 min
pH 10 :	14 min

Table 1 – Curcumin structure and general physico-chemical properties.

1.3 Overview of physico-chemical properties

The structure and major properties of curcumin are summarized in Table 1. Curcumin exists in enolic and β-diketonic form. In neutral and acidic aqueous (from pH 3 to 7), the diketonic form dominates. Above pH 8, the enolic form is the more abundant form (56). At low pH (≤6), curcumin is relatively stable compared to being almost immediately degraded at pH > 7 (57). Curcumin is highly protein bound (binding constant to bovine serum albumin = ~10^4 to 10^5 M^{-1}) (58) and can be stabilized by the

presence of protein such as fetal bovine serum in cell media (57). The major chemical degradation products of curcumin are ferulic acid and feruloylmethane, with vanillin being a minor product (57). As a solid, curcumin exists as an orange/yellow crystalline powder. Commercial curcumin contains 77% curcumin, 17% demethoxycurcumin and 3% bisdemethoxycurcumin (2).

1.3.1 Bioavailability of curcumin in vivo

Curcumin has very low bioavailability (<2%). The low aqueous solubility of curcumin limits the rate of dissolution in the gut after oral dosing, resulting in a significant portion of the dose being excreted in the feces. Curcumin has also been shown to be poorly absorbed with an in vitro intestinal apical to basolateral (A→B) P_{app} of $2.93 \pm 0.94 \times 10^{-6}$ cm/s in the in vitro Caco-2 model (59). Comparatively, the P_{app} of antipyrine, a well absorbed analgesic, was measured as $7.64 \pm 0.7 \times 10^{-5}$ cm/s. Further, curcumin undergoes extensive first pass metabolism, which contributes significantly to its poor oral bioavailability.

1.3.2 Pharmacokinetics of curcumin in vivo

Several studies have examined the pharmacokinetics of curcumin after oral dosing. In mice, a 1 g/kg oral dose (equivalent to a 70 g human dose) only produced a maximum serum concentration of 220 ng/mL (60). Other studies found similar results when dosing mice orally at 500 mg/kg (C_{max} = 60 ng/mL, $t_{1/2}$ = 45 minutes) (61) and 300 mg/kg (C_{max} = 266 ng/mL, $t_{1/2}$ = 20 minutes) (62). Perkins et al examined steady state curcumin levels in plasma and tissue after long term oral dosing in mice by addition to

mouse feed (0.1, 0.2, or 0.5% by weight) (63). Plasma levels were low, near the limit of detection of 5 pmol/mL, for all doses. Large amounts of curcumin were found in the feces and small intestinal mucosa, but no detectable amounts elsewhere. In the same study, I.P. injections (100 mg/kg) produced low levels of curcumin in the liver (73 nmol/g), intestinal mucosa, (200 nmol/g), brain, (2.9 nmol/g), heart, (9.1 nmol/g), lungs, (16 nmol/g), muscle (8.4 nmol/g) and kidney (78 nmol/g). Schiborr also examined tissue levels after oral (50 mg/kg) or I.P. (100 mg/kg) dosing (64). After oral dosing, no curcumin was detected in the brain, however, I.P. injections produced 4-5 μg/g levels one hour post dose.

Studies examining curcumin pharmacokinetics in humans have confirmed its low oral bioavailability. In human volunteers, an oral dose of 2 g of curcumin only produced 6 ng/mL serum levels (65). Phase I clinical trials were carried out in patients with high risk for various cancers. Patients ingested curcumin (4 g, 6 g , 8 g or 12 g daily) for 3 months (5). Curcumin was well tolerated at even very high doses (12 g/day). Serum average peak concentrations after taking 4 g, 6 g or 8 g of curcumin were 0.51±0.11 μM, 0.63±0.06 μM and 1.77±1.87 μM, respectively. A separate phase I clinical trial showed that daily oral consumption of 3.6 g curcumin resulted in 11.1 nM plasma concentrations one hour post-dose, with no accumulation seen after multiple dosing (up to 29 days) (66). Curcumin was detectable in urine (0.1 – 1.3 μM), an outcome unique to this study, as other studies did not detect curcumin or its metabolites in urine. A phase II clinical trial carried out by Dhillon et al dosed 8 g curcumin daily, resulting in none to trace amounts of curcumin in plasma (67). Curcumin metabolites (glucuronide and sulfate forms) were present, though concentrations were highly variable.

1.3.3 Clearance of curcumin after in vivo dosing

Besides poor absorption, the low bioavailability of curcumin is due in large part to extensive intestinal and hepatic metabolism. Both phase I and II metabolic pathways are important for curcumin clearance (Figure 1).

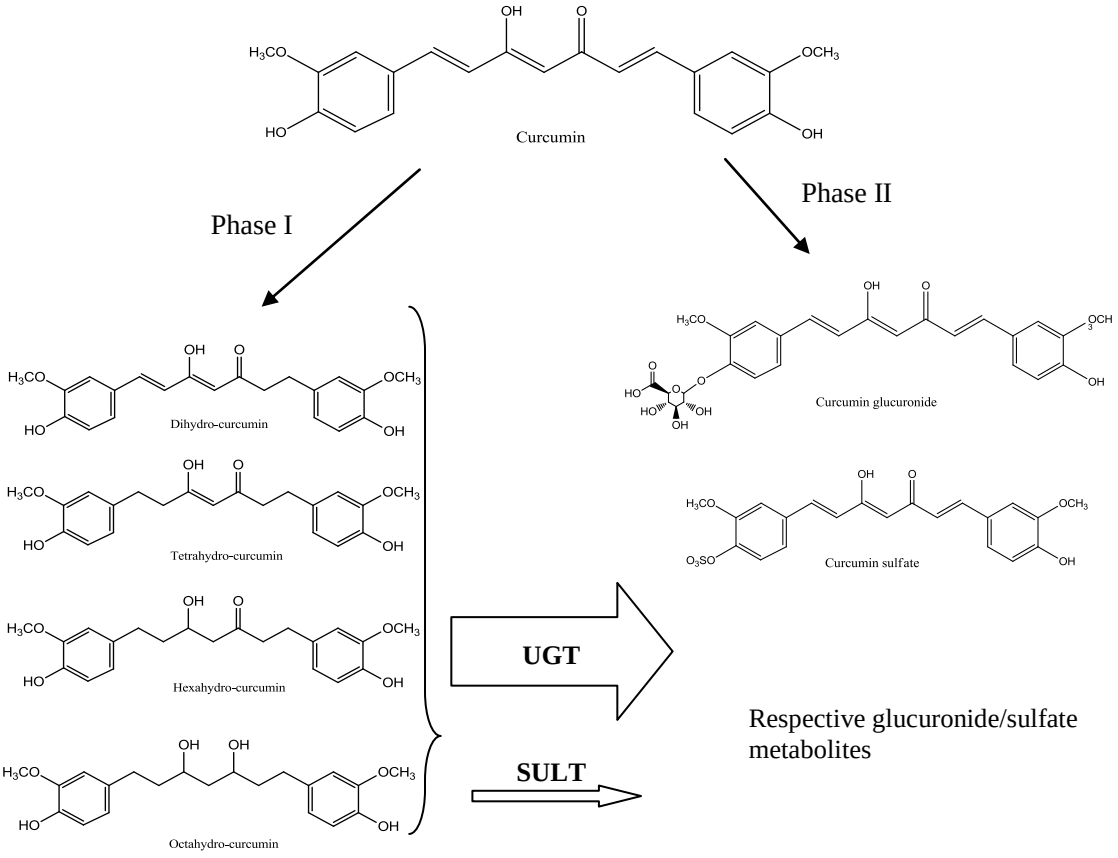

Figure 1 – Various Phase I and Phase II metabolites of curcumin.

1.3.3.1 Phase one metabolism

Curcumin is primarily reduced to its di-, tetra-, hexa- and octohydro forms after intravenous (I.V.) or I.P. injections (Figure 1, left) (68). This conversion has been

attributed to alcohol dehydrogenase in the liver. In vitro conversion of curcumin to these phase I metabolites was carried out in mouse liver slice incubations and confirmed by microsomal incubations (69). Incubating curcumin with pure alcohol dehydrogenase resulted in transformation to the reduced forms, further confirming this metabolic pathway. However, this process is not well understood, and the metabolic intermediates for this pathway are yet to be reported.

1.3.3.2 Phase two metabolism

UDP-glucuronosyltransferase (UGT) and sulfotransferase (SULT) are involved in curcumin conjugation reactions (Figure 1, right). Both enzyme families contain many different isozymes, with only a few being important for curcumin. The liver specific UGT1A1 isozyme has the highest activity for curcumin metabolism as shown using recombinant UGTs (70). Intestinal UGT1A8 and UGT 1A10 both account for significant curcumin metabolism; however, these have marginally lower overall activity compared to UGT1A1 (70). Phenolic curcumin monoglucuronides are the most common metabolic product seen after I.P. dosing (60). Overall hepatic and intestinal metabolic conversion of curcumin is high but differs between humans and rodents. Metabolic activity with human liver microsomes was significantly lower (4641 ± 126 pmol/min/mg) than human intestinal microsomes (12687 ± 1138 pmol/min/mg). However, in rodents the activity in liver and intestinal microsomes was relatively equal (4589 ± 170 and 3933 ± 104 pmol/min/mg, respectively) (71). An in vivo study administering curcumin I.P. concluded that 99% of the curcumin in the plasma was glucuronidated (60). SULT1A1 and 1A3 also account for a fraction of curcumin metabolism (68). Curcumin monosulfate

was shown to only account for 15% of metabolic products. Overall, phase II metabolism dominates after oral dosing and is one of the major obstacles that limits curcumin's oral bioavailability.

1.4 Inhibition of UGT enzymes for improving curcumin bioavailability

Since curcumin is mainly metabolized by UGT enzymes, inhibition of these enzymes could increase curcumin oral bioavailability. Depending on the molecular interaction with the enzyme, a chemical can have different inhibitory effects. In general, reversible enzymatic inhibitors fall into four categories: competitive, non-competitive, uncompetitive, and mixed inhibition (72). Competitive inhibitors bind directly to the active site and are metabolized, and thus the substrate V_{max} is not affected but K_m typically increases. Uncompetitive compounds are similar but bind to the enzyme-substrate complex, preventing conversion to the product. This reduces substrate V_{max} and K_m. In non-competitive inhibition, the inhibitor binds to the enzyme outside the active site, reducing its activity. This reduces substrate V_{max}, but K_m remains constant. Mixed inhibition is where the inhibitor binds to the active site but is not metabolized, resulting in decreased V_{max} and increased K_m.

Irreversible inhibitors can also be used. These typically bind irreversibly to the enzyme active site, reducing the V_{max} dramatically. For adjuvant therapy, a reversible inhibitor should ideally be used, since normal intestinal and hepatic metabolic activity needs to be restored once the oral absorption of curcumin is complete. This would minimize the potential for drug-drug interactions during long term dosing.

1.4.1 Inhibitors of UGT activity

Ideally, the inhibitory compound selected should show high affinity for both hepatic and intestinal UGT enzymes important to curcumin metabolism. Several exogenous drugs modulate UGT activity. HIV protease inhibitors, such as atazanavir, have been shown to inhibit bilirubin glucuronidation (73), leading to side effects such as jaundice. Non-steroidal anti-inflammatory drugs (NSAIDs) have shown UGT and SULT inhibition in previous studies (74). NSAIDS are metabolized primarily by UGT1A1 and have shown in vitro inhibition of β-estradiol glucuronidation. Opioids such as morphine have similar inhibitory effects (75). Gefitinib and erlotinib, tyrosine kinase inhibitors used for treating certain cancers, also show UGT inhibition in vitro (76). Unfortunately, many of these drugs have severe side effects and a narrow therapeutic window, making them not suitable for use in this particular application.

Any natural compound metabolized by UGT can be used as a competitive inhibitor. These also offer the advantage of safety at high doses based on normal ingestion through food. Several flavonoids have been shown to inhibit UGT1A1 activity at concentrations ranging from 0.5-10 μM (75, 77). The most potent of these compounds was tangeretin, an extract from orange peels. Other flavonoids showing inhibitory effects were quercetin, silibinin, and nobiletin. Piperine, an alkaloid extracted from black pepper, has also shown modulatory effects on several metabolic enzymes (78). Oral co-administration of piperine was shown to increase the bioavailability of curcumin in vivo (65). In human subjects given curcumin and piperine together orally, systemic bioavailabilty was increased by 2000% compared to curcumin alone. As an added

benefit, these natural compounds have anti-cancer activity (79-81), which could complement the anticancer activity of curcumin in vivo.

1.5 Formulation-based approaches to improve curcumin delivery

In order for curcumin to be used effectively as a chemopreventive or chemotherapeutic, its low bioavailability and short half life need to be overcome. Previous studies have examined a curcumin analogue with improved half life as well as increased potency compared to curcumin (82). Carrier-mediated drug delivery (via micelles, liposomes or phospholipids complexes) also shows great potential. Ma et al used poly(ethylene-oxide)-*co*-poly(caprolactone) (PEO-*co*-PCL) to form polymeric micelles loaded with curcumin (83). After I.V. injection, the half life of curcumin in this formulation was reported to be 60.5 hours, compared to 0.57 hours for a solubilized curcumin formulation. Anand et al loaded curcumin into poly(lactide-co-glycolide) (PLGA) nanoparticles and examined their bioactivity in vitro (84). Curcumin loaded PLGA nanoparticles showed increased cellular accumulation and increased potency versus soluble curcumin controls. However, these studies did not examine the pharmacokinetic parameters associated with their formulations. Additionally, in order to fabricate a successful system for chemoprevention, the ease of use must be considered in many ways. An ideal chemopreventive formulation must introduce active drug over a long period of time or be suitable for oral delivery. Microparticle and self microemulsifying drug delivery systems (SMEDDS) both offer possible avenues for long-term curcumin drug delivery.

1.5.1 Polymeric microparticles for drug delivery

Some small molecular weight compounds are not suitable for oral delivery for a variety of reasons including poor absorption, extensive first pass metabolism and low solubility. Injectable microparticles can deliver the drug systemically in a controlled manner, bypassing oral absorption (85, 86). This is also ideal for drugs with short half-lives or potent compounds that have a narrow therapeutic window. Drugs loaded into these systems are steadily released into systemic circulation. The desired rate of release is based on the rate of drug clearance and the desired steady state concentration ($C_{ss} = R_o/CL$, where C_{ss} is the steady state concentration, R_o is zero-order rate of drug release, and CL is the total clearance of the drug). The R_o can be fine-tuned depending on the drug as well as the excipient (polymer, etc) used for encapsulation (86). Polymer molecular weight, crystallinity, drug loading, glass transition temperature and the microparticle porosity all affect drug release rate. These parameters can be optimized during the fabrication process to achieve the desired release rate. As an example, lower molecular weight polymers tend to degrade faster than high molecular weight polymers and therefore release drug more quickly (87). Highly crystalline polymers, such as poly(lactic acid) (PLA), degrade slower than amorphous polymers like poly(glycolic acid) (PGA) (86, 88).

The biocompatibility and biodegradability of a polymer excipient is important when designing a microparticle drug delivery system. After intramuscular or subcutaneous injection, microparticles form a depot. A local foreign body response to the injection is typical, with acute inflammation at the injection site (89). Blood and tissue fluid proteins adhere on the microparticle surface. Inflammatory cells coat the

microparticle bulk surface and eventually form a fibrous coat. This is a typical response to any implant and is considered normal. Biodegradable polymers degrade by hydrolysis into monomers that are easily cleared by the body. The use of biodegradable polymers helps avoid surgery needed to remove a non-degradable delivery system at the end of drug release.

PLGA is one of the most commonly used biopolymers on the market. PLGA is amorphous but has a moderate release rate (weeks to months) depending on the microparticle diameter, porosity and polymer molecular weight (86, 90). In general, high microparticle porosity increases the drug release rate. Higher polymer molecular weight and microparticle size decrease drug diffusion through the polymer matrix, resulting in slower drug release. PLGA microparticles undergo bulk erosion by hydrolysis of the ester backbone. PLGA degrades to form its monomeric subunits lactic acid and glycolic acid. Both of these are cleared by the body readily after conversion to carbon dioxide and water via the tricarboxylic acid cycle (91). Drug release from PLGA is bimodal. A short burst release of drug is often observed and is considered to be due to release of unencapsulated drug on the surface. This is followed by sustained drug release, the kinetics of which depend on a number of formulation factors (92).

Disadvantages of polymeric microparticles mostly center on drug loading and injectability. Drugs, which are not potent or encapsulate poorly, require large microparticle doses or frequent dosing. Neither of these outcomes is patient-friendly, requiring repeated injections or an uncomfortably large depot size.

1.5.2 SMEDDS

The oral route is the most convenient for long term drug treatment. However, most drugs currently on their way to the clinic are classified as BCS class III or IV, indicating low solubility and/or low permeability (93). BCS class III (such as curcumin) or IV drugs are typically the hardest to formulate in an oral dosage form. Low solubility leads to poor drug dissolution while low permeability indicates poor gut absorption. Oral delivery of class III or IV drugs is associated with low bioavailability, high variability and non-linear pharmacokinetics. Self microemulsifying drug delivery systems (SMEDDS) can solubilize hydrophobic compounds at high concentrations so that otherwise poorly soluble drugs can be dosed orally in a soluble form (94). Once added to water, SMEDDS form a stable nanoemulsion with a dispersed phase typically less than <50 nm in diameter. The emulsion can be formed either prior to dosing by adding SMEDDS to an aqueous phase or can be formed *in situ* with the fluid present in the intestine (95).

SMEDDS are typically comprised of two components: oil and surfactant. The oil phase is responsible for dissolving the drug. Additionally, the oil component increases intestinal drug absorption and therefore bioavailability. Naturally occurring oils (such as olive, corn, peanut or palm oil) are preferable to synthetic oils (such as ethyl oleate or Captex®) due to decreased side effects after ingestion (96). However, modified (hydrolyzed) vegetable oils are typically capable of dissolving greater amounts of drug than unmodified oils due to increased hydrophobicity (95).

Surfactants assist in creating a stable nanoemulsion. Surfactant hydrophilic-lipophilic balance (HLB), ionic strength and chain length can affect the nanoemulsion

size and charge. Additionally, surfactants can enhance drug permeability by disrupting cell membrane organization (97). For instance, a negatively charged SMEDDS formulation decreased transepithelial electrical resistance (a measure of tight junctions) in the Caco-2 model and lead to greater mannitol permeability (98). Typical surfactants used include Cremophor EL®, Tween 80 and Labrasol®. The choice of oil and surfactant(s) is based on the drug used and needs to be optimized. Results of solubilization/phase studies shown in tertiary plots reveal the effects of varying component concentrations on the formulation. A successful SMEDDS can typically be identified by the naked eye as a clear solution with no phase separation or drug particulates. However, the formulation should be characterized by dynamic light scattering and zeta potential for size distribution and surface charge, respectively.

Clinical use of SMEDDS is limited but is increasing. Cyclosporin A (CsA) is an immunosuppressant used after organ transplant. CsA is poorly soluble, and a SMEDDS (Sandimmune® and Sandimmune Neoral®) showed greater bioavailability and dose proportional pharmacokinetics (99). Studies evaluating SMEDDS for other drugs such as Coenzyme Q_{10}, used for hypertension (100), and several HIV protease inhibitors have shown improved oral bioavailability of the respective drugs (101).

1.6 Breast cancer clinical overview

While curcumin has shown activity against a wide spectrum of cancers, the goal of this thesis is to evaluate curcumin's chemopreventive potential in breast cancer. Breast cancer is the most prevalent cancer in women. As of 2008, it is estimated that 2.6 million living women have some history of breast cancer (both benign and malignant)

and that a woman has a 1 in 8 chance of having breast cancer in her lifetime (102, 103). In 2011, an estimated 230,480 new cases of invasive breast cancer were diagnosed in the United States alone, accounting for 1 in 3 new cancer diagnoses in women. Breast cancer accounts for 24.5 deaths per 100,000 women of all races, but goes up to 33 per 100,000 for African-American women. Overall, breast cancer has a 90% five-year survival rate, but this survival figure precipitously drops with a higher stage of cancer upon diagnosis.

The three main types of normal breast tissue are the fat pad, the connective tissue, and the mammary gland (104, 105). The fat pad and connective tissue provide structure, support, and protection for the mammary glands. Typical human mammary glands are comprised of about 20 milk secreting lobules, which are themselves comprised of milk-producing epithelial cells (arranged in a ductile) covered by myoepithelial cells. These lobules are connected to the milk duct, which in turn is connected to the nipple. Development of this tissue is dependent on progesterone and estrogen during puberty. The majority of this information is based on mouse studies, and therefore can only infer the similarity to human development (106).

Breast cancer begins as cellular dysplasia (disordered cellular structuring) or carcinoma *in situ* (precancerous state) in the duct or lobule (57, 107-109). From 2004-2008, ductal carcinoma *in situ* accounted for 83% of diagnosed non-invasive breast cancers. Without intervention, this growth can breach the basement membrane of the tissue and become invasive. Depending on the tumor type and aggressiveness, distant metastasis will develop (110, 111). The most common metastasis locations are the lymph node (first to be seen typically), brain, liver, bones, and lungs. From this point, the metastases can grow larger and eventually inhibit normal function of these tissues.

The most important factor affecting prognosis is the stage of breast cancer at diagnosis (112-114). If diagnosed early (Stage 0-1), prognosis is very good. Women diagnosed at Stage 0 have a five year survival rate of 98%. However, due to the favored sites of metastasis of breast cancer (brain, lung, and bone especially), survival decreases dramatically if breast cancer is not diagnosed until Stage 4. Complications with breast cancer stem mostly from distant metastasis into other tissues, which can then cause a host of problems including interference with normal function (lungs) and damage to healthy tissue through increased pressure resulting from increased mass in the skull (brain).

Breast cancer most likely arises from a collection of genetic mutations in epithelial cells in the mammary tissue (6, 115). There is a clear genetic component in certain subtypes of breast cancer, as supported by evidence of the BRCA1 and BRCA2 gene mutations, which have been shown to lead to breast cancer at early ages and have strong hereditary correlation. Five main subtypes of breast cancer have been proposed based on gene expression arrays of patient breast tissue: normal breast-like, basal, luminal A, luminal B and HER-2 (110). Treatment options include surgery (single or double mastectomy) or combinations of radiation and chemotherapy depending on the subtype, grade and stage at time of diagnosis.

Surface receptor overexpression guides treatment options. For instance, estrogen receptor (ER+) and progesterone receptor (PR+) tumors are treated with hormonal therapies (116). HER-2+ tumors are treated with tyrosine kinase inhibitors in combination with other first line cytotoxics such as doxorubicin, docetaxel, and paclitaxel (44, 102). Triple negative (overexpressing none of the above receptors) are the most difficult to treat but are responsive to radiation and cytotoxic chemotherapy.

1.6.1 HER-2 overexpression in breast cancer

Since the studies described in this thesis focus heavily on HER-2+ breast cancer, this sub-type will be discussed further. HER-2 (ErbB2, neu or p185) is a 185 kDa tyrosine kinase receptor present on the cell surface (43). HER-2 is a member of the epidermal growth factor receptor (EGFR) family. It forms heterodimers with other members of the EGFR family (EGFR1, EGFR3 and EGFR4) in the presence of activating EGF-like ligands. HER-2 itself does not bind growth factor ligands, and must heterodimerize to activate downstream pathways.

Overexpression of HER-2 leads to increased activation of several EGFR family-mediated pathways that regulate cell division and survival. Like most tyrosine kinase receptors, HER-2 mediated signaling leads to activation of the Ras pathway (43). The Ras pathway can lead to inflammation through NF-κB signaling pathways (25) or cellular proliferation via MAPK and Akt/PI3K activation (117). These pathways also lead to expression of COX-2, an important inflammatory mediator (118).

HER-2 overexpression causes increased cell proliferation and inflammation, leading to tumorigenesis. HER-2+ tumors have high incidence of metastasis to the brain, lung and bone (25, 119). Overexpression of HER-2 is associated with MMP-9 (120, 121) and VEGF (122) overexpression, both important for EMT.

1.6.2 Models for studying breast cancer in vivo

Breast cancer is a multifaceted disease. In order to study breast cancer chemoprevention, a model that mimics the typical steps of tumorigenesis seen in humans needs to be used (123). This is difficult to achieve for breast cancer especially because of

the heterogeneity seen in human tumors (21, 22). However, xenograft and transgenic models representing specific subtypes are available and have been used for testing chemopreventive and chemotherapeutic compounds in vivo.

1.6.2.1 Xenograft models

Xenograft models typically consist of injecting human breast cancer cells into an immunocompromised mouse (123). The route and location of injection defines the type of xenograft. Injection of breast cancer cells into the mammary fat pad is called an orthotopic xenograft. Cells known to cause metastasis can also be injected intravenously to colonize a common metastasis site. Both models are useful depending on the stage of tumorigenesis being studied. A large number of well-characterized breast cancer cell lines are available, which mimic genetic profiles seen clinically (124, 125). This allows the targeting of specific pathways by selecting cell lines with specific phenotypes such as ER, EGFR or HER-2 overexpression. Additionally, cell lines can be modified to express luciferase (for luminescence imaging) or fluorescent tags such as GFP (126). Tagging cells with fluorescence allows the imaging of tumor growth and metastasis in live animals.

Xenografts have several disadvantages. They are not useful for studying the initiation step of tumorigenesis since cells are already tumorigenic. Additionally, breast cancer cell lines do not typically possess the same genetic alterations as primary breast tumors, which could lead to differences in treatment outcomes. Further, since xenografts must be carried out in immunocompromised mice, the involvement of the immune system cannot be examined (123).

1.6.2.2 Transgenic models

Transgenic models incorporate genetic alterations in order to overexpress an oncogene or suppress a tumor suppressor gene (123, 127). Therefore the effect of a specific treatment against that specific genotype can be tested in these models. The main advantage of these models is that treatment effects on tumorigenesis can be studied beginning at the initiation stage. Genetically altered mice have a defined genetic background, decreasing overall variability in tumor growth and response to treatments. Gene expression specific to the mammary tissue can be carried out using the mouse mammary tumor virus (MMTV) and whey acidic protein (WAP) promoters (115). A variety of different transgenic models using these promoters have been developed. Specifically for breast cancer, models overexpressing Myc (128), Ccnd1 (oncogene for cyclin D1) (129) and Erbb2 have been developed (115, 130). Additionally, transgenic models using SV40 large T-antigen, which inactivates p53 in the mammary tissue leading to tumorigenesis, have been characterized (131).

Transgenic models are expensive and the experimental time commitment is much longer than in xenografts. However, transgenic models more closely mimic human tumor development and animals are immunocompetent.

1.6.2.2.1 Balb-neuT

Efficacy studies carried out in this thesis use the Balb-neuT transgenic mouse model. This model overexpresses an activated form of the rat ortholog of HER-2 oncogene, neuT, under the control of the mouse mammary tumor virus-long terminal repeat (MMTV-LTR) promoter (132). This promoter responds to progesterone and

dihydrotestosterone, limiting its promotion to the mammary tissue (115). A valine to glutamic acid mutation enables the neuT protein to activate downstream signaling in the absence of growth factors (133). This allows for little to no further genetic alteration to initiate mammary cell transformation.

Tumors formed in this model are of lobular origin (132, 134). Between 3 and 4 weeks, hyperplasia can be observed in the terminal lobular buds. From 4-6 weeks, an increase in the number of microvessels is observed, which correlates with high levels of VEGF, bFGF and β_3 integrin (pro-angiogenic factors) (134). *In situ* carcinoma is present by 8-12 weeks of age, and invasive lobular carcinoma is detectable by 17 weeks of age. Although tumorigenesis is driven by overexpression of neuT, a distinct inflammatory contribution is present. IFN-γ, TNF-α and IL-1β were found to be overexpressed in mammary tissue taken from mice between 10 and 15 weeks of age (135). Microvessel count and growth factor levels are decreased at 15 weeks of age compared to 5 weeks of age, indicating that the majority of angiogenesis has ended by that age. At least one palpable tumor is typically seen at 17 weeks of age, with all ten mammary glands having a palpable tumor by 28 weeks of age. High levels of IL-1β and IL-6, but not TNF-α were found in 7 mm diameter tumors by PCR (135). The cancer stem cell population for this model has been identified as Sca-1+, confirmed by flow cytometry, mammosphere and in vivo tumorigenesis assays (136).

A number of studies have used Balb-neuT to determine the efficacy of anti-HER-2 treatments. This model was used initially for studying the anti-tumorigenic effects of IL-12 (132). Administration of IL-12 delayed time to 100% tumor penetration significantly and decreased tumor cytokine levels. A separate study showed that gefitinib

(an EGFR tyrosine kinase inhibitor) dramatically reduced tumor development by inhibiting EGFR and HER-2 phosphorylation (107). Addition of benzyl isothiocyanate (BITC, a constituent of cruciferous vegetables) to the Balb-neuT diet (3 mmol/kg) was shown to significantly decrease proliferation and increase apoptosis in mammary tissue (137). However, this study did not report tumor incidence results. Capriani et al used an in vivo electroporation to vaccinate Balb-neuT mice against neu (138). Treatment significantly delayed tumor appearance, with 40% of mice tumor-free at 44 weeks, compared to all control mice having ten tumors by 27 weeks. Importantly, this study established that 13 weeks of age (coinciding with *in situ* carcinoma) represents an important time point in tumor progression in these mice. Beginning treatment after this point proved to be futile, while treatments beginning before 13 weeks of age showed efficacy.

1.7 Statement of problem and hypothesis

Women with HER-2+ breast cancer have a high incidence of metastasis and low five-year survival rate. Curcumin offers the potential for chemoprevention of HER-2+ breast cancer but is limited by its unfavorable pharmacokinetics. A previous study from our laboratory has shown that polymeric microparticles can improve the pharmacokinetic properties of curcumin. However, injectable formulations such as microparticles, even when dosed infrequently, may not be accepted by some patients.

Curcumin has poor oral bioavailability due to low solubility and extensive gut and hepatic metabolism. SMEDDS can solubilize curcumin to negate the poor dissolution. Moreover, co-delivery of natural metabolic inhibitors can decrease curcumin metabolism

and thus improve oral bioavailability. The central hypothesis of this thesis is that *novel microparticle and SMEDDS formulations will be effective in improving curcumin pharmacokinetics and therapeutic efficacy*.

1.8 Specific aims

The following were the specific aims for this thesis:

(1) – Determine the chemopreventive efficacy of curcumin loaded microparticles in the Balb-neuT transgenic mouse model of HER-2+ breast cancer (covered in Chapter 2).

(2) – Determine suitable inhibitors of curcumin metabolism and co-deliver these compounds in a SMEDDS formulation to improve curcumin bioavailability (covered in Chapter 3).

CHAPTER 2

EFFECT OF CURCUMIN LOADED PLGA MICROPARTICLES ON TUMOR PROGRESSION IN A TRANSGENIC MOUSE MODEL OF BREAST CANCER

Curcumin has shown promising inhibitory activity against HER-2 positive tumor cells in vitro but suffers from poor oral bioavailability in vivo. Our lab has previously developed a polymeric microparticle formulation for sustained delivery of curcumin for chemoprevention. The goal of this study was to examine the anticancer efficacy of curcumin loaded polymeric microparticles in a transgenic mouse model of HER-2 cancer, Balb-neuT. Microparticles were injected monthly, and mice were examined for tumor appearance and growth. Initiating curcumin microparticle treatment at 2 or 4 weeks of age delayed tumor appearance by 2-3 weeks compared to that in control mice that received empty microparticles. At twelve weeks, abnormal (lobular hyperplasia, carcinoma *in situ*, and invasive carcinoma) mammary tissue area was significantly decreased in curcumin microparticle-treated mice, as was CD-31 staining. Curcumin treatment decreased mammary VEGF levels significantly, which likely contributed to slower tumor formation. When compared to saline controls, however, blank microparticles appeared to accelerate tumorigenesis and curcumin treatment appeared to abrogate this effect, suggesting that PLGA microparticles enhance tumorigenesis in this model. PLGA microparticle administration was shown to be associated with higher plasma lactic acid levels and increased activation of NF-κB. High lactic acid levels have been previously shown to stimulate tumor angiogenesis. Further studies are needed to

elucidate the mechanism of PLGA microparticle-mediated enhanced angiogenesis and tumorigenesis in this mouse model of breast cancer.

2.1 Introduction

Human epidermal growth factor receptor-2 (HER-2), a membrane receptor tyrosine kinase, is an upstream effector of Ras, Akt, and NF-κB (44, 139, 140). Overexpression of HER-2 leads to dysregulation of cellular division as well as induction of inflammation. Patients who have HER-2+ tumors are at high risk for metastases in the lung, bone and brain (110, 141). Availability of targeted therapies (the HER-2-targeted monoclonal antibody, trastuzumab, and the receptor tyrosine kinase inhibitor, lapatinib) has improved the five-year survival rate in these patients (102, 142, 143). However, these targeted therapies do not cross the blood-brain barrier effectively, making it difficult to treat brain metastases (144, 145). In addition, HER-2+ breast cancer is associated with higher incidence of recurrence (146). Therefore, a chemopreventive approach to HER-2+ breast cancer would be highly valuable.

Curcumin induces HER-2 ubiquitination and subsequent degradation resulting in the inhibition of HER-2+ tumor cells (45, 46). Curcumin's other anti-cancer effects mainly stem from inhibition of NF-κB activation (3, 16, 23). Despite promising preclinical studies, the use of curcumin in the clinic has been severely limited by its very low bioavailability (147).

Injectable microparticle (MP) based drug delivery offers the ability to bypass gut absorption and first pass metabolism (85, 86, 148, 149). Formulation parameters can be fine-tuned to sustain drug plasma levels over a course of weeks to months depending on

the excipients used (85). Our laboratory has previously developed an injectable microparticle formulation using the FDA-approved polymer, poly(lactide-*co*-glycolic acid) (PLGA) for sustained curcumin delivery (150, 151). This formulation maintained curcumin blood levels for at least 1 month and effectively inhibited tumor growth in a mouse xenograft MDA-MB-231 model of triple negative breast cancer.

The goal of the current study was to examine the efficacy of curcumin-loaded PLGA microparticles in a transgenic mouse model of HER-2+ breast cancer, Balb-neuT. Mice were treated with curcumin loaded microparticles beginning at varying time points in tumor progression to determine the optimal time of intervention. The effect of curcumin treatment on tumor multiplicity, growth and angiogenesis was determined.

2.2 Material and Methods

2.2.1 Materials

PLGA (intrinsic viscosity = 0.95-1.20 dL/g) and poly(ε-caprolactone) (PCL, intrinsic viscosity = 1.0-1.3 dL/g) were purchased from LACTEL Absorbable Polymers (Birmingham, AL). High purity curcumin (>98% curcuminoids), casein, Tween 80 and polyvinyl alcohol (PVA, 30-70 kDa MW) were purchased from Sigma-Aldrich (St. Louis, MO). Acetonitrile, methanol and chloroform were purchased from Fisher Scientific (Pittsburg, PA). Anti-HER-2 and anti-VEGF antibodies were purchased from Santa Cruz Biotechnology (Santa Cruz, CA). Anti-β-tubulin antibody and HRP linked anti-rabbit IgG was purchased from Cell Signaling Technology (Beverly, MA). HRP linked anti-β-actin antibody was purchased from Sigma-Aldrich. 1X RIPA buffer,

endotoxin free water and SuperSignal West Pico Chemiluminescent Substrate were purchased from Thermo Scientific (Waltham, MA).

2.2.2 Microparticle fabrication

Curcumin loaded MP were prepared using a rapid solvent evaporation technique published previously (150, 151). Briefly, curcumin (20 mg) and PLGA (20 mg) were dissolved in 1.65 mL of chloroform-methanol mixture (10:1 v/v). This solution was emulsified in 6 mL of 2% w/v PVA for 2 minutes using a digital vortex (FisherSci) set at 1000 rpm. Chloroform was removed from the emulsion over 25 minutes using a benchtop rotary evaporator (Heidolph, Schwabach, Germany). Particles were collected by centrifugation and washed twice with 10% w/v Tween 80 and then twice with water. Particles were then lyophilized for 48 hrs (Labconco, Kansas City, MO). Non-drug loaded (blank) PLGA and PCL MP were prepared similarly but without curcumin. Endotoxin-free water was used for preparing all the aqueous solutions. Curcumin content was measured by extracting a known amount of curcumin loaded MP with methanol at room temperature overnight on a rotary extractor. The suspension was centrifuged at 20000 x g for 10 minutes (Eppendorf, Hamburg, Germany) and supernatant was analyzed by HPLC. HPLC was performed on a Beckman HPLC system connected to a PDA detector (Brea, CA). Curcumin was eluted on a XBD C-18 Agilent column (250 x 4.6 mm, 5 μm) (Santa Clara, CA). Mobile phase consisted of 10 mM ammonium acetate (pH 4, adjusted with glacial acetic acid) and acetonitrile (35:65) run isocratically at 1 mL/min. Curcumin (λ_{max} = 430 nm) eluted at 4.9 minutes. Curcumin produced a linear standard plot over the range of 1.56 – 25 μg/mL with a R^2 >0.999 (Figure 2). Drug loading was

calculated by dividing the amount of curcumin recovered after extraction by the amount of microparticles from which it was extracted. Percent encapsulation efficiency was calculated as the amount of curcumin recovered from extraction divided by the 500 μg multiplied by 100.

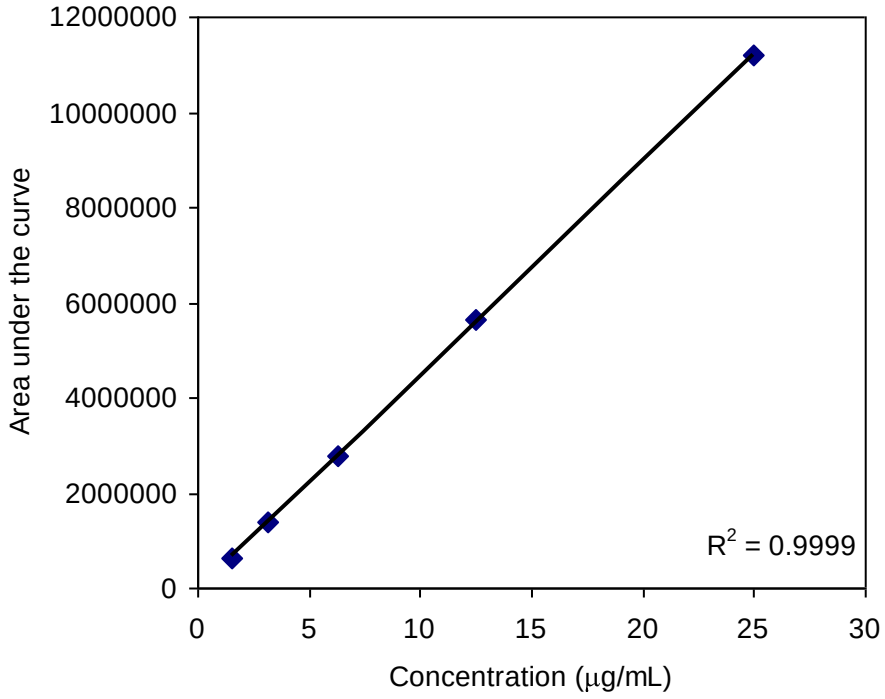

Figure 2 – Standard curve for curcumin concentration analyzed by HPLC.

2.2.3 Animal care

All animal studies were approved by the University of Minnesota Institutional Animal Care and Use Committee. Balb-neuT mice were bred according to established

protocols (132, 152). Mice were given access to food and water *ad libitum*. Genotyping was preformed by Transnetyx Inc (Cordova, TN) using tail snips collected at 1-3 weeks of age.

2.2.4 Pharmacokinetic studies

Balb/c mice (10-12 weeks old) were given a single subcutaneous (S.C.) injection of curcumin loaded PLGA MP (equivalent to 58.2 mg of curcumin). A set of mice were sacrificed at various time points to collect blood and tissues. Mammary tissue was homogenized in distilled water using a handheld homogenizer (Omni International, Kennesaw, GA) and then lyophilized. Curcumin was extracted from the tissues with ethyl acetate (0.5 mL for whole blood, 2 mL for mammary tissue) overnight at room temperature. Samples were centrifuged at 3200 x g for 10 minutes and supernatant was dried under nitrogen stream. Curcumin was reconstituted in methanol and analyzed by liquid chromatography tandem mass spectroscopy (LC-MS/MS) using a previously published protocol (153).

Chromatography was performed on an Agilent Technologies 1200 series system with negative ESI connected to a TSQ Quantum system. An Agilent XDB-C18 1.8 µm, 4.6×50 mm column was used for separation. Mobile phase consisted of (A) 10 mM ammonium acetate and (B) acetonitrile. Linear gradient flow (0.5 mL/min) with a total run time of 10 min was used: 0–4.5 min: 45–100% B, 4.5–5.5 min: 100% B, 5.5–6 min: 100-45% B, 6–10 min: 45% B. The following mass transitions were monitored: curcumin – 367→216, hydroxybenzophenone (internal standard) – 197→92. Elution time was 4.3

min for curcumin and for 3.4 min hydroxybenzophenone. Curcumin produced a linear standard plot with a range from 0.013 – 1.25 μM and a $R^2 > 0.999$ (Figure 3).

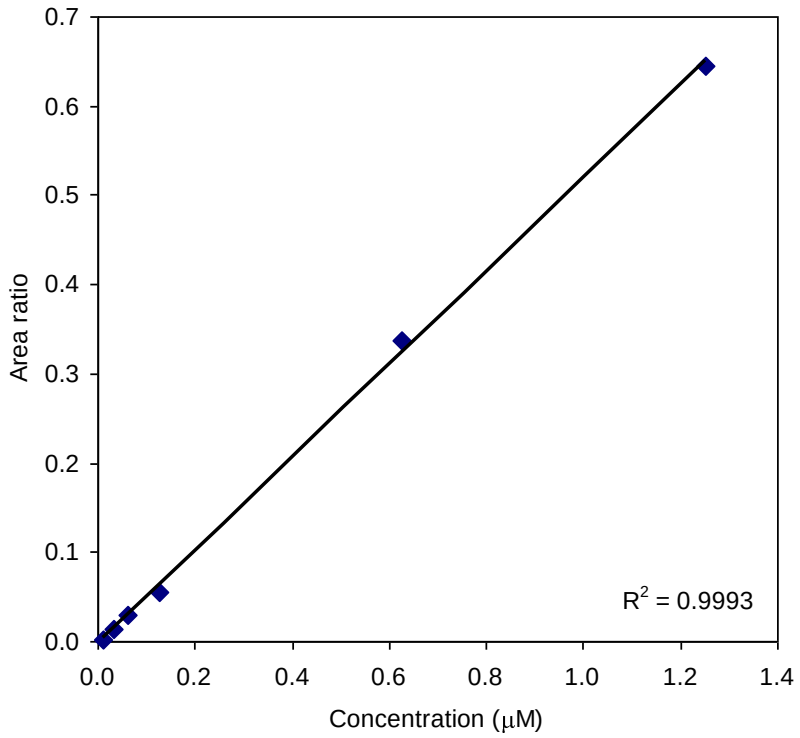

Figure 3 – Standard curve for curcumin quantitation by LC-MS/MS.

2.2.5 Tumorigenesis studies

Female Balb-neuT mice were injected S.C. with curcumin-loaded PLGA MP (140 mg, corresponding to 58.2 mg of curcumin suspended in 750 μL sterile 1X PBS) or blank PLGA MP (90 mg) initially at 2, 4, 7 or 12 weeks of age, and once a month thereafter. Mice treated initially at 2 weeks received a reduced dose (100 mg curcumin loaded MP, 60 mg blank MP) to account for lower body weight. Microparticle dose was returned to

normal beginning at 6 weeks of age in these mice. In control animals, saline was injected starting at 2 weeks (550 μL), and once a month thereafter (750 μL). Beginning at 8 weeks, mouse mammary pads were palpated once a week for tumors, with a one mm^3 mass considered as tumor formation. Volume of the right ventral anterior tumor was measured weekly using calipers. Volume was calculated as $V = (L \times W^2)/2$, where L is the tumor diameter parallel to the tail, and W is the tumor diameter perpendicular to the tail. Mice were euthanized when tumors in all ten mammary pads were detected.

2.2.6 Histology

Female Balb-neuT mice were S.C. injected with curcumin loaded PLGA MP, blank PLGA MP, or saline as described above. Mice were sacrificed at 8 or 12 weeks of age and mammary tissue was harvested. A portion of the tissue was fixed with 10% buffered formalin for histology while the other part was stored at -80º C for Western blotting studies. Formalin-fixed mammary tissues were switched to 70% ethanol after 24 hours. Tissue processing and staining for hematoxylin and eosin (H&E), Ki-67, and CD-31 were carried out by the Comparative Pathology Shared Resource at the University of Minnesota. All samples were received by the Comparative Pathology Shared Resource laboratory in 70% v/v ethanol/water, processed accordingly for routine histology and embedded in paraffin. The samples were then cut into 4 μm sections and stained with H&E. Abnormal tissue areas (lobular hyperplasia, carcinoma *in situ*, and invasive carcinoma) were measured in 10X magnification photographs using ImageJ software (Bethesda, MD). Ki-67 and CD-31 staining were quantified by taking 15-20 unique 400X pictures per tissue and manually counting positively stained cells.

2.2.7 Western blotting

Mammary tissues were minced into fine pieces, and protein was extracted using 1X RIPA buffer. Protein content was determined using the BCA assay kit (Pierce, Rockford, IL). Western blotting was carried out using the BioRad Criterion system (Hercules, CA). Proteins were separated by SDS-PAGE on a 4-15% polyacrylamide gradient gel and then transferred to a nitrocellulose membrane. Blots were probed with antibodies against HER-2, VEGF, or p65 NF-κB. β-actin or β-tubulin served as loading controls. Bands were visualized with SuperSignal West Pico Chemiluminescent Substrate. Band intensities were determined using ImageJ and Origins (Northhampton, MA) software.

2.2.8 Plasma and mammary tissue inflammatory cytokine levels

Mice were injected with 60 mg of empty PLGA MP, 60 mg of empty PCL MP, 100 mg of curcumin loaded PLGA MP, saline (750 μL) or 5% casein solution at two weeks of age. Casein was injected intraperitoneally (200 μL, I.P.) while all other treatments were administered S.C. Casein has been used previously to induce systemic inflammation (154). One month after treatment, mice were sacrificed. Plasma and mammary tissues were collected. Mammary tissues were minced fine and protein was extracted using 1X RIPA buffer. Plasma and mammary protein extracts were analyzed using a Multiplex cytokine assay (Millipore, Billerica, MA) by the Cytokine Lab, School of Medicine, University of Minnesota.

In a separate study, 12 week old female BALB/c mice were injected with 750 μL saline or 90 mg blank PLGA MP and sacrificed after 24 hours. Plasma and tissues were collected. Plasma was examined for IL-1β, IL-6 and TNF-α concentrations using ELISA kits (Invitrogen, Grand Island, NY) according to manufacture's protocol.

2.2.9 Lactic acid quantitation

Plasma lactic acid levels were determined using a lactic acid quantitation kit (Abnova, Walnut, CA) using a part of the tissues collected for the one month cytokine analysis described above. Plasma was used without additional processing.

2.2.10 Bioluminescence imaging

Transgenic mice carrying a NF-κB response element upstream of an inserted luciferase transgene (BALB/c-Tg[NF-κB-RE-luc]) were purchased from Taconic (Hudson, NY). These mice express luciferase when NF-κB is activated. Seven week old female mice were injected S.C with saline or 90 mg empty PLGA MP, or given an I.P. injection of a 5% casein solution, as described in previous sections. Bioluminescence imaging was carried out on a Caliper LifeScience (Hopkinton, MA) IVIS® Spectrum instrument at various times after initiating treatment. Mice were injected I.P. with luciferin (150 mg/kg) 15 minutes before imaging. Data was analyzed using Living Image® software.

2.2.11 Endotoxin detection

Microparticles were tested for the presence of endotoxin using a LAL chromogenic endotoxin quantitation kit (Pierce). PLGA MP were suspended (120 mg/mL) in endotoxin free water and vortexed. The MP suspension was centrifuged at 20000 x g for 10 minutes and the supernatant was tested directly.

2.2.12 Statistical Analysis

Significance of observed differences was tested using Student's t-test when applicable. Comparisons between more than two groups were carried out using ANOVA followed by Newman Keuls testing, with $p<0.05$ being considered statistically significant.

2.3 Results

2.3.1 Formulation of curcumin microparticles and pharmacokinetic characterization

Curcumin loaded microparticles (curcumin MP) were prepared by a modified solvent evaporation technique. Average particle diameter was 18.7 ± 7.7 mm (Figure 2) with ~39% w/w drug loading (78% encapsulation efficiency). These results are similar to that described for curcumin MP reported in previous studies (150, 151). Empty PLGA (blank) MP were examined for endotoxin levels. The endotoxin levels were undetectable in MP (limit of quantitation = 0.1 endotoxin units/mL). A single injection of curcumin MP sustained blood (~0.2 μM) and mammary tissue (~1 μM) levels in BALB/c mice for

up to 45 days (Figure 5). Significantly higher blood and mammary tissue concentrations were observed one and forty five days after injection.

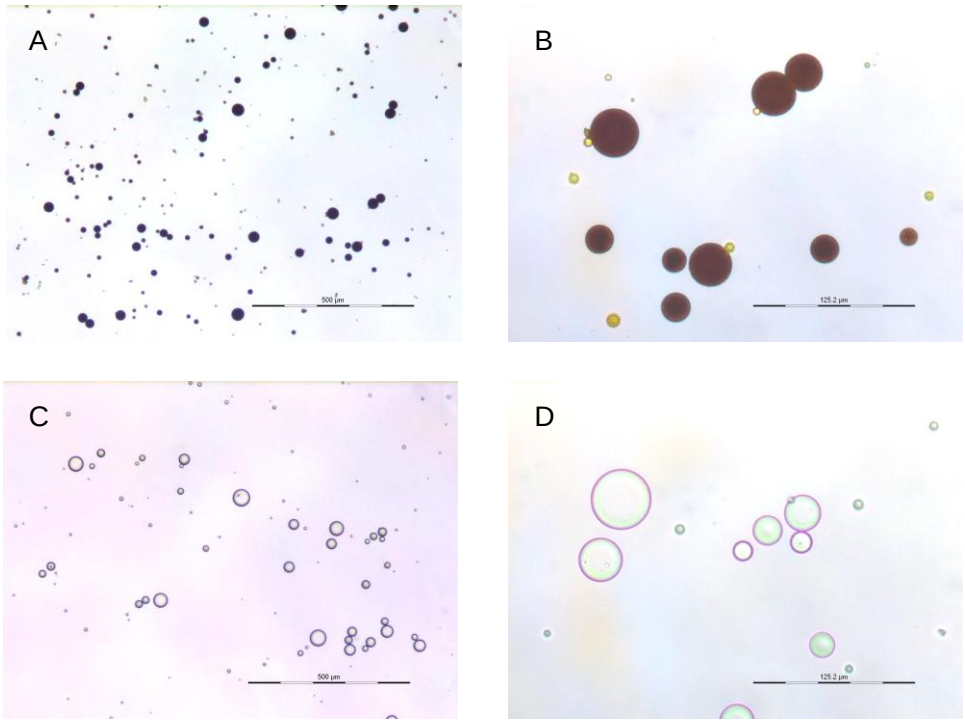

Figure 4 – Curcumin loaded and blank PLGA microparticles. Curcumin loaded (A, B) or blank (C, D) microparticles were suspended in water and photographed using an optical microscope at 100X (A and C, scale bar represents 500 μm) and 400X (B and D, scale bar represents 125 μm) magnifications.

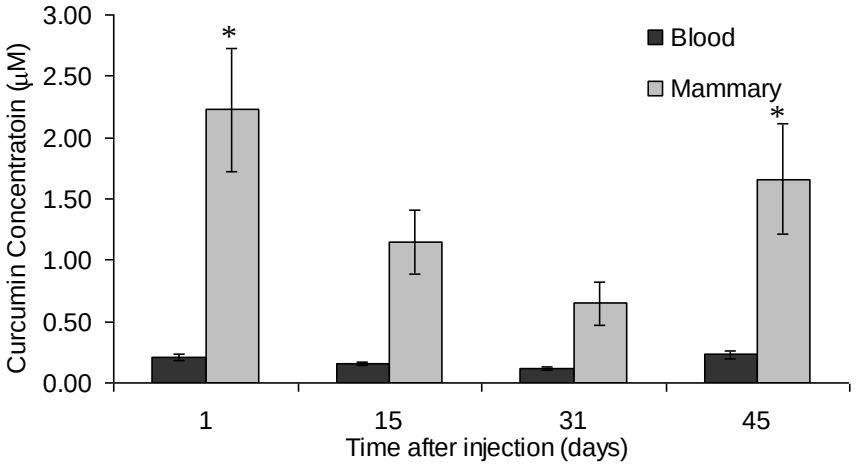

Figure 5 – Curcumin loaded PLGA microparticles sustain blood and mammary curcumin levels for at least 45 days. Female BALB/c mice (n=5-6) were administered a single dose of curcumin loaded microparticles (equivalent to 58.2 mg of curcumin). A set of mice were sacrificed at various time points and tissues were collected and analyzed for curcumin content by LC-MS. Data are presented as average curcumin concentration ± S.D. *$p<0.05$ determined by ANOVA followed by post hoc Newman Keuls testing compared to other time points of the same tissue.

2.3.2 Curcumin loaded microparticles delay tumorigenesis in Balb-neuT mice

The effect of beginning curcumin MP treatment at various stages of tumorigenesis was examined. In Balb-neuT mice initially injected with curcumin MP at 2 or 4 weeks of age and once a month thereafter, tumorigenesis was significantly delayed compared to that in mice which received blank MP (Figure 6A, 7A). Average time to first tumor was significantly increased in mice initially receiving curcumin MP at 2 weeks (15.5 vs 14.2 weeks, $p<0.05$) or 4 weeks (16.5 vs 14.4 weeks, $p<0.05$) compared to empty microparticles (Figure 6B, 7B). Time to reach 100% tumorigenesis also

increased with curcumin MP treatment compared to blank microparticles in mice beginning treatment at 2 weeks (21.3 vs 18.5 weeks, $p<0.05$) or 4 weeks (21.1 vs 19.1, $p<0.05$). Rate of tumor growth in mice receiving curcumin MP initially at 2 weeks was significantly decreased compared to blank MP treatment (30.6 vs 77.6 mm^3/week, $p<0.05$). Curcumin MP administration also significantly decreased abnormal mammary tissue area (Figures 8-11).

Saline-treated controls developed tumors later than those receiving blank MP or curcumin MP (Figures 6, 7). Abnormal area was also significantly lower in saline-treated mice compared to that in other groups ($p<0.05$). Mice that started receiving MP treatment at 7 or 12 weeks of age (after the onset of *in situ* carcinoma) showed no significant difference in tumorigenesis (data not shown).

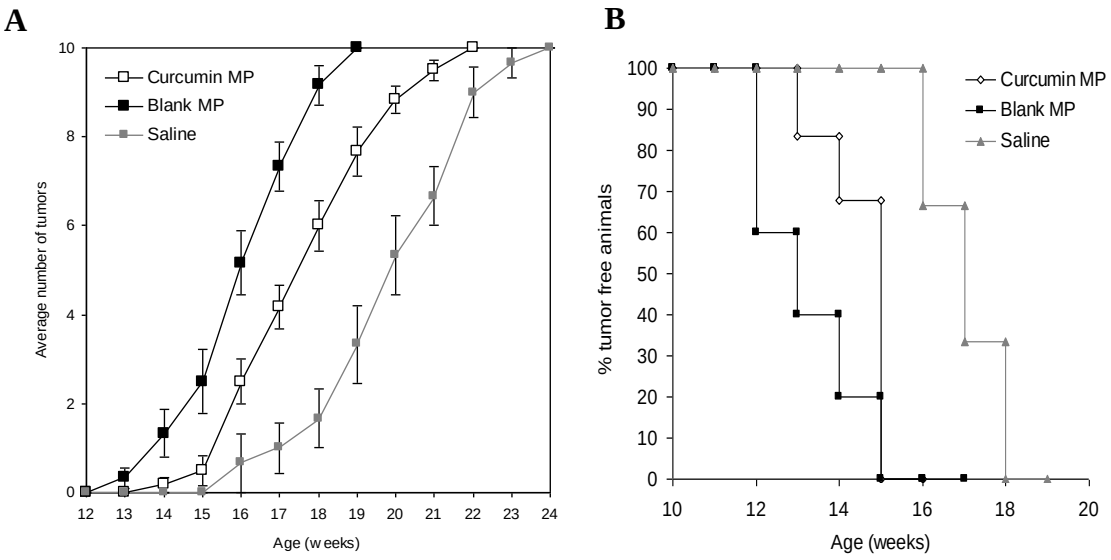

Figure 6 – PLGA microparticles speed up tumor appearance when initially injected at 2 weeks but this effect is partially offset by curcumin. A – Female Balb-neuT mice (n=6) initially began receiving curcumin, empty microparticle injections or saline once a month at 2 weeks of age. Data are presented as average number of palpable tumors present ± S.E. B – Time to first tumor was significantly delayed with curcumin microparticle treatment.

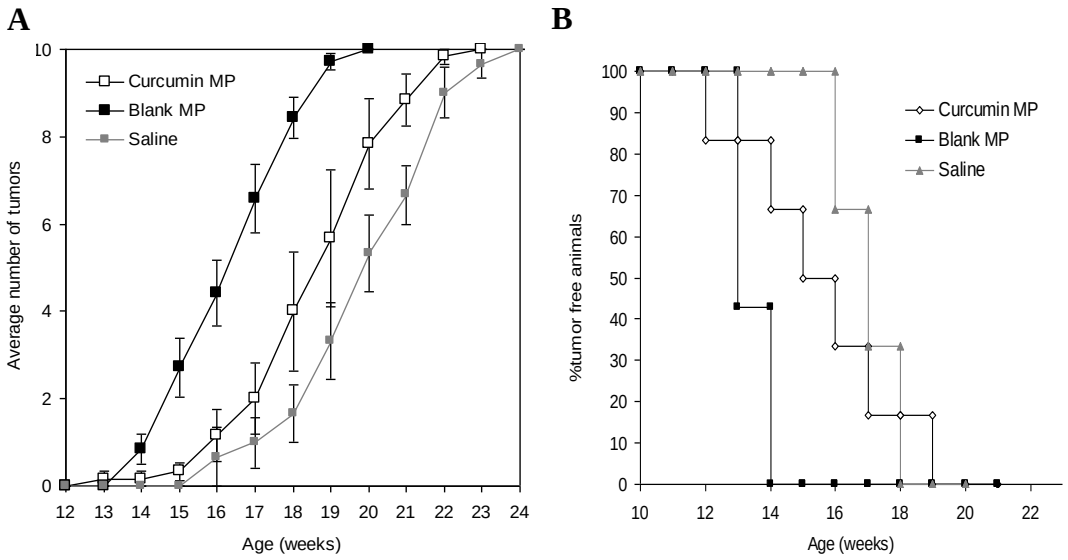

Figure 7 – PLGA microparticles speed up tumor appearance when initially injected at 4 weeks of age but this effect is partially offset by curcumin. A – Female Balb-neuT mice (n=6) initially began receiving curcumin, empty microparticle injections or saline once a month at 4 weeks of age. Data are presented as average number of palpable tumors present ± S.E. B – Time to first tumor was significantly delayed with curcumin microparticle treatment.

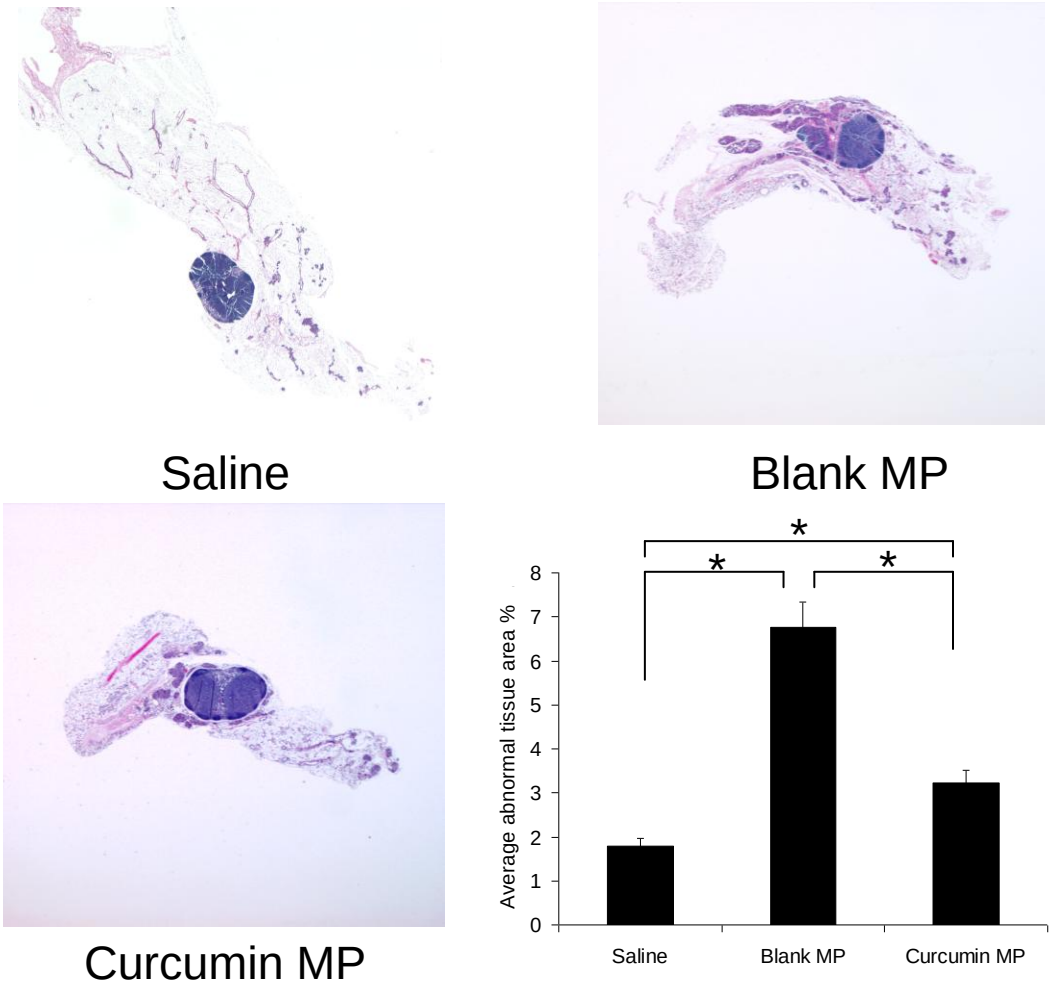

Figure 8 – Curcumin microparticle treatment reduces abnormal tissue area in Balb-neuT mice initially treated at 2 weeks of age. 10X magnification of H&E stained mammary tissues taken from 8 week old female Balb-neuT mice (n=4) after 6 weeks of curcumin microparticle (MP), blank PLGA MP or saline administration. Abnormal tissue was quantified using ImageJ software. Data are presented as average abnormal tissue area ± S.D. *$p<0.05$ compared to indicated group by ANOVA followed by post-hoc Newman Keuls testing.

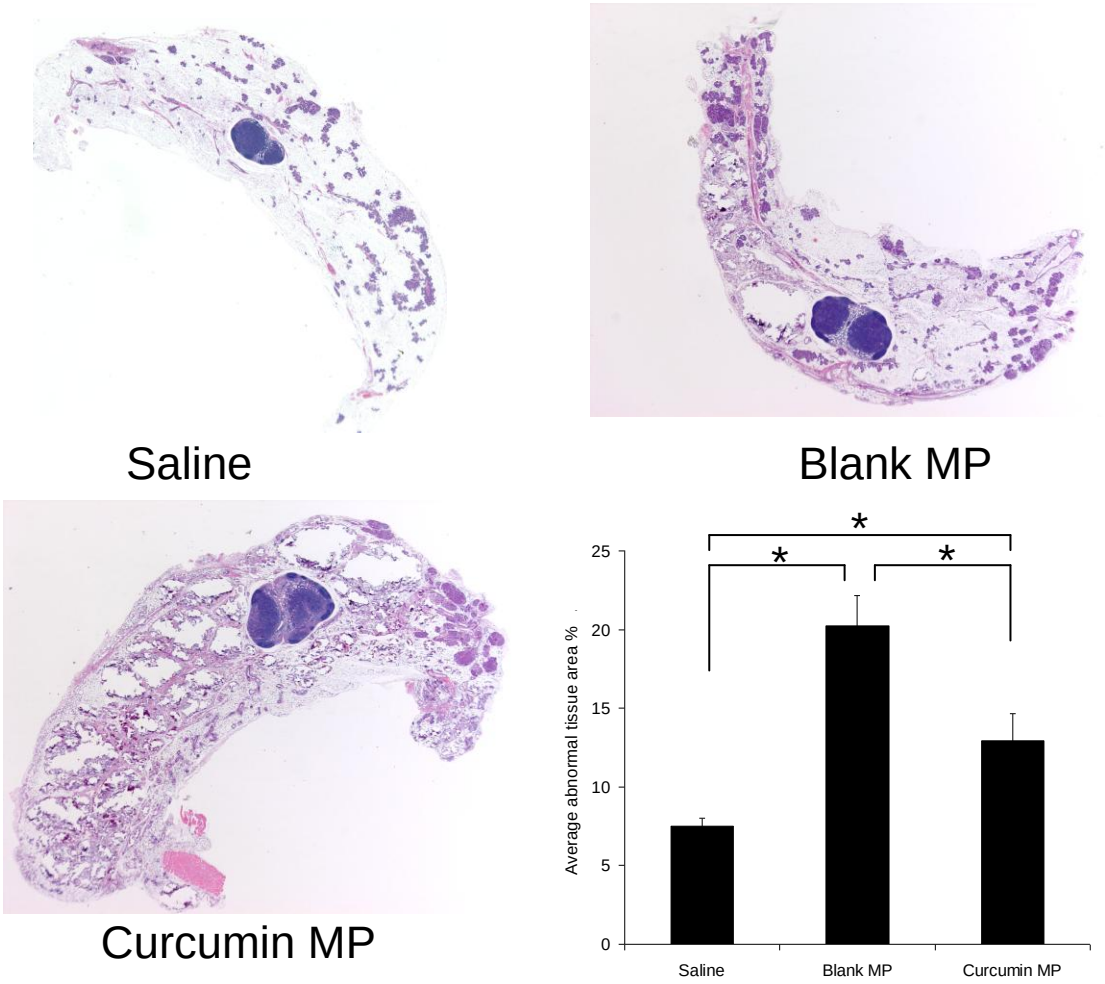

Figure 9 – Curcumin microparticle treatment reduces abnormal tissue area in Balb-neuT mice initially treated at 2 weeks of age. 10X magnification of H&E stained mammary tissues taken from 12 week old female Balb-neuT mice (n=4) after 10 weeks of curcumin microparticle (MP), blank PLGA MP or saline administration. Abnormal tissue was quantified using ImageJ software. Data are presented as average abnormal tissue area ± S.D. *$p<0.05$ compared to indicated group by ANOVA followed by post-hoc Newman Keuls testing.

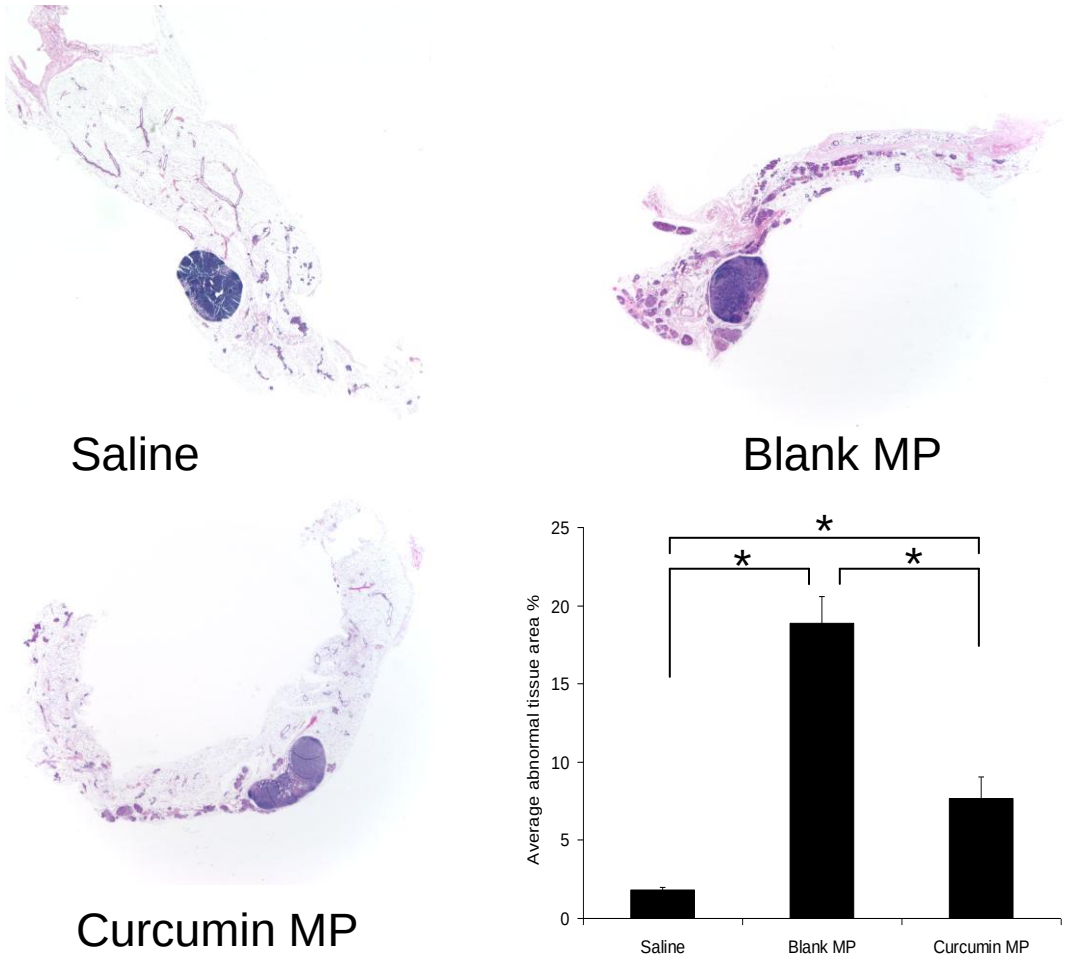

Figure 10 – Curcumin microparticle treatment reduces abnormal tissue area in Balb-neuT mice initially treated at 4 weeks of age. 10X magnification of H&E stained mammary tissues taken from 8 week old female Balb-neuT mice (n=4) after 4 weeks of curcumin microparticle (MP) blank PLGA MP or saline administration. Abnormal tissue was quantified using ImageJ software. Data are presented as average abnormal tissue area ± S.D. *$p<0.05$ compared to indicated group by ANOVA followed by post-hoc Newman Keuls testing.

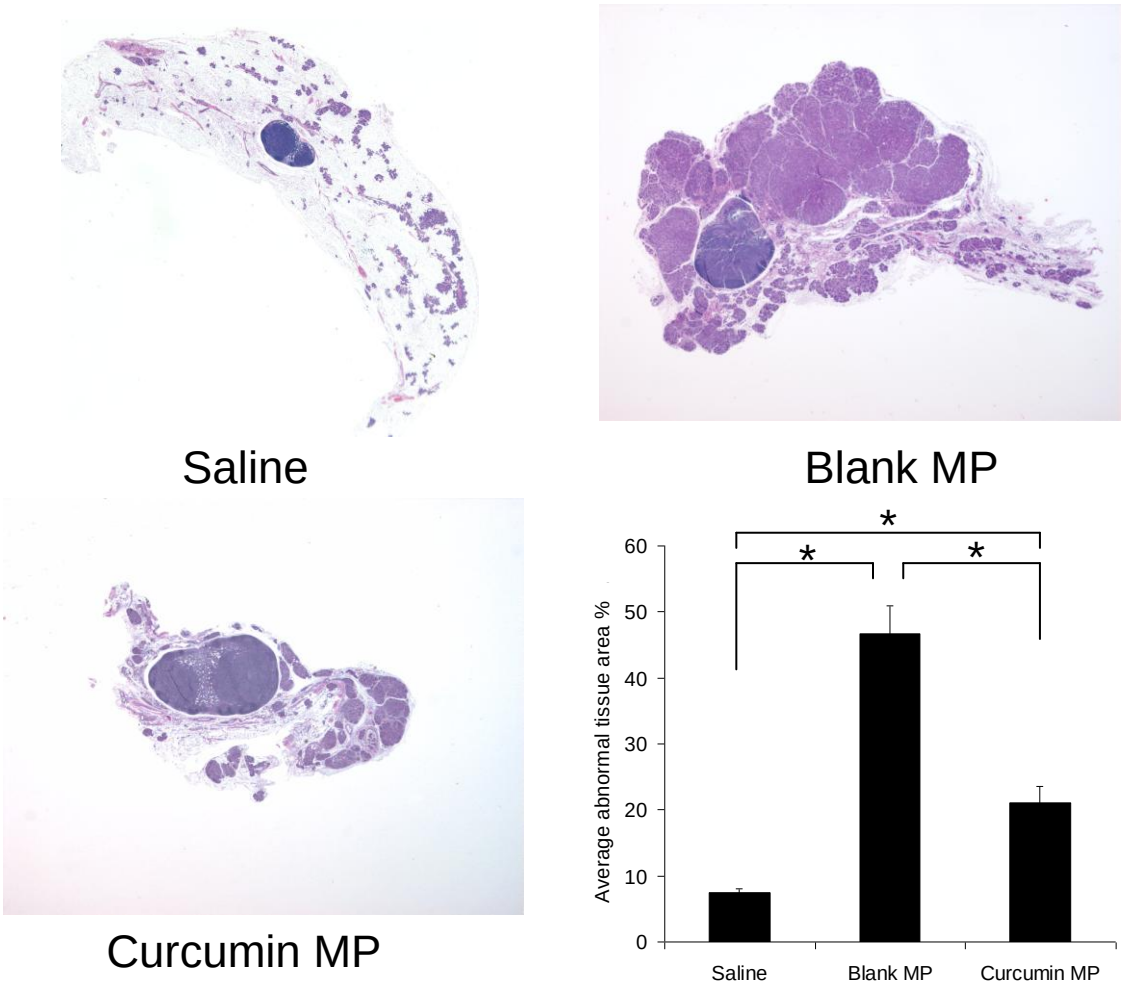

Figure 11 – Curcumin microparticle treatment reduces abnormal tissue area in Balb-neuT mice initially treated at 4 weeks of age. 10X magnification of H&E stained mammary tissues taken from 12 week old female Balb-neuT mice (n=4) after 8 weeks of curcumin microparticle (MP) blank PLGA MP or saline administration. Abnormal tissue was quantified using ImageJ software. Data are presented as average abnormal tissue area ± S.D. *$p<0.05$ compared to indicated group by ANOVA followed by post-hoc Newman Keuls testing.

2.3.3 Curcumin loaded microparticles decrease HER-2 and VEGF protein levels

Starting curcumin MP treatment at 2 or 4 weeks of age resulted in decreased HER-2 protein levels by 12 weeks of age (Figure 12) but not by 8 weeks of age (data not shown). One caveat to this data is that b-actin was used as the loading control when an epithelial cell protein control such as K8 or K18 would have been more suitable. Ki-67 staining (marker for cell division) was not decreased in any treatment group receiving curcumin MP compared to blank MP controls. However, Ki-67 was substantially increased in mice receiving blank MP compared to saline controls (Figures 13-16).

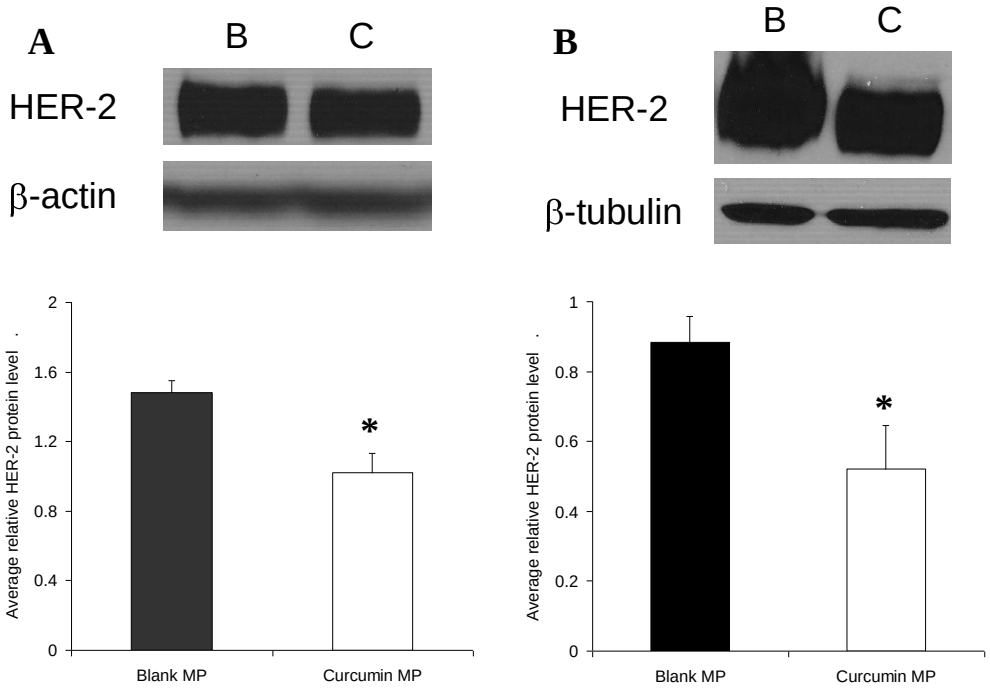

Figure 12 - Curcumin loaded microparticles decrease mammary HER-2 protein levels. Female BALB-neuT mice (n = 2-4) began receiving curcumin loaded (C, Curcumin MP) or blank microparticles (B, Blank MP) at 2 (A) or 4 (B) weeks, then once a month thereafter. Mice were sacrificed at 12 weeks and mammary tissue was harvested. Proteins were separated by SDS-PAGE then transferred to a nitrocellulose blot. β-actin and β-tubulin served as loading control. Data are presented as average relative protein level ± S.D. *$p<0.05$ compared to blank microparticle control.

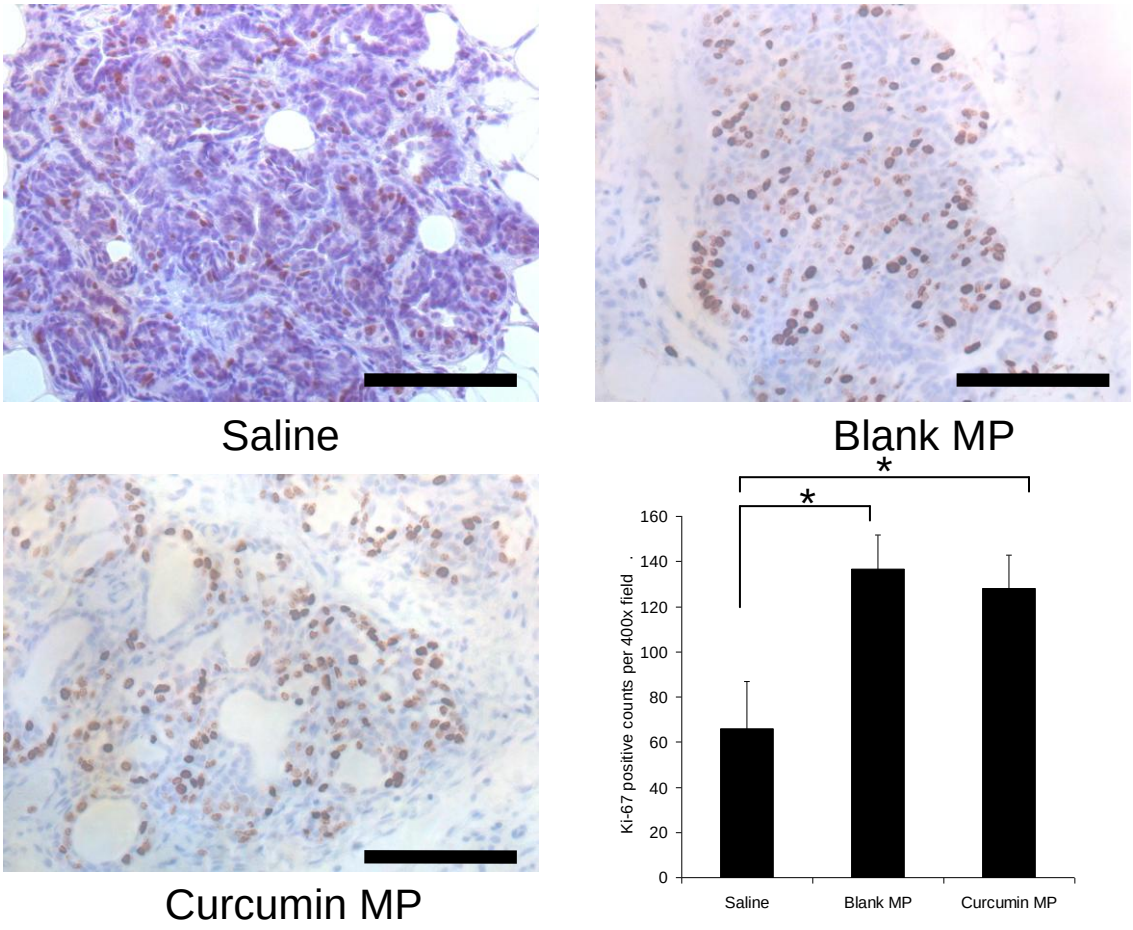

Figure 13 – PLGA microparticles increase cell proliferation when injected at two weeks of age. Female BALB-neuT mice were initially treated with saline, curcumin microparticles or blank microparticles beginning at 2 weeks of age. Mice were sacrificed at 8 weeks of age and mammary tissue was harvested and stained with anti-Ki-67 antibody. Positive Ki-67 staining was manually counted using 15-20 individual 400X magnification pictures. Black bars represent 100 μm. Data are presented as average number of Ki-67 positive counts per a 400X field ± S.D. *$p<0.05$ by ANOVA followed by post-hoc Newman Keuls testing.

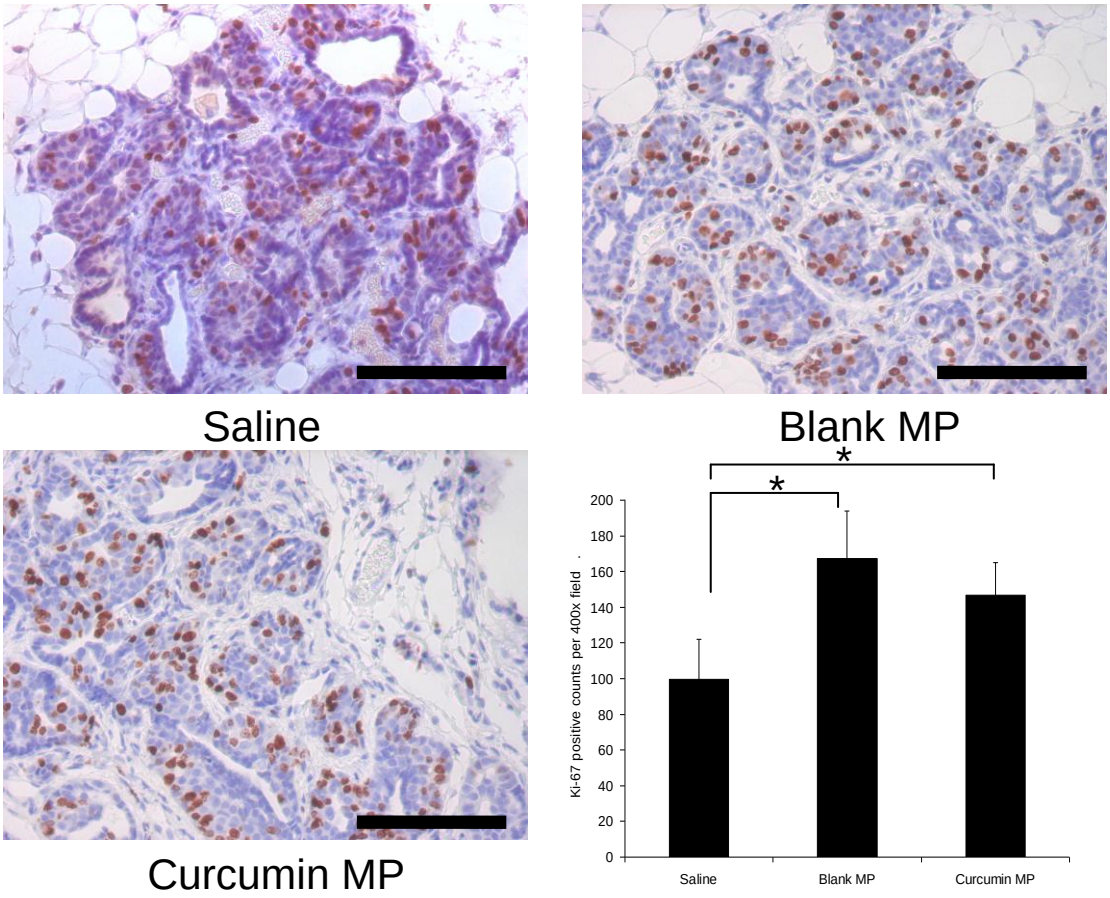

Figure 14 – PLGA microparticles increase cell proliferation at 12 weeks of age. Female BALB-neuT mice were initially treated with saline, curcumin microparticles or blank microparticles beginning at 2 weeks of age. Mice were sacrificed at 12 weeks of age and mammary tissue was harvested stained with anti-Ki-67 antibody. Positive Ki-67 staining was manually counted using 15-20 individual 400X magnification pictures. Black bars represent 100 μm. Data are presented as average number of Ki-67 positive counts per a 400X field ± S.D. *$p<0.05$ by ANOVA followed by post-hoc Newman Keuls testing.

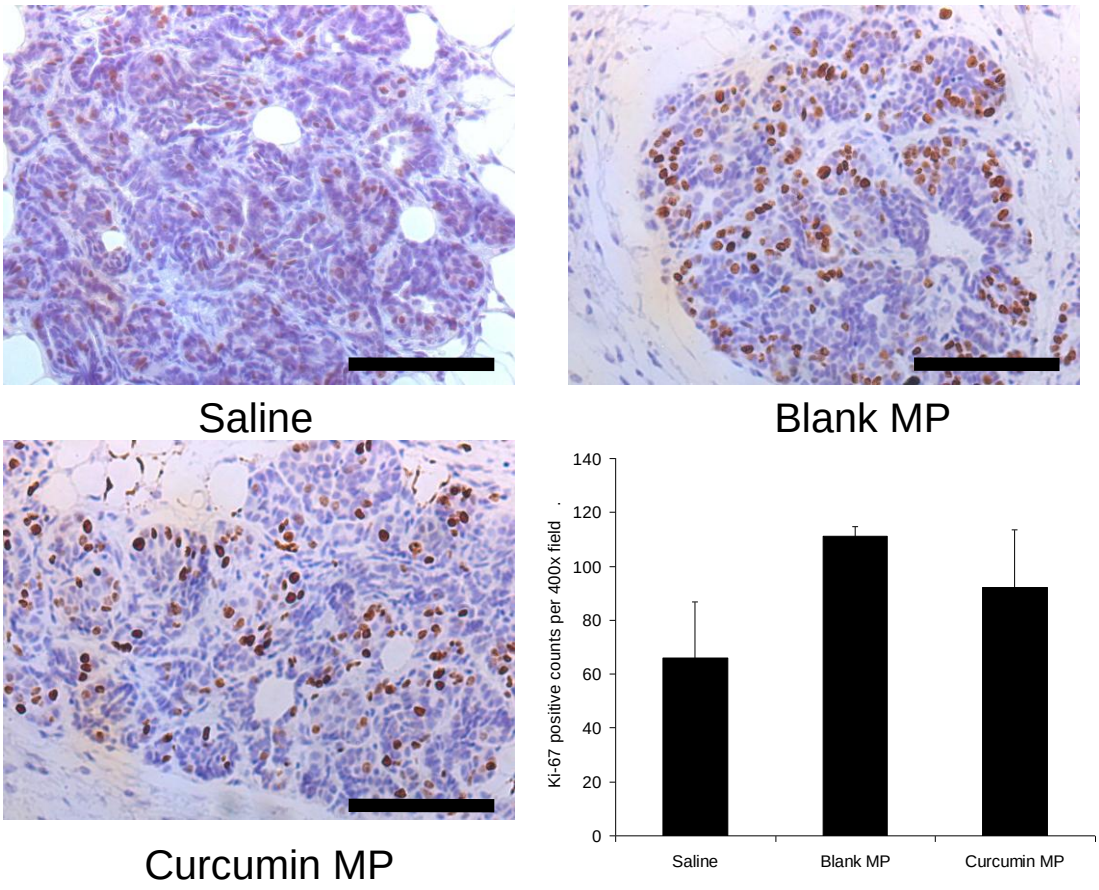

Figure 15 – PLGA microparticles do not increase cell proliferation when treatment was started at 4 weeks of age. Female BALB-neuT mice were initially treated with saline, curcumin microparticles or blank microparticles beginning at 4 weeks of age. Mice were sacrificed at 8 weeks of age and mammary tissue was stained with anti-Ki-67 antibody. Positive Ki-67 staining was manually counted using 15-20 individual 400X magnification pictures. Black bars represent 100 μm. Data are presented as average number of Ki-67 positive counts per a 400X field ± S.D. *$p<0.05$ by ANOVA followed by post-hoc Newman Keuls testing.

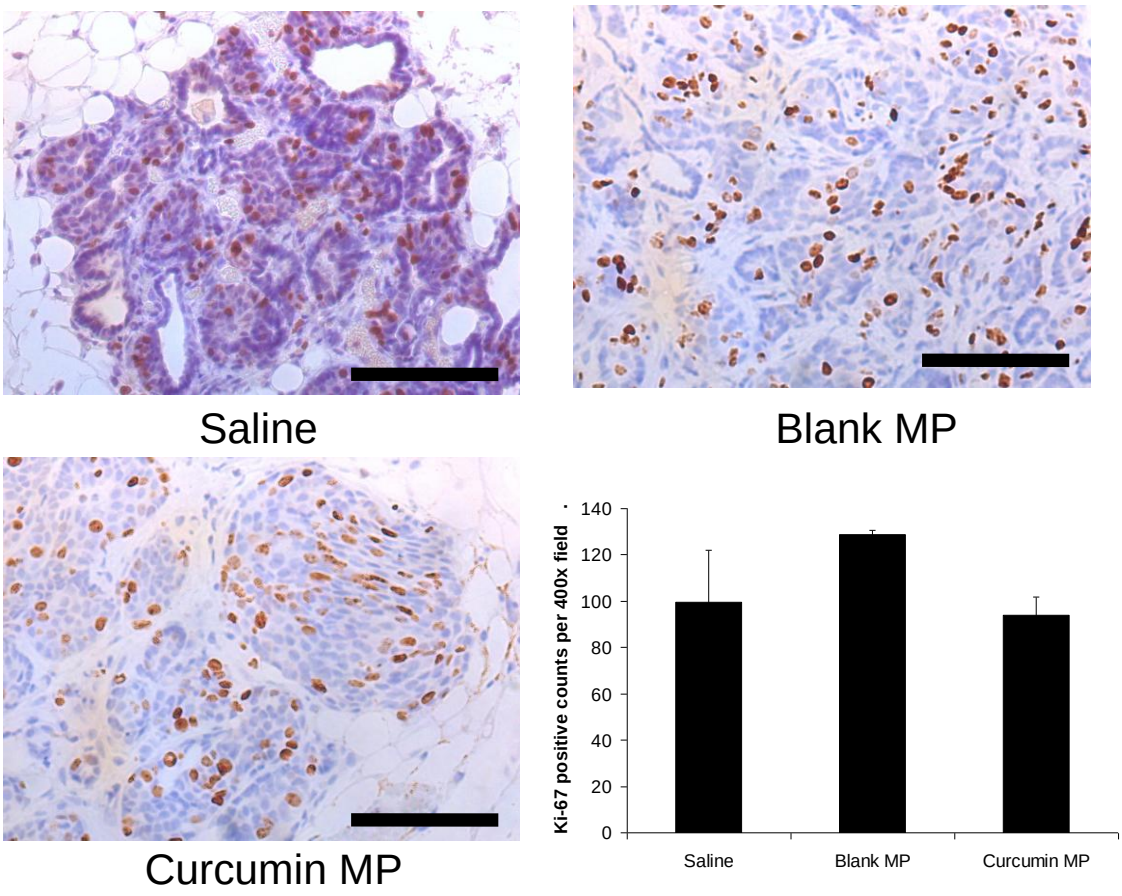

Figure 16 – PLGA microparticles do not increase cell proliferation when treatment was started at 4 weeks of age. Female BALB-neuT mice were initially treated with saline, curcumin microparticles or blank microparticles beginning at 4 weeks of age. Mice were sacrificed at 12 weeks of age and mammary tissue was harvested stained with anti-Ki-67 antibody. Positive Ki-67 staining was manually counted using 15-20 individual 400X magnification pictures. Black bars represent 100 μm. Data are presented as average number of Ki-67 positive counts per a 400X field ± S.D. *$p<0.05$ by ANOVA followed by post-hoc Newman Keuls testing.

VEGF levels were significantly decreased in curcumin MP treatment groups at 12 weeks of age (Figure 17). Again, K-8 or K-18 would have served as a better control protein, and so this data is possibly skewed. Immunohistochemistry revealed a significant decrease in CD-31 staining (a marker for angiogenic microvasculature) in mice initially treated with curcumin MP at 2 weeks of age compared to blank MP (Figures 18-21). Mice receiving curcumin MP at 4 weeks of age showed no significant difference in CD-31 staining compared to blank MP.

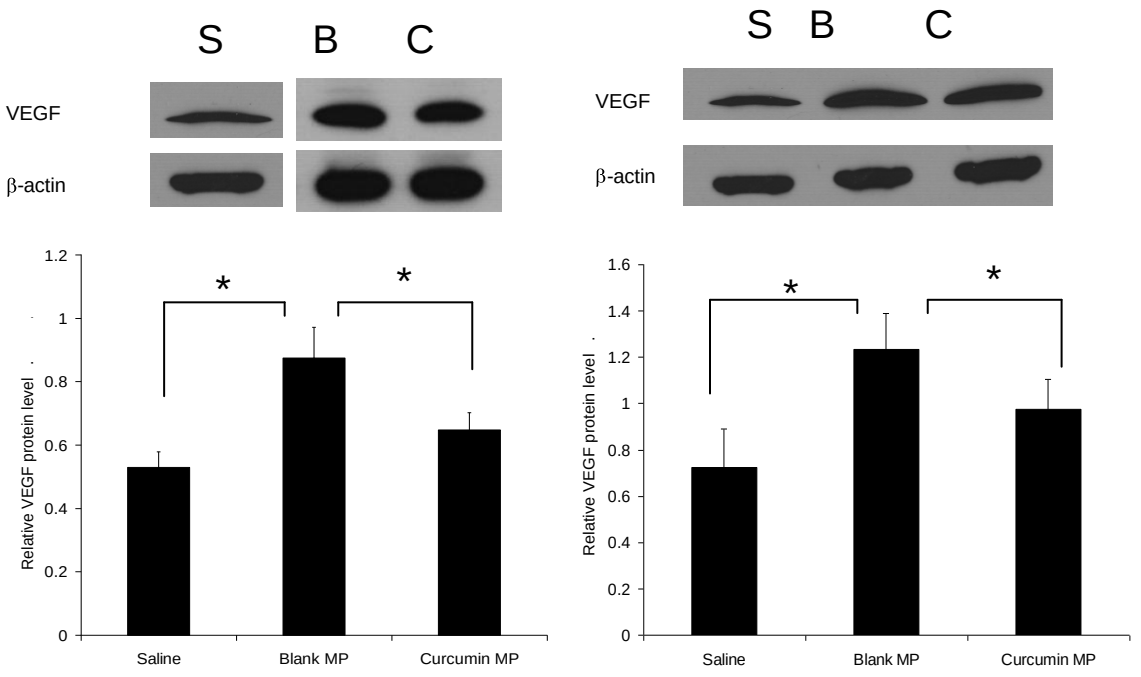

Figure 17 – Empty PLGA microparticles increase VEGF levels compared to saline controls. Female Balb-neuT mice began receiving curcumin microparticle (C) blank MP (B), or saline injections (S) at 2 (left) or 4 (right) weeks of age and were sacrificed at 12 weeks of age. Protein extracts were separated by SDS-PAGE and probed for VEGF protein. Data are presented as average protein level relative to β-actin ± S.D. *$p<0.05$

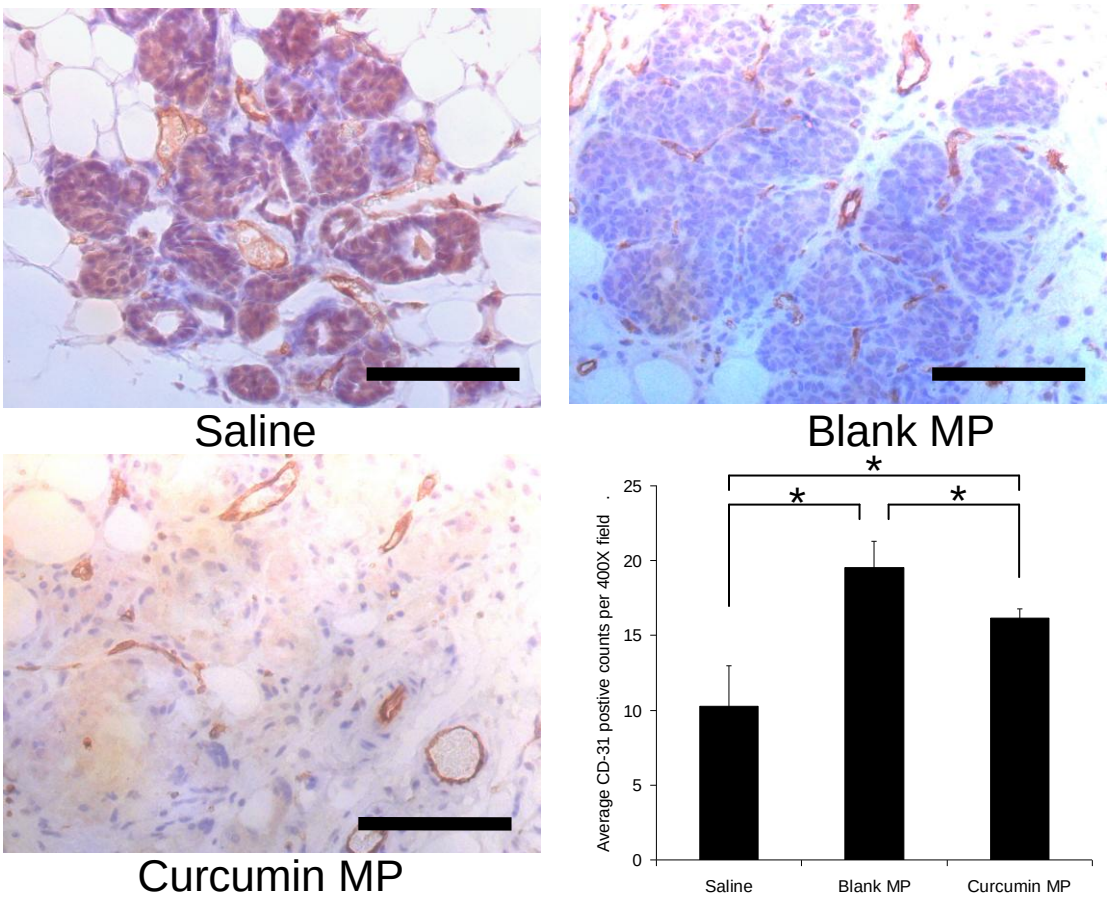

Figure 18 – PLGA microparticles increase microvasculature in mammary tissues of BALB-neuT mice compared to saline controls. Female BALB-neuT mice were initially treated with saline, curcumin microparticles or blank microparticles beginning at 2 weeks of age. Mice were sacrificed at 8 weeks of age and mammary tissue was stained with anti-CD-31 antibody. CD-31 staining was manually counted using 15-20 individual 400X magnification pictures. Black bars represent 100 μm. Data are presented as average number of CD-31 positive counts per a 400X field ± S.D. *$p<0.05$ by ANOVA followed by post-hoc Newman Keuls testing.

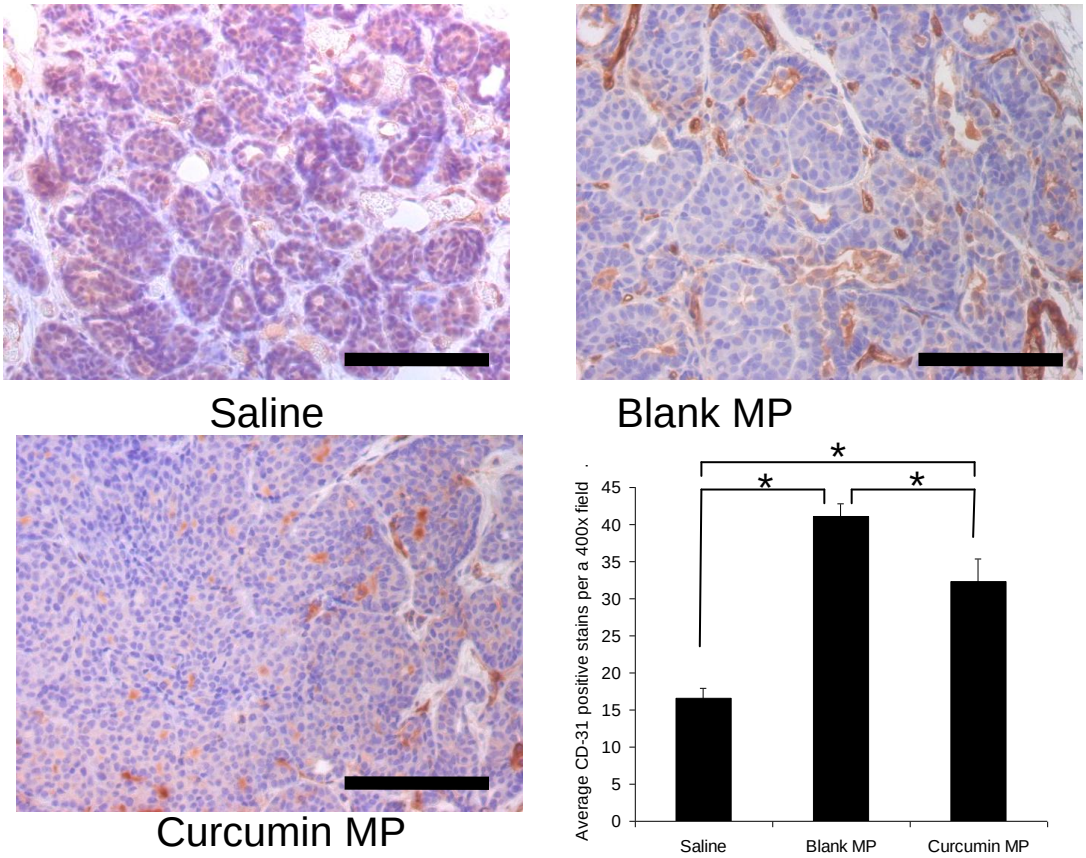

Figure 19 – PLGA microparticles increase microvasculature in mammary tissues of BALB-neuT mice compared to saline controls. Female BALB-neuT mice were initially treated with saline, curcumin microparticles or blank microparticles beginning at 2 weeks of age. Mice were sacrificed at 12 weeks of age and mammary tissue was stained with anti-CD-31 antibody. CD-31 staining was manually counted using 15-20 individual 400X magnification pictures. Black bars represent 100 μm. Data are presented as average number of CD-31 positive counts per a 400X field ± S.D. *$p<0.05$ by ANOVA followed by post-hoc Newman Keuls testing.

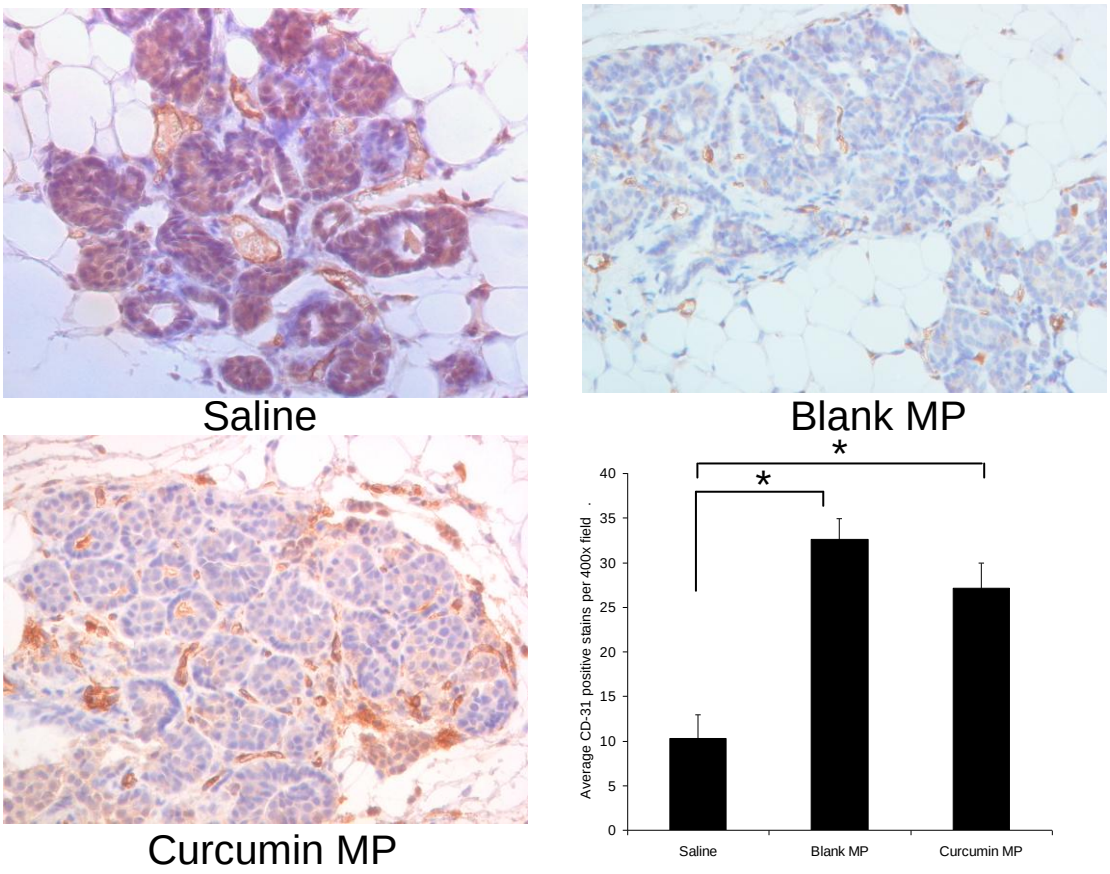

Figure 20 – PLGA microparticles increase microvasculature in mammary tissues of BALB-neuT mice compared to saline controls. Female BALB-neuT mice were initially treated with saline, curcumin microparticles or blank microparticles beginning at 4 weeks of age. Mice were sacrificed at 8 weeks of age and mammary tissue was stained with anti-CD-31 antibody. CD-31 staining was manually counted using 15-20 individual 400X magnification pictures. Black bars represent 100 μm. Data are presented as average number of CD-31 positive counts per a 400X field ± S.D. *$p<0.05$ by ANOVA followed by post-hoc Newman Keuls testing.

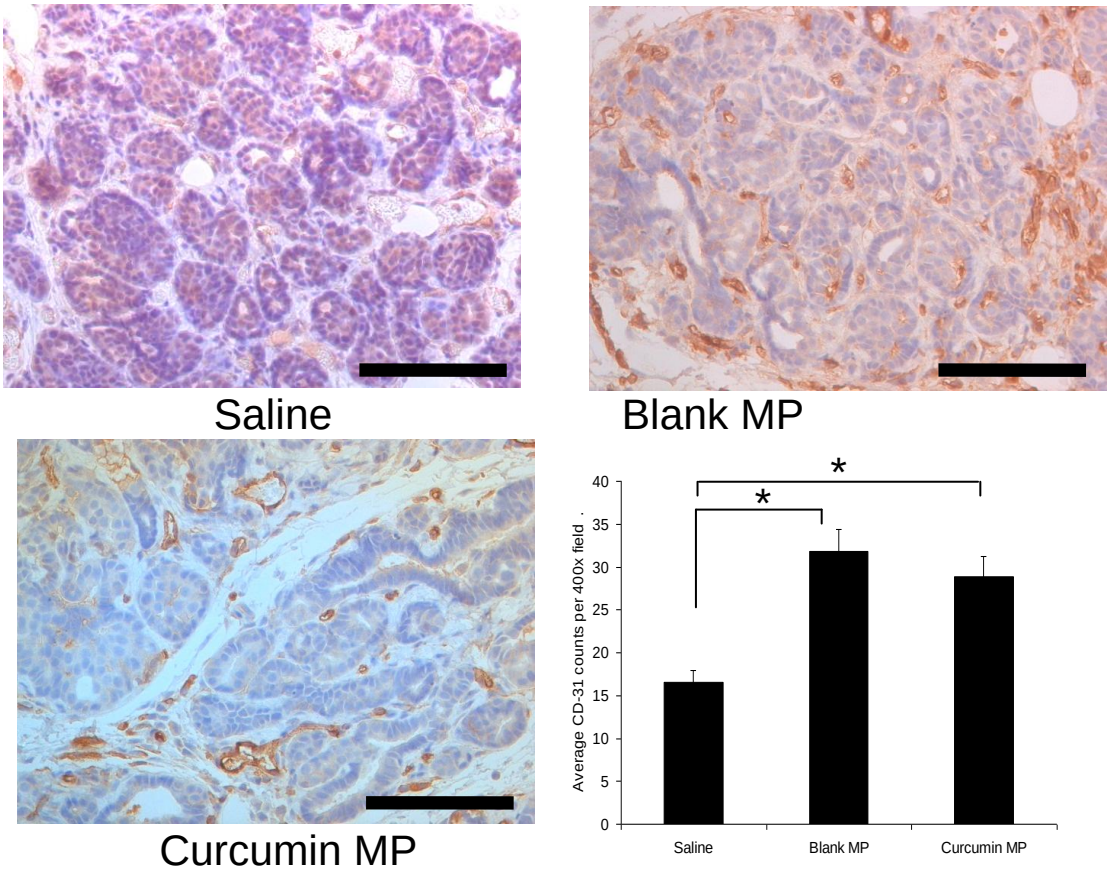

Figure 21 – PLGA microparticles increase microvasculature in mammary tissues of BALB-neuT mice compared to saline controls. Female BALB-neuT mice were initially treated with saline, curcumin microparticles or blank microparticles beginning at 4 weeks of age. Mice were sacrificed at 12 weeks of age and mammary tissue was stained with anti-CD-31 antibody. CD-31 staining was manually counted using 15-20 individual 400X magnification pictures. Black bars represent 100 μm. Data are presented as average number of CD-31 positive counts per a 400X field ± S.D. *$p<0.05$ by ANOVA followed by post-hoc testing.

Saline controls showed significantly lower VEGF levels compared to both curcumin and blank MP treatment groups. Additionally, saline treated animals showed significantly lower CD-31 staining at both 8 and 12 weeks of age. Total p65 NF-κB mammary tissue levels were not significantly changed with curcumin MP treatment compared to blank MP (data not shown).

2.3.4 Lactic acid levels are increased in mice receiving PLGA microparticles

The excess lactic acid produced by PLGA MP may have contributed to the increase in VEGF and angiogenesis observed. Thus, the contribution of blank MP to circulating lactic acid was examined one month after injection. Treatment with blank MP resulted in significantly increased levels of lactic acid in plasma compared to that following saline treatment (Figure 22).

2.3.5 NF-κB is activated in mice receiving PLGA microparticles

NF-κB is the main regulator of acute and systemic inflammatory responses in the body. Activiation of NF-κB would be a biomarker for systemic inflammation after PLGA MP injection. NF-κB-RE-luc mice express luciferase when NF-κB is activated. To determine if NF-κB was activated, mice were treated with blank MP. Introduction of blank MP significantly increased bioluminescence 2.4-fold ($p<0.05$) compared to saline controls after 24 hours, with NF-κB continuously activated for at least 72 hours (Figure 23). Casein showed a modest effect (~1.5 fold) on NF-κB activation and for a shorter

duration than PLGA microparticles (data not shown). In BALB/c mice, plasma IL-1β and IL-6 levels were significantly increased compared to saline controls 24 hours after PLGA MP injection (Figure 24). TNF-α levels were undetectable in plasma for both groups. No significant difference in IL-1α, IL-6, TNF-α or GM-CSF was observed in plasma or mammary tissue one month after dosing (data not shown).

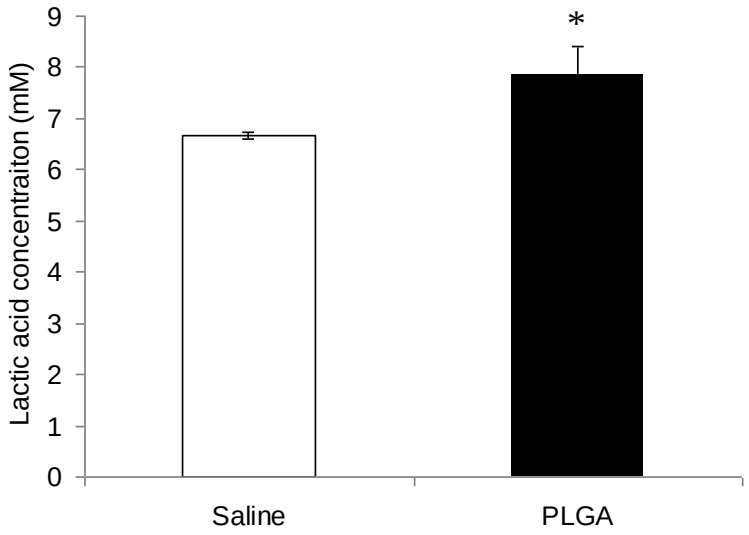

Figure 22 – PLGA MP increase lactic acid levels in plasma. Female BALB-neuT mice were administered PLGA microparticles at 2 weeks of age. After one month, mice were sacrificed and blood was collected. Plasma lactic acid levels were determined using a lactate assay kit. Data are presented as average lactic acid concentration ± S.D. *$p<0.05$, compared to saline injected control.

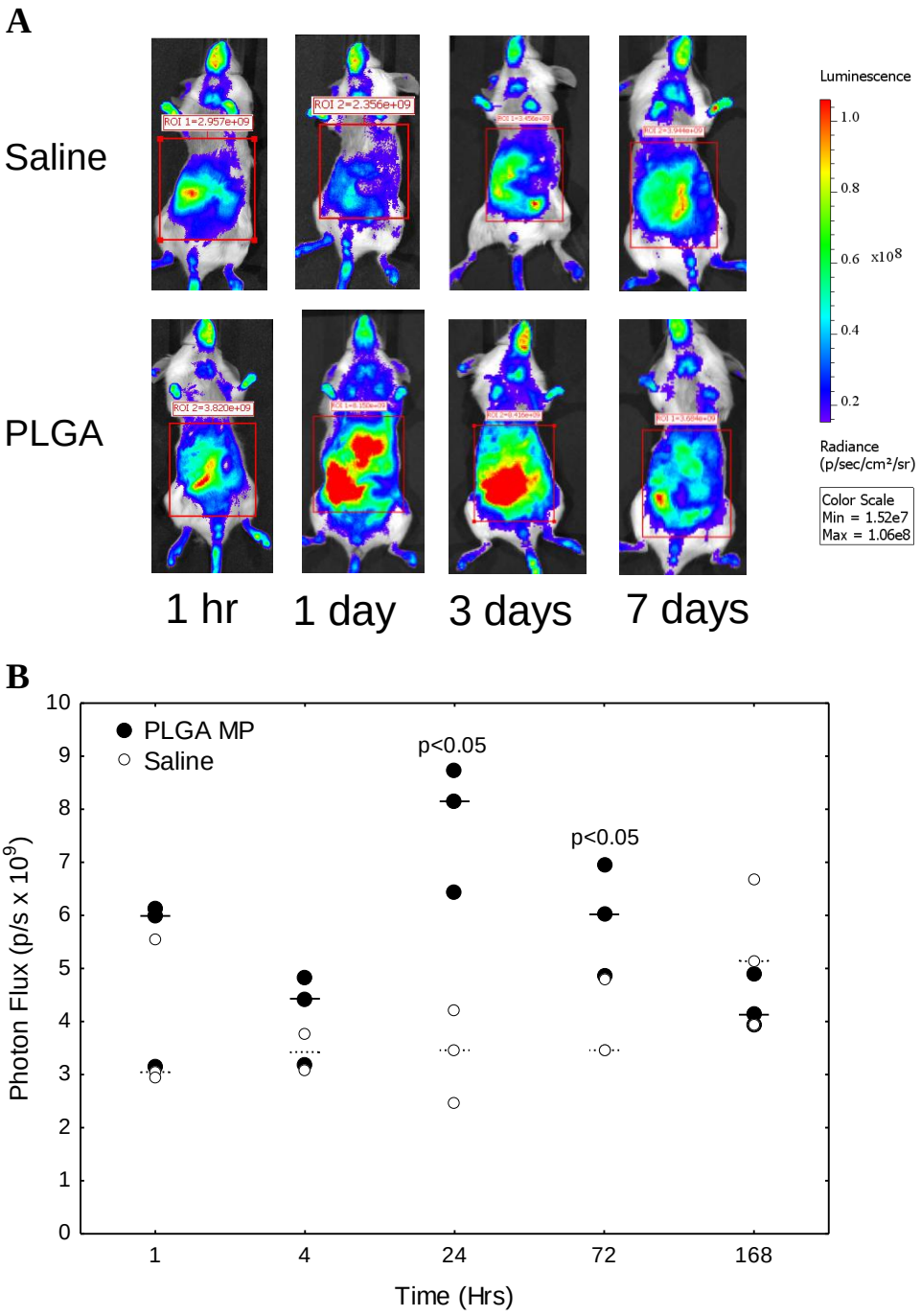

Figure 23– PLGA induces NF-κB activation in vivo. Female NF-κB-RE luc mice (n=3) were injected with saline or 90 mg PLGA microparticles and imaged at various time points after injection. A – Mice were administered luciferin (150 mg/kg) 15 minutes prior to imaging. B – Bioluminescence was calculated using LivingImage software and values were compared. Data are presented as individual photon flux measurements (photons/sec). $p<0.05$ as measured by Student's t-test.

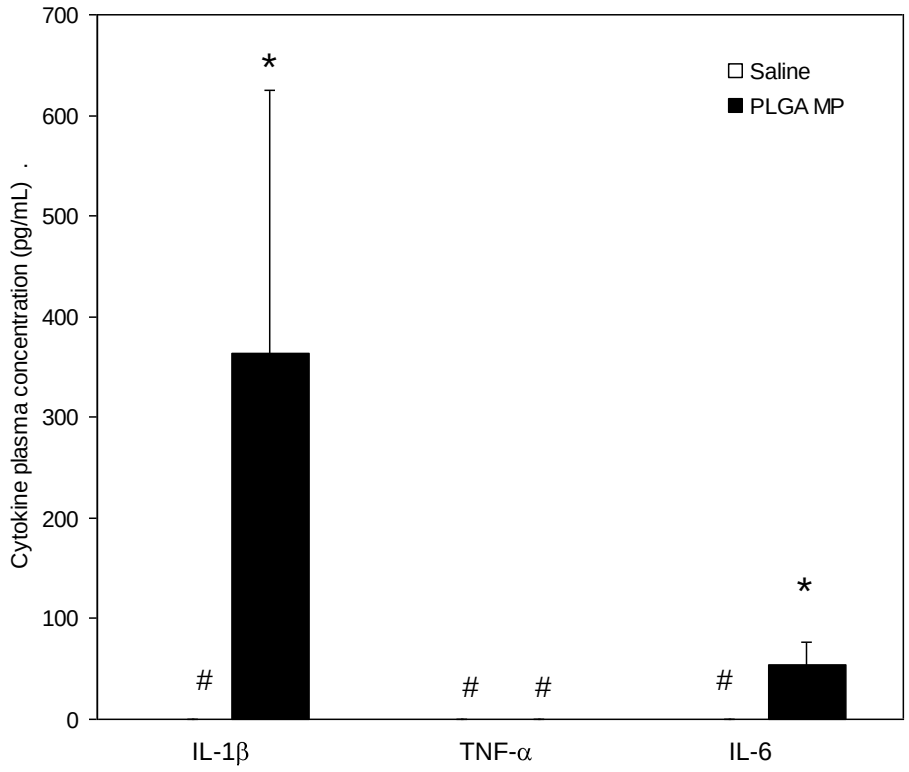

Figure 24 – PLGA microparticles increase plasma inflammatory cytokine levels. Female balb/c mice were administered saline or 90 mg PLGA microparticles (MP) and sacrificed after 24 hours. Cytokine levels were determined by ELISA. *$p<0.05$ as determined by a Student's t-test. # - values were below the detection limit of the ELISA kit.

2.4 Discussion

Curcumin has been shown to affect several cellular pathways important in breast cancer (2, 155). The wide array of curcumin effects is due in large part to the inhibition of IκB kinase (16, 23), resulting in reduced activation of NF-κB. This leads to a decrease in downstream activation of pathways important for inflammation and angiogenesis. In HER-2 positive tumor cells, curcumin has been shown to deplete HER-2 protein levels in a time- and concentration-dependent manner (45, 46). The concentration needed to deplete HER-2 by 50% was decreased from 40 μM to 10 μM by increasing the

incubation time by just twelve hours. We hypothesized that low, sustained levels of curcumin would be effective in inhibiting HER-2 positive breast cancer in vivo.

The therapeutic usefulness of curcumin is limited by its poor solubility and bioavailability, which is due to poor absorption and extensive gut and hepatic metabolism (60, 66, 156). To bypass these problems, curcumin loaded PLGA MP were formulated capable of sustaining blood and mammary tissue levels for at least 45 days after a single injection. The significantly higher curcumin levels in the blood and mammary tissue one day after administration are due to the burst release typically seen in implants. Drug absorbed on the surface has no diffusional polymer barrier is released quickly. Previous in vitro release studies using this curcumin PLGA MP formulation showed 10% drug release within twenty four hours. Forty five days after administration, a similar event occurs due to the extensive degradation of the PLGA polymer. Average polymer molecular weight is decreased resulting in increased curcumin diffusion and therefore significantly higher tissue levels.

The transgenic mouse model Balb-neuT was used in order to examine the efficacy of curcumin treatment. The Balb-neuT model overexpresses neu protein via the MMTV-LTR promoter. The overexpressed protein is an activated form (neuT), which allows for signal transduction even in the absence of signaling molecules (133). The model is aggressive, with hyperplasia appearing as early as 3 weeks after birth, coinciding with initial mammary development. Microvasculature is increased from 4-6 weeks, with *in situ* carcinoma appearing around 7 weeks. By 17 weeks, at least one palpable tumor is present in the mouse. This mouse model thus allows for evaluating the effect of time of curcumin intervention on tumor progression.

Initiating curcumin treatment at 2 or 4 weeks of age, but not at 7 or 12 weeks of age (not shown), delayed the tumor onset compared to blank MP treatment group. When these results were compared to saline controls, the results were very surprising (Figures 6, 7). The time to first tumor and the overall tumorigenesis in saline-treated Balb-neuT mice was slower than in the other treatment groups. This suggested that blank MP accelerated tumorigenesis in this model, and curcumin inhibited this effect. The acute local inflammatory effects of PLGA MP are well established (89, 91) but no previous studies have reported systemic inflammation.

NF-κB is the major pathway for acute and systemic inflammation (24, 157). Activation of the NF-κB pathway in macrophages leads to release of pro-inflammatory cytokines such as IL-1β, IL-6 and TNF-α. Therefore, activation of this pathway would be a likely player in any inflammatory effects induced by blank MP. Bioluminescence in NF-κB-RE-luc mice was increased 2.4 fold in mice treated with blank MP. NF-κB activation was significantly elevated compared to saline controls for at least 72 hours but was near background one week after dosing. Additionally, IL-1β and IL-6 plasma levels were significantly higher in mice 24 hours after blank MP injection. Based on this data, it is likely that introduction of blank MP leads to systemic inflammation via ubiquitous activation of NF-κB. The microparticles used for all the studies were made with endotoxin-free water to prevent any bacterial contamination. Confirmation that microparticles are devoid of endotoxins prior to injection further supports that NF-κB activation was not a byproduct of contamination during microparticle fabrication. No significant difference in inflammatory cytokine (IL-1α, IL-6, TNF-α, GM-CSF) levels

were seen one month after injection with blank MP compared to saline control. It is likely that the systemic inflammation had subsided one month after blank MP injections, as evident by lack of NF-κB activation at 7 days post-dose. Curcumin is a known anti-inflammatory agent and has been shown to block the activation of NF-κB. It is possible that curcumin MP treatment offset the systemic inflammation caused by PLGA microparticles and this led to the observed delay in tumorigenesis.

Alternatively, lactic acid (existing as lactate in physiologic pH) can act as a signaling molecule during tumorigenesis. In developing tumors, pH is reduced due to excessive lactic acid produced from tumor cells. This is a byproduct of the Warburg effect, observed when tumor cells switch from oxidative phosphorylation to glycolysis as their main ATP pathway (158, 159). Lactic acid is exported by tumor cells via monocarboxylate transporter-4 (MCT-4) into the extracellular matrix. Excess lactate in the extracellular matrix has two fates. Lactate can be taken up by other tumor cells via the MCT-1 transporter and used to produce energy. This allows for faster tumor growth, as well as decreased glucose reliance. The glucose not taken up by these cells is free to diffuse farther into the tumor and provide energy for otherwise hypoxic cells. Addtionally, lactate can activate NF-κB in endothelial cells and lead to IL-8 production (160). Excess lactate has been shown to increase HIF-1α concentration, stimulating angiogenesis (161).

Our studies show that the systemic lactic acid concentration was elevated in animals that received blank microparticles. Excess lactate could lead to increased tumor growth and thus producing a faster time to palpable tumors. Increased systemic lactate

could also be taken up by endothelial cells already stimulated by the increased inflammation seen in this model, leading to enhanced angiogenesis. Tumorigenesis in this mouse model is initially driven by inflammation with neo-angiogenesis ending by 6 weeks of age. No difference in outcome was seen when MP were introduced after the angiogenic switch (mice injected at 7 or 12 weeks) and tumor growth was being driven solely by HER-2 overexpression. Western blotting confirmed that blank MP treatment increased VEGF levels. Similarly, immunohistochemistry studies showed that CD-31 positive blood vessels were increased in mice receiving PLGA MP, although the effect was more pronounced in mice beginning treatment at 2 weeks. Induction of VEGF and angiogenesis by lactate is well established, and these results further support the hypothesis that excess lactate produced by PLGA could contribute to enhanced angiogenesis and tumorigenesis in this model.

Curcumin showed bioactivity in the Balb-neuT mice, although it could not completely overcome the tumorigenic effects of blank MP. In mice initially receiving curcumin MP at 2 or 4 weeks, abnormal tissue area was significantly decreased compared to those receiving blank MP. At twelve weeks of age, curcumin MP treated mice had decreased HER-2 protein levels. This supported the hypothesis that low, steady curcumin levels could result in significant changes in cellular pathways. Previous studies using curcumin and other dietary polyphenols at sustained low doses showed similar effects (162). HER-2 is the main driver of tumorigenesis in this model, and its depletion is linked to decreased growth. However, the excess lactic acid may have offset the antiproliferative effects of curcumin, which would explain why Ki-67 staining was not significantly changed by curcumin MP treatment.

While PLGA MP are considered to be safe and are currently used in the clinic, our studies show that the systemic inflammation caused by PLGA MP can lead to accelerated tumorigenesis especially in this tumor model. In order to pursue a curcumin-based chemopreventive approach to breast cancer, future work may have to focus on reformulating the microparticles with a different polymer. However, these studies showed that curcumin has activity against HER-2+ tumors and should be further pursued for cancer chemoprevention.

2.5 Conclusions

Curcumin loaded microparticles were effective in delaying tumorigenesis in Balb-neuT mice compared to blank PLGA microparticle controls. Curcumin treatment led to a delay in tumor appearance and decrease in CD-31 staining. However, when compared to saline controls, PLGA microparticles were shown to speed up tumorigenesis. Future studies should examine this effect in depth, as well as evaluate other formulations of curcumin for chemoprevention.

CHAPTER 3

A NOVEL APPROACH FOR IMPROVING CURCUMIN BIOAVAILABILITY UTILIZING A SMEDDS FORMULATION AND METABOLIC INHIBITION

In spite of its well documented anticancer chemopreventive and therapeutic activity, the clinical development of curcumin has been limited by its poor oral bioavailability. Curcumin has low aqueous solubility and undergoes extensive first pass metabolism following oral dosing. We hypothesized that oral bioavailability of curcumin can be enhanced by increasing its absorption and decreasing its metabolic clearance simultaneously. To test this hypothesis, we formulated curcumin with naturally occurring UGT inhibitors (piperine, quercetin, tangeretin, and silibinin) in a self-microemulsifying drug delivery system (SMEDDS). Mouse liver microsome studies showed that silibinin and quercetin inhibited curcumin glucuronidation effectively. When dosed orally in mice, the SMEDDS formulation containing curcumin alone increased curcumin glucuronide concentrations in plasma without significantly affecting parent drug concentration. Of the four inhibitors examined in vivo, silibinin significantly improved the C_{max} (0.15 μM vs. 0.03 μM for curcumin SMEDDS) and overall bioavailability (3.5-fold vs. curcumin SMEDDS) of curcumin. Previous studies have shown that silibinin has anticancer activity as well. Thus, co-delivery of silibinin with curcumin in SMEDDS represents a novel and promising approach to improve curcumin bioavailability.

3.1 Introduction

Curcumin, a dietary polyphenol derived from turmeric, is a potent antioxidant and anti-inflammatory and has shown significant anti-cancer effects (3, 4, 9, 163). The clinical potential of curcumin, however, has been limited due to its short half-life (<0.5 hr) and low bioavailability (<2%) (61, 62, 147). This is the result of curcumin suffering from low aqueous solubility and extensive gut and hepatic and intestinal metabolism (60, 68, 69). Curcumin undergoes extensive phase one and phase two hepatic metabolism. Primarily, UDP-glucuronosyltransferase (UGT) and sulfotransferase (SULT) convert curcumin to its glucuronide and sulfate metabolites, respectively. Glucuronidation by UGT1A1, 1A8, and 1A10 accounts for the majority of curcumin metabolism (69, 71). Thus, to improve the oral bioavailability of curcumin, both low solubility and high metabolic clearance must be overcome.

Previous studies have shown that self-microemulsifying drug delivery systems (SMEDDSs) can be used to increase the solubility and oral absorption of hydrophobic compounds (94, 95, 164). SMEDDSs are comprised of one or more surfactants dispersed in an oil phase. When added to an aqueous phase (either prior to dosing or *in situ* in the gut), a thermodynamically-stable nanoemulsion is formed. Previous studies have shown that SMEDDSs can be used to dissolve high concentrations of curcumin (up to 50 mg/ml) (94, 165), making them a promising formulation for the oral delivery of curcumin.

There have been very few previous attempts to decrease curcumin metabolism through adjuvant therapies. One study by Shoba et al showed that administering piperine, an alkaloid found in black pepper, with curcumin improved curcumin bioavailability 2000% compared to curcumin alone (65). However, this study did not

firmly establish the mechanism of improved curcumin bioavailability with piperine. Several other natural compounds, particularly flavonoids, have been shown to inhibit UGT activity (75, 77). Many of these flavonoids also have chemopreventive and chemotherapeutic activity against a variety of cancers (81, 166). Thus, flavonoids offer great potential as an adjuvant therapy to increase curcumin bioavailability and anticancer activity.

The goal of the current study was to evaluate the effect of co-delivering a natural inhibitor of curcumin metabolism using a SMEDDS formulation on the oral bioavailability of curcumin. *In vitro* hepatic microsomal assays were used to identify promising UGT inhibitors. The ability of these inhibitors to improve the oral bioavailability of curcumin was then investigated *in vivo*.

3.2 Materials and methods

3.2.1 Materials

Curcumin (>98% curcuminoid content), piperine, silibinin, quercetin, epigallocatechin gallate (EGCG), uridine 5'-diphospho-glucuronic acid (UDPGA), alamethicin, Carbitol™ and dimethyl sulfoxide (DMSO) were purchased from Sigma (St. Louis, MO). Tangeretin was generously provided by the Florida Department of Citrus. Cremophor® EL was purchased from BASF (Florham Park, NJ). Captex® 355 was purchased from Abitec Corp (Columbus, OH). Acetonitrile was purchased from Fisher Scientific (Pittsburg, PA). CD-1 female pooled mouse liver microsomes were purchased from BD Biosciences (San Jose, CA).

3.2.2 Microsomal studies

Curcumin and a selected inhibitor (piperine, silibinin, quercetin, EGCG, tangeretin or salicylic acid) were first dissolved in DMSO. This solution was then added to Tris buffer (10 mM, pH 7.1) containing 5 mM magnesium chloride, 5 μg alamethicin, and 100 μg/mL of microsomal protein. Final DMSO concentration was 2% for all samples. Final volume of this reaction mix was 0.2 mL. The concentration of curcumin in the assay buffer was 1 μM, and was chosen based on reported K_m values for UGT1A1 metabolism (70). Samples were first incubated at 37 °C for two minutes, followed by the addition of UDPGA (3 mM) to start the reaction. The reaction was stopped after 5 minutes by addition of ice cold acetonitrile (3:1). Samples were refrigerated for 15 minutes and then centrifuged for 10 minutes at 14,000 rpm. Curcumin concentration in the supernatant was determined by HPLC.

3.2.3 SMEDDS

The SMEDDS formulation used for all the studies consisted of Cremophor® EL and Carbitol™ (2:1 w/w), mixed with Captex® 355 (10:1 w/w, surfactants to oil). Equilibrium solubility of flavonoids in this formulation was determined by adding excess solid compound to the formulation and incubating at room temperature overnight with stirring. The saturated formulation was centrifuged at 14000 rpm for 10 min. Supernatant was then diluted with methanol and analyzed by HPLC (see below). Particle size distribution was determined using a Beckman-Coulter Delsa Nano C Particle Analyzer (Brea, CA). SMEDDSs were diluted with distilled water (1:200 v/v) prior to analysis.

3.2.4 Pharmacokinetic studies

All animal studies were approved by the Institutional Animal Care and Use Committee of University of Minnesota. Animals were housed in specific pathogen-free environment, with access to food and water *ad libitum*. Female BALB/c or CD-1 mice, 8-12 weeks of age, were dosed by oral gavage with curcumin suspension prepared in 1% carboxymethylcellulose, curcumin solution (DMSO solubilized), curcumin SMEDDS, curcumin with piperine SMEDDS, curcumin with tangeretin SMEDDS, curcumin with quercetin SMEDDS, or curcumin with silibinin SMEDDS. All SMEDDS formulations were dosed in the oil phase, with no prior mixing with an aqueous solvent. Curcumin, quercetin, and silibinin were dosed at 100 mg/kg for all the studies, while piperine was dosed at 125 mg/kg and tangeretin was dosed at 33 mg/kg. Mice were sacrificed at 0.5, 1, 2, 4, or 6 hours post-dose. Blood was collected from the facial vein and/or by cardiac puncture into a heparinized tube (Terumo Capiject, Somerset, NJ) and then centrifuged at 20000 x g for 5 minutes to obtain plasma. Other tissues were collected in pre-weighed glass test tubes. Tissues and plasma were stored at -20° C until analysis.

3.2.5 Curcumin extraction from plasma and tissue

Acetonitrile was added to thawed plasma (1:4 v/v, plasma to acetonitrile) to precipitate proteins. Plasma samples were centrifuged at 20000 x g for 10 minutes, and the supernatant was used directly for HPLC analysis. Other tissues were weighed and homogenized in 4 mL distilled water using a hand-held homogenizer (Omni International, Kennesaw, GA) and then lyophilized for 48 hours (Labconco, Kansas City, MO). Curcumin was extracted from dried tissues using acetonitrile for ~18 hrs at room

temperature on a rotary extractor. Tissues were centrifuged twice, first at 3200 x g and then at 20000 x g to rid samples of tissue debris. Final supernatant was used directly for HPLC analysis. Stability of curcumin during the extraction and the efficiency of extraction were determined by spiking tissues from untreated animals with 50 μg of curcumin dissolved in DMSO prior to lyophilizing, followed by extraction and analysis of curcumin as described above. Extraction efficiency was calculated by dividing amount of curcumin recovered by 50 μg, multiplied by 100.

3.2.6 HPLC analysis

All HPLC analyses were performed using a Beckman Coulter HPLC system attached to UV-PDA and fluorescence (Jasco, Easton, MD) detectors. Sample injection volume was 50 μL for all analytes.

Curcumin and curcumin glucuronide. The mobile phase consisted of acetonitrile and 10 mM ammonium acetate (65:35 v/v) with a flow rate of 1 mL/min. Compounds were separated on a Scherzo SM C-18 (150 x 4.6 mm, 5 μm) column (Imtakt, Philadelphia, PA). Curcumin (retention time, 3.9 min) and curcumin glucuronide (retention time 6.6 min) were detected using a fluorescence detector (excitation 420 nm, emission 470 nm for both compounds) (Figure 24). Total run time was 9 minutes.

Curcumin, tangeretin and piperine. The three compounds were separated on an Agilent Zorbax SB-C18 column (250 x 4.6 mm; 5 μm, Santa Clara, CA), fitted with an Agilent Zorbax cartridge guard column (C-18, 12.5 x 4.6 mm). Mobile phase consisted of acetonitrile and 10 mM ammonium acetate buffer adjusted to pH 4 with glacial acetic

acid (65:35), running at a flow rate of 1 ml/min. Curcumin (λ_{max} = 430 nm) eluted at 4.9 min. Piperine (λ_{max} = 340 nm) eluted at 5.6 min. Tangeretin (λ_{max} = 280 nm) eluted at 6.7 min. Total run time was 9 min. Curcumin glucuronide co-eluted with the solvent front (1.6 min), making it difficult to accurately determine curcumin glucuronide concentrations. Incubation of plasma diluted with 50 mM phosphate buffer and 5000 U β-glucuronidase (Sigma) confirmed the identity of this peak (data not shown). Curcumin and piperine produced linear standard plots over the range of 0.015 – 0.5 μg/mL with R^2 > 0.99 (Figure 25).

Curcumin and quercetin. A gradient method was used to separate curcumin and quercetin (λ_{max} = 370 nm) using an Agilent Eclipse XBD-C18 (150 x 4.6 mm, 5 μm) column with a Agilent Zorbax cartridge guard column (C-18, 12.5 x 4.6 mm). The mobile phase consisted of A: 10 mM ammonium acetate, B: acetonitrile. The gradient conditions were – 0-2 min B 35%, 2-4 min B 35-65%, 4-9 min B 65%, 9-10 min B 65-35%. Quercetin eluted at 3.9 minutes. The retention time for curcumin was 7.9 minutes. Curcumin and quercetin produced linear standard plots over the range of 1–25 μg/mL with R^2 > 0.99 (Figure 26).

Curcumin and silibinin. Silibinin (λ_{max} = 288 nm) and curcumin were separated on the Agilent XBD Eclipse C-18 column with an Agilent Zorbax cartridge guard column (C-18, 12.5 x 4.6 mm). Mobile phase consisted of A: 10 mM ammonium acetate, B: acetonitrile. The gradient conditions were – B 35%. 0-2 min B 20%, 2-4 min B 20-70%, 4-8 min B 70%, 8-9 min B 70-20%. Retention time of curcumin and silibinin were 7.6 and 5.6 minutes, respectively. Retention time for curcumin was 7.9 minutes. Curcumin

and silibinin produced linear standard plots over the range of 0.015–0.5 μg/mL with R^2 > 0.99 (Figure 27).

3.2.7 Determination of pharmacokinetic parameters

Non-compartmental analysis of the plasma concentrations was performed using Phoenix WinNonLin software version 1.2 (Pharsight, St. Louis, MO). Area under the curve (AUC_{inf}) was calculated.

3.2.8 Statistical analysis

SigmaPlot software was used to test for the significance of differences using ANOVA followed by post-hoc Newman Keuls testing, with $p < 0.05$ being considered statistically significant.

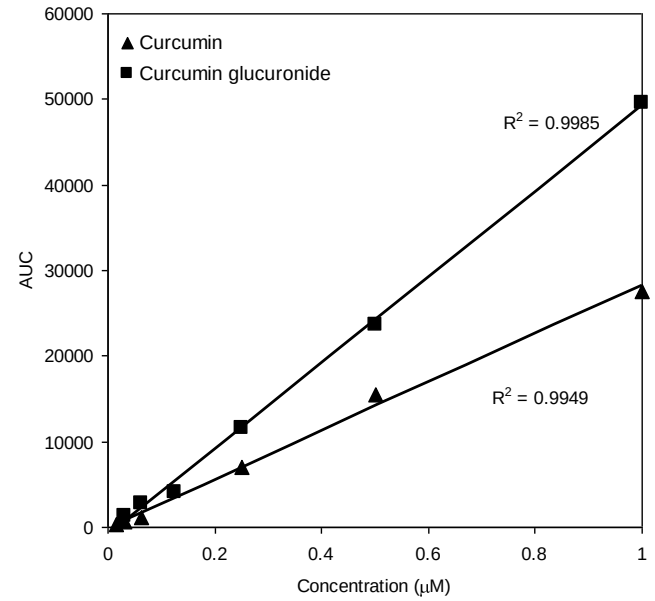

Figure 25 – Standard curve for the quantification of curcumin and curcumin glucuronide using HPLC analysis.

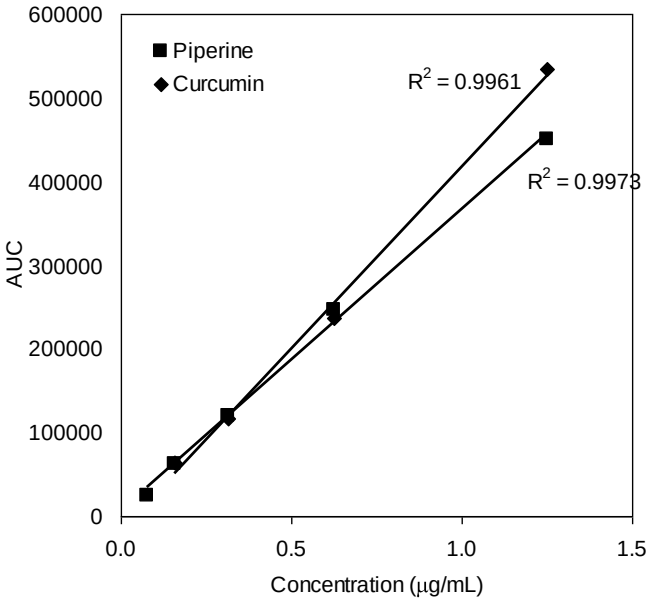

Figure 26– Standard curve for the quantitation of curcumin and piperine by HPLC analysis.

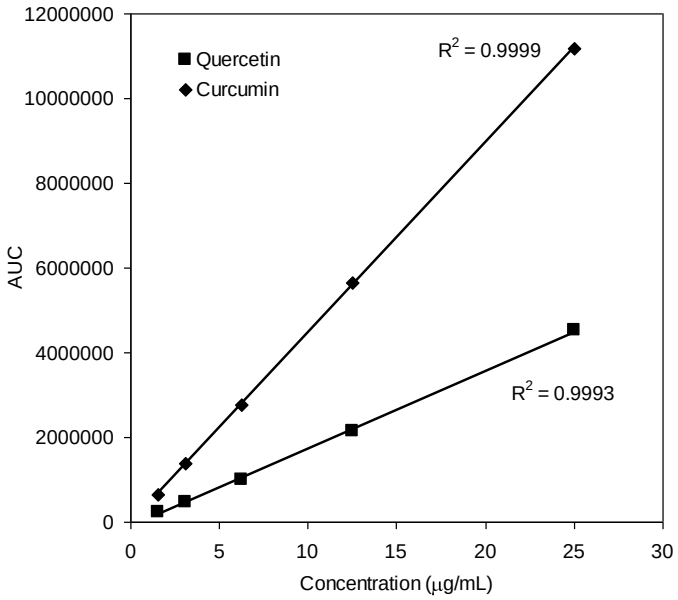

Figure 27 – Standard curve for the quantitation of curcumin and quercetin by HPLC analysis.

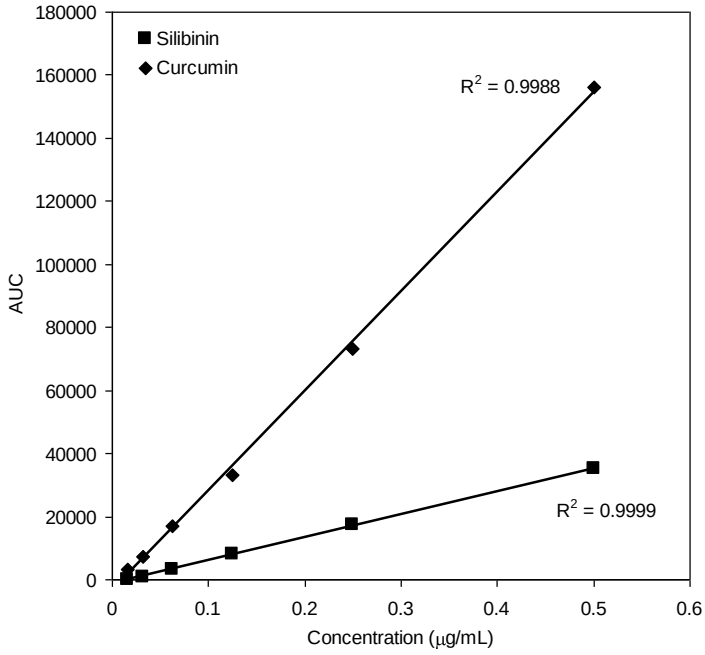

Figure 28 – Standard curve for the quantitation of curcumin and silibinin by HPLC analysis.

3.3 Results

3.3.1 Microsomal Studies

Flavonoids share chemical structure attributes with curcumin (Figure 28), making them attractive candidates for competitively inhibiting curcumin metabolism. Mouse liver microsomal assays were carried out with a panel of naturally occurring compounds to identify molecules that have inhibitory effects on curcumin glucuronidation. Members of the panel were selected based on previously reported inhibitory activity on UGTs as well as anticancer activity. For example, piperine has been shown to increase curcumin bioavailability (65) and to modulate a variety of metabolic enzymes and cancer pathways (78, 167, 168). Silibinin (derived from milk thistle) and quercetin (from fruit peels and onions) (77) have been shown to modulate UGT enzymatic activity and have anticancer effects (79, 169). In our studies, tangeretin, quercetin and silibinin showed significant inhibitory effects on curcumin metabolism (Figure 29). Inhibitor concentrations were limited to 10 μM to mimic concentrations achievable *in vivo*. Quercetin, silibinin and tangeretin showed 20-30% inhibition at the maximum concentration tested compared to blank controls. The other compounds used showed either no inhibitory effect (piperine) or significantly increased UGT activity (EGCG and salicylic acid).

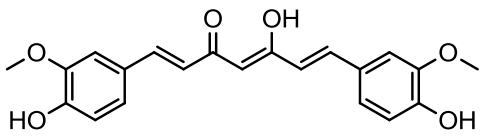

Curcumin

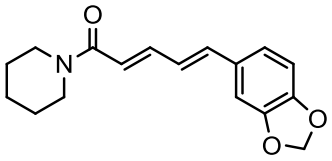

Piperine

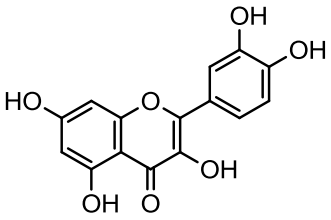

Quercetin

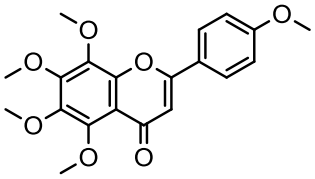

Tangeretin

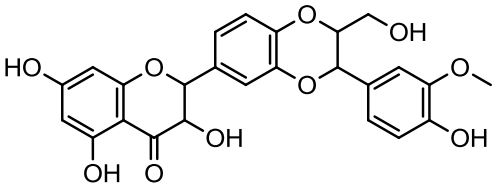

Silibinin

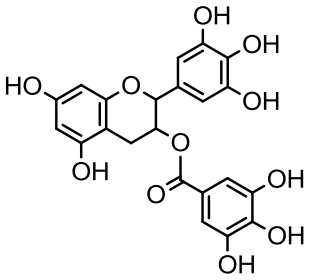

Epigallocatechin gallate (EGCG)

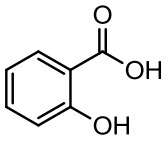

Salicylic acid

Figure 29 – Structure of curcumin and natural inhibitors of UGT metabolism.

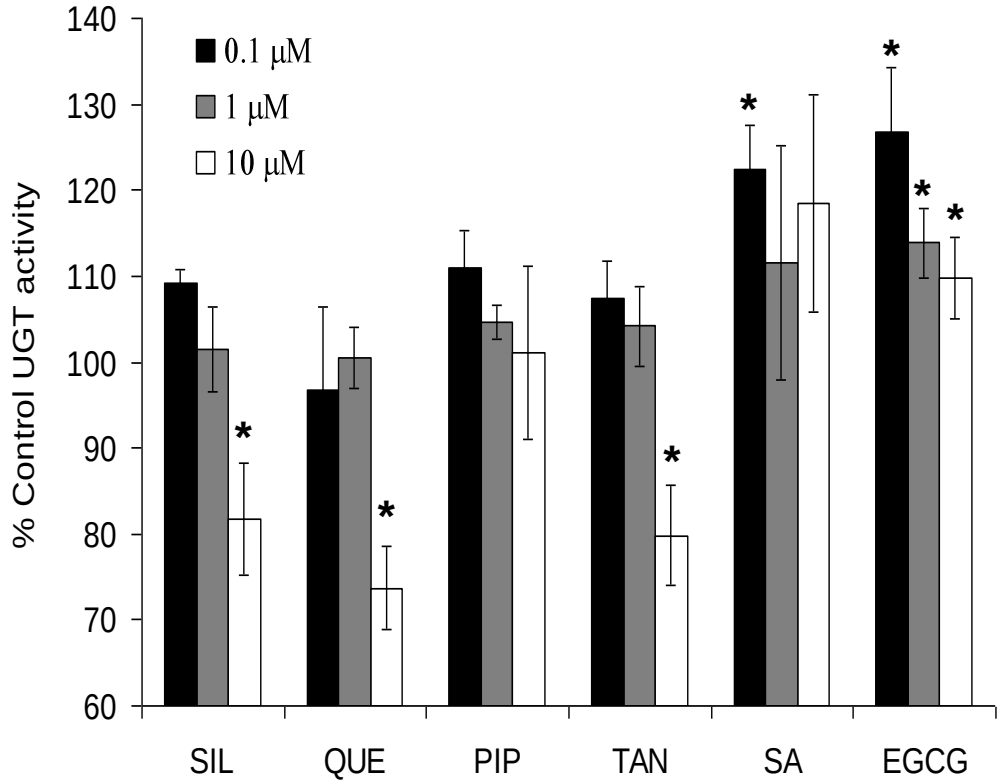

Figure 30 – Inhibition of curcumin glucuronidation. Curcumin (1 μM) was incubated with piperine (PIP), quercetin (QUE), silibinin (SIL), tangeretin (TAN), epigallocatechin gallate (EGCG) or salicylic acid (SA) at various concentrations with mouse liver microsomes (n = 3). Data are presented as % of control curcumin glucuronidation activity ± S.D. *$p<0.05$ as determined by a Students t-test versus incubations with no inhibitor.

3.3.2 SMEDDS formulation

Previous studies have shown that SMEDDSs containing Cremophor® EL solubilized curcumin to a greater extent than those formulated with some other surfactants (94, 170, 171). The SMEDDS used in our studies showed high curcumin and inhibitor (piperine, silibinin, or quercetin) solubility (Table 2). A concentration of 30 mg/ml was suitable for 100 mg/kg dosing (equivalent to 7 g dose in a human), making this formulation suitable for human dosing in the future. Dynamic light scattering was

used to characterize the nanoemulsion formed by the addition of SMEDDS to water. No significant difference in size was observed between curcumin-loaded and curcumin and inhibitor-loaded formulations.

Compound	Solubility (mg/g)	Particle size (nm)
Curcumin	51.5	17.6 ± 4.7
Piperine	45.2	21.5 ± 8.8
Quercetin	34.4	15.1 ± 3.0
Silibinin	32.8	16.8 ± 2.4

Table 2 – Solubility of compounds in SMEDDS formulation with corresponding particle size

3.3.3 Effect of formulation on curcumin plasma levels

Several different formulations were investigated for oral delivery of curcumin. Plasma concentrations observed one hour post-dose [suggested t_{max} of curcumin (171)] are shown in Figure 30. Curcumin solubilized in the SMEDDS formulation did not show a significant increase in plasma concentration compared to curcumin suspension or curcumin solubilized in DMSO. All formulations showed significant variability, with some animals having no detectable curcumin in the plasma. However, the SMEDDS resulted in much higher plasma concentrations of curcumin glucuronide, which was essentially absent in animals treated with either the suspension or solution formulations (data not shown).

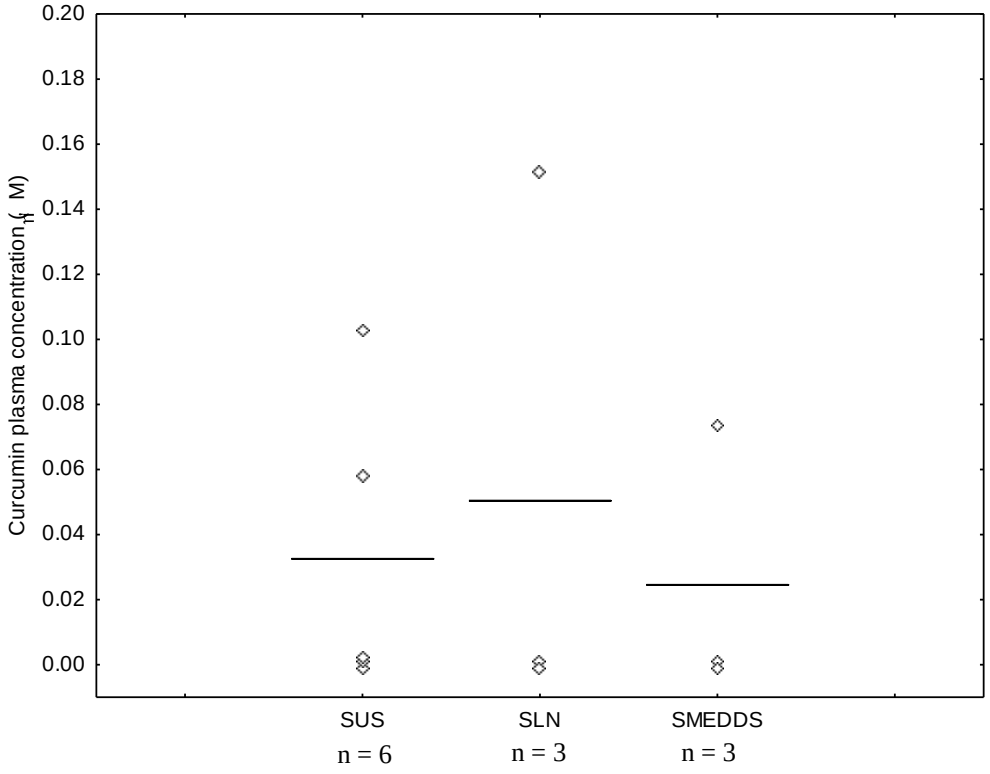

Figure 31 – SMEDDS formulation does not increase plasma levels of curcumin. Mice (n = 3-6) were dosed orally with curcumin (100 mg/kg) either as a suspension (SUS), solubilized in DMSO (SLN) or in the SMEDDS formulation (SMEDDS). Mice were sacrificed after one hour and curcumin plasma concentrations were determined by HPLC. Data points represent curcumin plasma concentration in individual animals, with lines signifying group mean.

3.3.4 Effect of metabolic inhibitors on curcumin pharmacokinetics

Administration of tangeretin with curcumin in the SMEDDS formulation produced no detectable levels of curcumin in the plasma one hour after administration (data not shown). However, co-administration of piperine with curcumin using the SMEDDS formulation resulted in higher average C_{max} values than administration of curcumin alone, but was also associated with high variability (Figure 31). Piperine was well absorbed from this formulation and resulted in high (~30 μM) plasma concentrations

one hour after dosing. However, piperine treatment appeared to stress the mice, as evidenced by decreased mobility and squinting eyes, almost immediately after dosing. Although piperine co-delivery resulted in higher curcumin levels in this study, the effect was highly variable (0 – 2.4 μM) and deemed unacceptable.

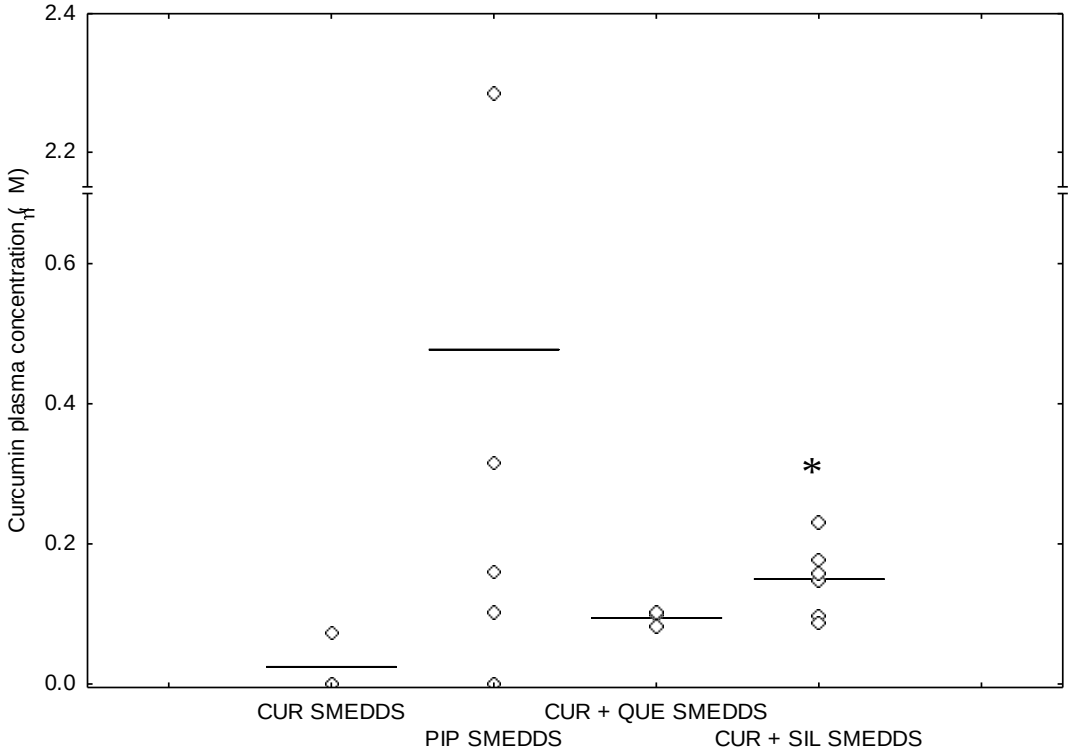

Figure 32 – Addition of quercetin (QUE) or silibinin (SIL) reduces variability and improves curcumin plasma concentrations. Mice were administered orally with SMEDDS formulations containing curcumin (100 mg/kg, n=3) and either piperine (125 mg/kg, n=6), QUE (100 mg/kg, n=3), or SIL (100 mg/kg, n=6). Mice were sacrificed after one hour and blood was collected and processed to obtain plasma. Curcumin plasma concentrations were analyzed by HPLC. Data points represent curcumin plasma concentration in individual animals, with lines signifying group mean. *$p<0.05$ as determined by ANOVA followed by post hoc Newman Keuls testing compared to CUR SMEDDS.

Co-administration of either quercetin or silibinin reduced the variability in plasma concentrations of curcumin and increased the average C_{max} of curcumin after oral dosing (Figure 32) compared to that without the inhibitor. Silibinin showed significantly higher plasma levels one hour after dosing ($p<0.05$) and therefore the highest potential to improve curcumin bioavailability. Based on this, a full time-course study was conducted for the curcumin and silibinin combination in the SMEDDS formulation. As can be seen from Figure 26A, plasma levels of curcumin were much higher and were still detectable four hours after dosing of the combination compared to that when curcumin was dosed alone. Silibinin plasma concentrations peaked at 30 minutes and remained steady throughout the study (Figure 32B). Mice tolerated the curcumin-silibinin combination formulation well, and no overt signs of toxicity were observed in this short-term study.

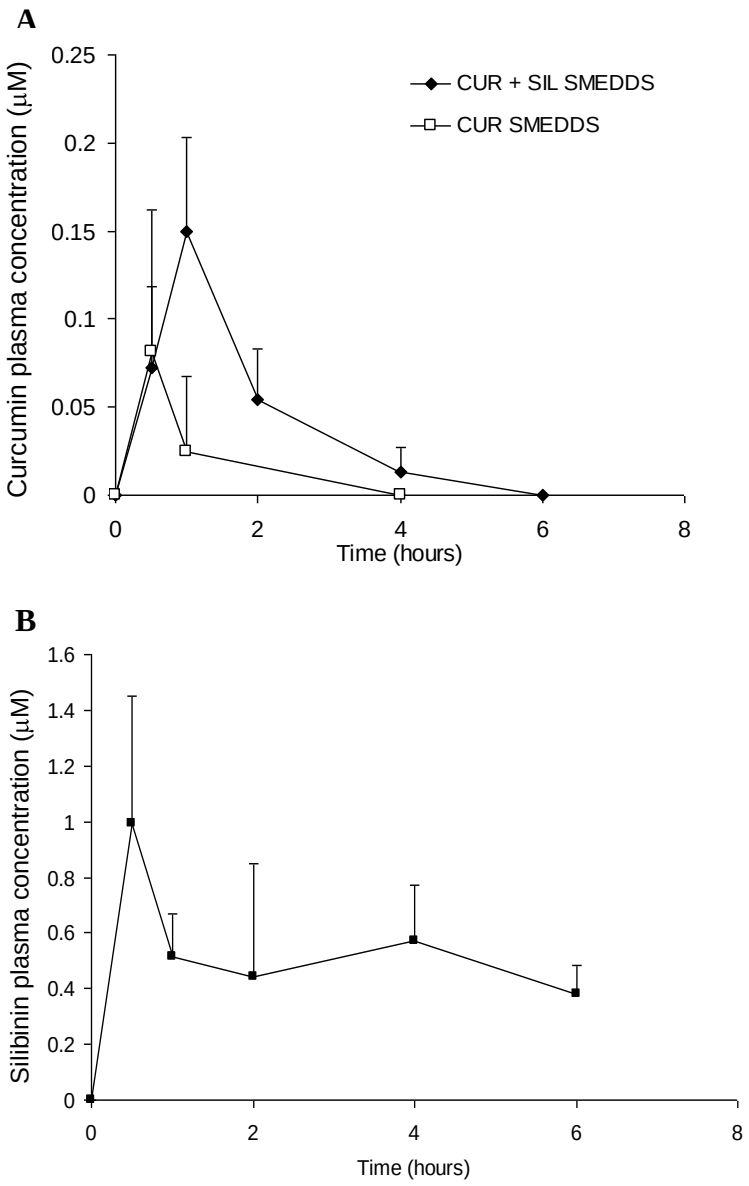

Figure 33 – Addition of silibinin improves curcumin oral bioavailability. Female mice (n = 3-6) were dosed orally with curcumin SMEDDS (CUR SMEDDS) or curcumin and silibinin combination SMEDDS (CUR + SIL SMEDDS). Mice were sacrificed at various time points, and plasma was analyzed for curcumin (A) and silibinin (B) concentrations. Data are presented as mean plasma concentration. Error bars are representative of S.D.

3.4 Discussion

The chemotherapeutic potential of curcumin is well documented. In various cancer cell lines, curcumin has been shown to inhibit the activation of NF-κB (23), a pathway critical for tumorigenesis and inflammation (24). However, many of these effects have been tested at curcumin concentrations ranging from 20-100 μM. These concentrations are likely unrealistic and not physiologically relevant, given the poor bioavailability of curcumin. Interestingly, the IC_{50} of curcumin has been shown to decrease with the duration of exposure (45, 162). These results suggest that a long-term dosing regimen, resulting in low, steady concentrations of curcumin, could be an effective chemopreventive approach. The overall goal of the current study was to examine an oral dosing strategy to improve curcumin bioavailability.

The low solubility of curcumin (~2 ng/mL in water) combined with its poor absorption through the small intestine (59) results in a significant portion of an oral dose being excreted in the feces (63). To overcome this problem, we used a SMEDDS capable of solubilizing large amounts of curcumin (Table 2). SMEDDSs have also been shown to improve the absorption of hydrophobic drugs and increase the shelf-life of otherwise unstable compounds (95). SMEDDSs have been used previously for oral dosing of curcumin. For example, Setthacheewakul et al (171) formulated a SMEDDS, consisting of Cremophor EL, Labrasol, Labrafac PG and Capryol 90. This formulation showed average plasma concentrations as high as 5 μM in rats, ~8-9 times higher than the suspension control. Compared to this previous study, the lower C_{max} observed in our study could be due to the differences in UGT enzyme levels between rodent species (172). The effectiveness of SMEDDS in other studies was less clear. Cui et al reported

the curcumin concentrations remaining in the gastrointestinal tract, rather than the plasma concentrations (94). Zhongfa et al (165) used a curcumin dose of 1.8 g/kg corresponding to a 126 g average human dose. It is not clear whether such high doses can be used in humans. Recently, Zhang et al successfully fabricated a folate-modified SMEDDS formulation for targeting colon cancer (173). Since this formulation is intended for colon cancer treatment, no systemic levels of curcumin were reported. However, our laboratory recently showed that folate modulated PLGA nanoparticles increase gut absorption in vitro (174), and so there is high potential that this formulation could be useful for systemic delivery.

In our studies, solubilizing curcumin in the SMEDDS formulation appeared to improve the absorption of curcumin, as evidenced by higher plasma concentrations of the glucuronide. The lack of significantly higher plasma concentrations of parent drug suggested that inhibition of curcumin metabolism in the gut and during first pass through the liver was probably necessary to improve its oral bioavailability. UGT enzymes account for the majority of curcumin metabolism in the gut and liver. UGT1A1 and 1A3 (liver) as well as UGT1A8 and UGT1A10 (gut) show high activity for curcumin compared to other UGT enzymes (70), with UGT1A1 showing the highest activity for curcumin of all UGT enzymes tested. Inhibition of UGT activity offered a possible avenue to decrease curcumin clearance, and thereby increase the overall systemic exposure of curcumin.

Previous studies have examined the effects of naturally occurring compounds on UGT activity (74, 75, 77). As an additional benefit, some of these natural compounds also have complementary anticancer activity (79-81, 169, 175). This is especially true for

piperine which, when combined with curcumin, affects cellular pathways important for cancer stem cells such as Wnt (167). Silibinin, quercetin and tangeretin decreased curcumin glucuronidation in mouse liver microsomes, while piperine, EGCG and salicylic acid did not (Figure 22). This was an unexpected finding for piperine, which was previously shown to increase curcumin bioavailability. Because prior reports suggested that piperine is highly effective in improving curcumin bioavailability (65), we included piperine in our in vivo studies. Addition of piperine to the SMEDDS formulation increased curcumin plasma levels but the results were highly variable. Shoba et al showed a 2000% increase in curcumin bioavailability in humans, with a lesser effect in rats (65). A closer look at the analytical technique used in the study could partly explain the dramatic increase in oral bioavailability observed with piperine. Prior to analysis, plasma samples were heated at 80˚ C for half an hour, which likely degraded curcumin glucuronide to the parent compound. The paper did not report on the stability of curcumin metabolites during the sample processing and extraction procedure used. Also, piperine has been shown to increase intestinal brush border membrane fluidity, leading to increased absorption of co-delivered molecules (176). Thus, in addition to potential effects on metabolism, the apparent effects of piperine on curcumin bioavailability are likely due to increased gut absorption. Plasma from animals treated with curcumin-piperine combination had high concentrations of curcumin glucuronide, providing further evidence that piperine improved the absorption of curcumin. Although some animals showed high plasma levels of curcumin, piperine was not investigated further because of the high variability and the observed side effects.

Both quercetin and silibinin increased curcumin bioavailability and were associated with reduced animal-to-animal variability. Extended pharmacokinetic studies showed a 3.5 fold increase in area under the curve (AUC) for curcumin and silibinin SMEDDS compared to SMEDDS with curcumin alone. Silibinin was previously shown to inhibit UGT1A1-mediated glucuronidation of β-estradiol (77) but is not a commonly used natural product for metabolic inhibition. To our knowledge, this is the first study showing an increase in bioavailability of curcumin using silibinin as an inhibitor. Similar to piperine, silibinin also modulates cellular pathways important for cancer proliferation and invasion. A decrease in epidermal growth factor receptor (EGFR) activation (177, 178) by silibinin led to apoptosis and decreased MAPK activity (169), a pathway important for tumor cell proliferation. Silibinin has been shown to decrease vascular endothelial growth factor (VEGF) production (179), leading to decreased angiogenesis in vivo (180). Additionally, silibinin has been shown to inhibit tumor invasion through up-regulation of E-cadherin (181) and decreased MDA-MB-231 migration in vitro (182). Silibinin has been combined previously with curcumin to effectively induce apoptosis in adult myeloid leukemia cells in vitro through activation of caspase pathways (183). Pharmacokinetic studies using the combination SMEDDS improved plasma concentrations of both curcumin and silibinin, and this formulation can therefore be expected to have enhanced chemopreventive activity.

3.5 Conclusions

Our studies showed that oral bioavailability of curcumin can be increased by formulating curcumin in a soluble form using the SMEDDS and by decreasing its

metabolic clearance. Co-delivery of silibinin was used as a novel approach to decrease UGT-mediated clearance of curcumin and to improve curcumin bioavailability *in vivo*. Both curcumin and silibinin have complementary antioxidant, anti-inflammatory and anticancer activities. Therefore, there is a great potential for this combination formulation to be utilized as an oral dosage form for chemoprevention. Future studies will examine the safety and chemopreventive efficacy of this formulation following chronic dosing.

CHAPTER 4

SUMMARY AND FUTURE DIRECTIONS

Curcumin, a dietary polyphenol derived from turmeric, has been shown to modulate cellular pathways important for cancer chemoprevention in vitro and in vivo. The clinical utility of curcumin is limited by its poor solubility and extensive gut and hepatic metabolism, resulting in a low bioavailability and short half life after oral dosing. Our lab has previously formulated a microparticle drug delivery system for sustained curcumin delivery. This formulation showed efficacy in inhibiting tumor growth in a triple negative xenograft model of breast cancer.

The overall objective of the first portion of this thesis was to test curcumin loaded PLGA microparticles in a HER-2 overexpressing transgenic mouse model of breast cancer. HER-2 is overexpressed in 30% of breast cancers and is associated with poor five-year survival. Curcumin has been shown to deplete HER-2 protein in vitro in a time- and concentration-dependant manner. Studies in Chapter 2 showed that curcumin loaded microparticles delayed tumorigenesis by 2-3 weeks in Balb-neuT mice compared to blank microparticle injections. Western blotting revealed a decrease in HER-2 and VEGF protein levels and immunohistochemistry showed decreased CD-31+ microvasculature in mammary tissue. When these results were compared to saline controls; however, saline treated mice showed the longest delay to 100% tumorigenesis. Additionally, saline treated animals showed significantly lower VEGF protein levels compared to curcumin loaded and blank PLGA microparticles. Cell proliferation and microvasculature were significantly lower in saline treated Balb-neuT mice. These results suggested that blank PLGA microparticles may accelerate tumor formation in this model. Bioluminescence

studies in NF-κB-RE-luc mice showed that blank PLGA microparticles activated NF-κB signaling for at least 72 hours after injection, suggesting that sustained systemic inflammation caused by PLGA microparticles may have resulted in increased tumorigenesis. It was concluded that while curcumin showed bioactivity, PLGA microparticles may not be a suitable formulation in this disease model.

Studies in Chapter 3 examined a novel oral formulation to improve curcumin bioavailability. Previous studies have used SMEDDS to administer curcumin orally in a soluble form, with mixed results. We hypothesized that the addition of a natural metabolic enzyme inhibitor in a SMEDDS formulation will increase curcumin bioavailability. Potential inhibitors of UGT enzymatic activity were evaluated by microsomal assay. Silibinin and quercetin both showed 20-30% inhibition at 10 μM concentrations. Surprisingly, piperine, which had been shown to increase curcumin bioavailability previously, did not inhibit curcumin metabolism in vitro. Acute pharmacokinetic studies showed that oral administration of curcumin in the SMEDDS formulation did not result in significantly higher plasma concentrations of curcumin relative to that with a conventional suspension formulation. Coadministration with piperine in the SMEDDS formulation produced highly variable results, with plasma concentrations ranging from 0 to 2.4 μM. Dosing curcumin and silibinin together in the SMEDDS formulation showed the highest, least variable plasma concentrations one hour after dosing. Extended pharmacokinetic studies showed that curcumin and silibinin coadministration improved curcumin AUC 3.5-fold compared to curcumin alone. Based on its ability to improve curcumin bioavailability and its own potential chemopreventive

properties, it was concluded that co-delivering silibinin was a highly promising approach to improve curcumin anti-cancer efficacy.

Future studies need to be designed to determine the mechanism by which PLGA microparticles induced tumorigenesis in the Balb-neuT model. The activation of NF-κB by PLGA microparticle injection points to a systemic inflammatory effect. Acute local inflammation is a normal reaction at the injection site but no previous study has shown systemic inflammation to PLGA microparticles previously. Additionally, studies are needed to determine what effects, if any, lactic acid (produced by degrading PLGA) has on tumorigenesis. As discussed in Chapter 2, lactic acid can act as a signaling molecule to stimulate angiogenesis. Studies examining the dose-response relationship between PLGA/lactic acid and tumorigenesis/angiogenesis should be carried out to determine a maximum safe dose for chemoprevention. This will provide the critical preliminary data to determine the safety of using PLGA in patients who are at high risk for inflammatory diseases.

Beyond the effects of PLGA, curcumin should still be pursued as a chemopreventive compound for breast cancer. Although the results of the studies in Chapter 2 were mixed, curcumin delayed tumorigenesis. Repackaging curcumin into an alternate polymeric microparticle delivery system should be an important goal in the future. Other future studies should focus on the complementarity of curcumin and silibinin combination. As discussed in Chapter 3, silibinin has its own chemopreventive potential. Studies are already underway to look at the potential additive or synergistic effects of curcumin and silibinin against breast cancer, with particular attention given to

their effects on metastasis. Curcumin has great potential as a chemopreventive compound, and these studies will contribute to further advancing it to the clinic.

REFERENCES

1. Aggarwal, B.B., Sundaram, C., Malani, N., and Ichikawa, H. 2007. Curcumin: the Indian solid gold. *Adv Exp Med Biol* 595:1-75.
2. Anand, P., Sundaram, C., Jhurani, S., Kunnumakkara, A.B., and Aggarwal, B.B. 2008. Curcumin and cancer: an "old-age" disease with an "age-old" solution. *Cancer Lett* 267:133-164.
3. Goel, A., Kunnumakkara, A.B., and Aggarwal, B.B. 2008. Curcumin as "Curecumin": from kitchen to clinic. *Biochem Pharmacol* 75:787-809.
4. Kunnumakkara, A.B., Anand, P., and Aggarwal, B.B. 2008. Curcumin inhibits proliferation, invasion, angiogenesis and metastasis of different cancers through interaction with multiple cell signaling proteins. *Cancer Lett* 269:199-225.
5. Cheng, A.L., Hsu, C.H., Lin, J.K., Hsu, M.M., Ho, Y.F., Shen, T.S., Ko, J.Y., Lin, J.T., Lin, B.R., Ming-Shiang, W., et al. 2001. Phase I clinical trial of curcumin, a chemopreventive agent, in patients with high-risk or pre-malignant lesions. *Anticancer Res* 21:2895-2900.
6. Hanahan, D., and Weinberg, R.A. 2000. The hallmarks of cancer. *Cell* 100:57-70.
7. Poulsen, H.E., Prieme, H., and Loft, S. 1998. Role of oxidative DNA damage in cancer initiation and promotion. *Eur J Cancer Prev* 7:9-16.
8. Nguyen, D.X., Bos, P.D., and Massague, J. 2009. Metastasis: from dissemination to organ-specific colonization. *Nat Rev Cancer* 9:274-284.
9. Singh, U., Barik, A., Singh, B.G., and Priyadarsini, K.I. Reactions of reactive oxygen species (ROS) with curcumin analogues: Structure-activity relationship. *Free Radic Res* 45:317-325.
10. Ruby, A.J., Kuttan, G., Babu, K.D., Rajasekharan, K.N., and Kuttan, R. 1995. Anti-tumour and antioxidant activity of natural curcuminoids. *Cancer Lett* 94:79-83.
11. Joe, B., and Lokesh, B.R. 1994. Role of capsaicin, curcumin and dietary n-3 fatty acids in lowering the generation of reactive oxygen species in rat peritoneal macrophages. *Biochim Biophys Acta* 1224:255-263.
12. Ohshima, H., and Bartsch, H. 1994. Chronic infections and inflammatory processes as cancer risk factors: possible role of nitric oxide in carcinogenesis. *Mutat Res* 305:253-264.
13. Thomsen, L.L., Miles, D.W., Happerfield, L., Bobrow, L.G., Knowles, R.G., and Moncada, S. 1995. Nitric oxide synthase activity in human breast cancer. *Br J Cancer* 72:41-44.
14. Chan, M.M., Huang, H.I., Fenton, M.R., and Fong, D. 1998. In vivo inhibition of nitric oxide synthase gene expression by curcumin, a cancer preventive natural product with anti-inflammatory properties. *Biochem Pharmacol* 55:1955-1962.
15. Yang, C., Zhang, X., Fan, H., and Liu, Y. 2009. Curcumin upregulates transcription factor Nrf2, HO-1 expression and protects rat brains against focal ischemia. *Brain Res* 1282:133-141.
16. Biswas, S.K., McClure, D., Jimenez, L.A., Megson, I.L., and Rahman, I. 2005. Curcumin induces glutathione biosynthesis and inhibits NF-kappaB activation and

interleukin-8 release in alveolar epithelial cells: mechanism of free radical scavenging activity. *Antioxid Redox Signal* 7:32-41.
17. Piper, J.T., Singhal, S.S., Salameh, M.S., Torman, R.T., Awasthi, Y.C., and Awasthi, S. 1998. Mechanisms of anticarcinogenic properties of curcumin: the effect of curcumin on glutathione linked detoxification enzymes in rat liver. *Int J Biochem Cell Biol* 30:445-456.
18. Syng-Ai, C., Kumari, A.L., and Khar, A. 2004. Effect of curcumin on normal and tumor cells: role of glutathione and bcl-2. *Mol Cancer Ther* 3:1101-1108.
19. Weinstein, I.B., and Joe, A. 2008. Oncogene addiction. *Cancer Res* 68:3077-3080; discussion 3080.
20. Weinstein, I.B. 2002. Cancer. Addiction to oncogenes--the Achilles heal of cancer. *Science* 297:63-64.
21. Bertucci, F., and Birnbaum, D. 2008. Reasons for breast cancer heterogeneity. *J Biol* 7:6.
22. Campbell, L.L., and Polyak, K. 2007. Breast tumor heterogeneity: cancer stem cells or clonal evolution? *Cell Cycle* 6:2332-2338.
23. Jobin, C., Bradham, C.A., Russo, M.P., Juma, B., Narula, A.S., Brenner, D.A., and Sartor, R.B. 1999. Curcumin blocks cytokine-mediated NF-kappa B activation and proinflammatory gene expression by inhibiting inhibitory factor I-kappa B kinase activity. *J Immunol* 163:3474-3483.
24. Karin, M. 2006. Nuclear factor-kappaB in cancer development and progression. *Nature* 441:431-436.
25. Merkhofer, E.C., Cogswell, P., and Baldwin, A.S. Her2 activates NF-kappaB and induces invasion through the canonical pathway involving IKKalpha. *Oncogene* 29:1238-1248.
26. Sakurai, H., Suzuki, S., Kawasaki, N., Nakano, H., Okazaki, T., Chino, A., Doi, T., and Saiki, I. 2003. Tumor necrosis factor-alpha-induced IKK phosphorylation of NF-kappaB p65 on serine 536 is mediated through the TRAF2, TRAF5, and TAK1 signaling pathway. *J Biol Chem* 278:36916-36923.
27. Pomerantz, J.L., and Baltimore, D. 2002. Two pathways to NF-kappaB. *Mol Cell* 10:693-695.
28. Lee, J., Im, Y.H., Jung, H.H., Kim, J.H., Park, J.O., Kim, K., Kim, W.S., Ahn, J.S., Jung, C.W., Park, Y.S., et al. 2005. Curcumin inhibits interferon-alpha induced NF-kappaB and COX-2 in human A549 non-small cell lung cancer cells. *Biochem Biophys Res Commun* 334:313-318.
29. Plummer, S.M., Holloway, K.A., Manson, M.M., Munks, R.J., Kaptein, A., Farrow, S., and Howells, L. 1999. Inhibition of cyclo-oxygenase 2 expression in colon cells by the chemopreventive agent curcumin involves inhibition of NF-kappaB activation via the NIK/IKK signalling complex. *Oncogene* 18:6013-6020.
30. Lee, J.Y., Lee, Y.M., Chang, G.C., Yu, S.L., Hsieh, W.Y., Chen, J.J., Chen, H.W., and Yang, P.C. Curcumin induces EGFR degradation in lung adenocarcinoma and modulates p38 activation in intestine: the versatile adjuvant for gefitinib therapy. *PLoS One* 6:e23756.
31. Chen, Y.R., and Tan, T.H. 1998. Inhibition of the c-Jun N-terminal kinase (JNK) signaling pathway by curcumin. *Oncogene* 17:173-178.

32. Woo, M.S., Jung, S.H., Kim, S.Y., Hyun, J.W., Ko, K.H., Kim, W.K., and Kim, H.S. 2005. Curcumin suppresses phorbol ester-induced matrix metalloproteinase-9 expression by inhibiting the PKC to MAPK signaling pathways in human astroglioma cells. *Biochem Biophys Res Commun* 335:1017-1025.
33. Rajasingh, J., Raikwar, H.P., Muthian, G., Johnson, C., and Bright, J.J. 2006. Curcumin induces growth-arrest and apoptosis in association with the inhibition of constitutively active JAK-STAT pathway in T cell leukemia. *Biochem Biophys Res Commun* 340:359-368.
34. Turkson, J., and Jove, R. 2000. STAT proteins: novel molecular targets for cancer drug discovery. *Oncogene* 19:6613-6626.
35. Iavnilovitch, E., Groner, B., and Barash, I. 2002. Overexpression and forced activation of stat5 in mammary gland of transgenic mice promotes cellular proliferation, enhances differentiation, and delays postlactational apoptosis. *Mol Cancer Res* 1:32-47.
36. Marcu, M.G., Jung, Y.J., Lee, S., Chung, E.J., Lee, M.J., Trepel, J., and Neckers, L. 2006. Curcumin is an inhibitor of p300 histone acetylatransferase. *Med Chem* 2:169-174.
37. Woo, J.H., Kim, Y.H., Choi, Y.J., Kim, D.G., Lee, K.S., Bae, J.H., Min, D.S., Chang, J.S., Jeong, Y.J., Lee, Y.H., et al. 2003. Molecular mechanisms of curcumin-induced cytotoxicity: induction of apoptosis through generation of reactive oxygen species, down-regulation of Bcl-XL and IAP, the release of cytochrome c and inhibition of Akt. *Carcinogenesis* 24:1199-1208.
38. Vishvakarma, N.K., Kumar, A., and Singh, S.M. Role of curcumin-dependent modulation of tumor microenvironment of a murine T cell lymphoma in altered regulation of tumor cell survival. *Toxicol Appl Pharmacol* 252:298-306.
39. Furuya, M., Yonemitsu, Y., and Aoki, I. 2009. III. Angiogenesis: complexity of tumor vasculature and microenvironment. *Curr Pharm Des* 15:1854-1867.
40. Shan, B., Schaaf, C., Schmidt, A., Lucia, K., Buchfelder, M., Losa, M., Kuhlen, D., Kreutzer, J., Perone, M., Arzt, E., et al. Curcumin suppresses HIF-1A synthesis and VEGFA release in pituitary adenomas. *J Endocrinol*.
41. Yoysungnoen, P., Wirachwong, P., Bhattarakosol, P., Niimi, H., and Patumraj, S. 2006. Effects of curcumin on tumor angiogenesis and biomarkers, COX-2 and VEGF, in hepatocellular carcinoma cell-implanted nude mice. *Clin Hemorheol Microcirc* 34:109-115.
42. Tung, Y.T., Chen, H.L., Lai, C.W., Shen, C.J., Lai, Y.W., and Chen, C.M. Curcumin reduces pulmonary tumorigenesis in vascular endothelial growth factor (VEGF)-overexpressing transgenic mice. *Mol Nutr Food Res* 55:1036-1043.
43. Hynes, N.E., and Stern, D.F. 1994. The biology of erbB-2/neu/HER-2 and its role in cancer. *Biochim Biophys Acta* 1198:165-184.
44. Yarden, Y. 2001. Biology of HER2 and its importance in breast cancer. *Oncology* 61 Suppl 2:1-13.
45. Hong, R.L., Spohn, W.H., and Hung, M.C. 1999. Curcumin inhibits tyrosine kinase activity of p185neu and also depletes p185neu. *Clin Cancer Res* 5:1884-1891.

46. Jung, Y., Xu, W., Kim, H., Ha, N., and Neckers, L. 2007. Curcumin-induced degradation of ErbB2: A role for the E3 ubiquitin ligase CHIP and the Michael reaction acceptor activity of curcumin. *Biochim Biophys Acta* 1773:383-390.
47. Lai, H.W., Chien, S.Y., Kuo, S.J., Tseng, L.M., Lin, H.Y., Chi, C.W., and Chen, D.R. The Potential Utility of Curcumin in the Treatment of HER-2-Overexpressed Breast Cancer: An In Vitro and In Vivo Comparison Study with Herceptin. *Evid Based Complement Alternat Med* 2012:486568.
48. Hu, G., Kang, Y., and Wang, X.F. 2009. From breast to the brain: unraveling the puzzle of metastasis organotropism. *J Mol Cell Biol* 1:3-5.
49. Ray, S., Chattopadhyay, N., Mitra, A., Siddiqi, M., and Chatterjee, A. 2003. Curcumin exhibits antimetastatic properties by modulating integrin receptors, collagenase activity, and expression of Nm23 and E-cadherin. *J Environ Pathol Toxicol Oncol* 22:49-58.
50. Prasad, C.P., Rath, G., Mathur, S., Bhatnagar, D., and Ralhan, R. 2009. Potent growth suppressive activity of curcumin in human breast cancer cells: Modulation of Wnt/beta-catenin signaling. *Chem Biol Interact* 181:263-271.
51. Wang, S., Yu, S., Shi, W., Ge, L., Yu, X., Fan, J., and Zhang, J. Curcumin inhibits the migration and invasion of mouse hepatoma Hca-F cells through down-regulating caveolin-1 expression and epidermal growth factor receptor signaling. *IUBMB Life* 63:775-782.
52. Aggarwal, B.B., Shishodia, S., Takada, Y., Banerjee, S., Newman, R.A., Bueso-Ramos, C.E., and Price, J.E. 2005. Curcumin suppresses the paclitaxel-induced nuclear factor-kappaB pathway in breast cancer cells and inhibits lung metastasis of human breast cancer in nude mice. *Clin Cancer Res* 11:7490-7498.
53. Lin, S.S., Lai, K.C., Hsu, S.C., Yang, J.S., Kuo, C.L., Lin, J.P., Ma, Y.S., Wu, C.C., and Chung, J.G. 2009. Curcumin inhibits the migration and invasion of human A549 lung cancer cells through the inhibition of matrix metalloproteinase-2 and -9 and Vascular Endothelial Growth Factor (VEGF). *Cancer Lett* 285:127-133.
54. Ibrahim, A., El-Meligy, A., Fetaih, H., Dessouki, A., Stoica, G., and Barhoumi, R. Effect of curcumin and Meriva on the lung metastasis of murine mammary gland adenocarcinoma. *In Vivo* 24:401-408.
55. Kunnumakkara, A.B., Guha, S., Krishnan, S., Diagaradjane, P., Gelovani, J., and Aggarwal, B.B. 2007. Curcumin potentiates antitumor activity of gemcitabine in an orthotopic model of pancreatic cancer through suppression of proliferation, angiogenesis, and inhibition of nuclear factor-kappaB-regulated gene products. *Cancer Res* 67:3853-3861.
56. Jovanovic, S.V., Steenken, S., Boone, C.W., Simic‖ , M.G. 1999. H-Atom Transfer Is A Preferred Antioxidant Mechanism of Curcumin. *J Amer Chem Soc* 41:9677-9681.
57. Wang, Y.J., Pan, M.H., Cheng, A.L., Lin, L.I., Ho, Y.S., Hsieh, C.Y., and Lin, J.K. 1997. Stability of curcumin in buffer solutions and characterization of its degradation products. *J Pharm Biomed Anal* 15:1867-1876.

58. Barik, A., Priyadarsini, K.I., and Mohan, H. 2003. Photophysical studies on binding of curcumin to bovine serum albumins. *Photochem Photobiol* 77:597-603.
59. Wahlang, B., Pawar, Y.B., and Bansal, A.K. Identification of permeability-related hurdles in oral delivery of curcumin using the Caco-2 cell model. *Eur J Pharm Biopharm* 77:275-282.
60. Pan, M.H., Huang, T.M., and Lin, J.K. 1999. Biotransformation of curcumin through reduction and glucuronidation in mice. *Drug Metab Dispos* 27:486-494.
61. Yang, K.Y., Lin, L.C., Tseng, T.Y., Wang, S.C., and Tsai, T.H. 2007. Oral bioavailability of curcumin in rat and the herbal analysis from Curcuma longa by LC-MS/MS. *J Chromatogr B Analyt Technol Biomed Life Sci* 853:183-189.
62. Liu, A., Lou, H., Zhao, L., and Fan, P. 2006. Validated LC/MS/MS assay for curcumin and tetrahydrocurcumin in rat plasma and application to pharmacokinetic study of phospholipid complex of curcumin. *J Pharm Biomed Anal* 40:720-727.
63. Perkins, S., Verschoyle, R.D., Hill, K., Parveen, I., Threadgill, M.D., Sharma, R.A., Williams, M.L., Steward, W.P., and Gescher, A.J. 2002. Chemopreventive efficacy and pharmacokinetics of curcumin in the min/+ mouse, a model of familial adenomatous polyposis. *Cancer Epidemiol Biomarkers Prev* 11:535-540.
64. Schiborr, C., Eckert, G.P., Rimbach, G., and Frank, J. A validated method for the quantification of curcumin in plasma and brain tissue by fast narrow-bore high-performance liquid chromatography with fluorescence detection. *Anal Bioanal Chem* 397:1917-1925.
65. Shoba, G., Joy, D., Joseph, T., Majeed, M., Rajendran, R., and Srinivas, P.S. 1998. Influence of piperine on the pharmacokinetics of curcumin in animals and human volunteers. *Planta Med* 64:353-356.
66. Sharma, R.A., Euden, S.A., Platton, S.L., Cooke, D.N., Shafayat, A., Hewitt, H.R., Marczylo, T.H., Morgan, B., Hemingway, D., Plummer, S.M., et al. 2004. Phase I clinical trial of oral curcumin: biomarkers of systemic activity and compliance. *Clin Cancer Res* 10:6847-6854.
67. Dhillon, N., Aggarwal, B.B., Newman, R.A., Wolff, R.A., Kunnumakkara, A.B., Abbruzzese, J.L., Ng, C.S., Badmaev, V., and Kurzrock, R. 2008. Phase II trial of curcumin in patients with advanced pancreatic cancer. *Clin Cancer Res* 14:4491-4499.
68. Ireson, C.R., Jones, D.J., Orr, S., Coughtrie, M.W., Boocock, D.J., Williams, M.L., Farmer, P.B., Steward, W.P., and Gescher, A.J. 2002. Metabolism of the cancer chemopreventive agent curcumin in human and rat intestine. *Cancer Epidemiol Biomarkers Prev* 11:105-111.
69. Hoehle, S.I., Pfeiffer, E., Solyom, A.M., and Metzler, M. 2006. Metabolism of curcuminoids in tissue slices and subcellular fractions from rat liver. *J Agric Food Chem* 54:756-764.
70. Hoehle, S.I., Pfeiffer, E., and Metzler, M. 2007. Glucuronidation of curcuminoids by human microsomal and recombinant UDP-glucuronosyltransferases. *Mol Nutr Food Res* 51:932-938.

71. Pfeiffer, E., Hoehle, S.I., Walch, S.G., Riess, A., Solyom, A.M., and Metzler, M. 2007. Curcuminoids form reactive glucuronides in vitro. *J Agric Food Chem* 55:538-544.
72. Fowler, S., and Zhang, H. 2008. In vitro evaluation of reversible and irreversible cytochrome P450 inhibition: current status on methodologies and their utility for predicting drug-drug interactions. *AAPS J* 10:410-424.
73. Zhang, D., Chando, T.J., Everett, D.W., Patten, C.J., Dehal, S.S., and Humphreys, W.G. 2005. In vitro inhibition of UDP glucuronosyltransferases by atazanavir and other HIV protease inhibitors and the relationship of this property to in vivo bilirubin glucuronidation. *Drug Metab Dispos* 33:1729-1739.
74. Mano, Y., Usui, T., and Kamimura, H. 2005. In vitro inhibitory effects of non-steroidal antiinflammatory drugs on UDP-glucuronosyltransferase 1A1-catalysed estradiol 3beta-glucuronidation in human liver microsomes. *Biopharm Drug Dispos* 26:35-39.
75. Grancharov, K., Naydenova, Z., Lozeva, S., and Golovinsky, E. 2001. Natural and synthetic inhibitors of UDP-glucuronosyltransferase. *Pharmacol Ther* 89:171-186.
76. Liu, Y., Ramirez, J., House, L., and Ratain, M.J. Comparison of the drug-drug interactions potential of erlotinib and gefitinib via inhibition of UDP-glucuronosyltransferases. *Drug Metab Dispos* 38:32-39.
77. Williams, J.A., Ring, B.J., Cantrell, V.E., Campanale, K., Jones, D.R., Hall, S.D., and Wrighton, S.A. 2002. Differential modulation of UDP-glucuronosyltransferase 1A1 (UGT1A1)-catalyzed estradiol-3-glucuronidation by the addition of UGT1A1 substrates and other compounds to human liver microsomes. *Drug Metab Dispos* 30:1266-1273.
78. Srinivasan, K. 2007. Black pepper and its pungent principle-piperine: a review of diverse physiological effects. *Crit Rev Food Sci Nutr* 47:735-748.
79. Bischoff, S.C. 2008. Quercetin: potentials in the prevention and therapy of disease. *Curr Opin Clin Nutr Metab Care* 11:733-740.
80. Chen, D., and Dou, Q.P. 2008. Tea polyphenols and their roles in cancer prevention and chemotherapy. *Int J Mol Sci* 9:1196-1206.
81. Weng, C.J., and Yen, G.C. Flavonoids, a ubiquitous dietary phenolic subclass, exert extensive in vitro anti-invasive and in vivo anti-metastatic activities. *Cancer Metastasis Rev*.
82. Ohori, H., Yamakoshi, H., Tomizawa, M., Shibuya, M., Kakudo, Y., Takahashi, A., Takahashi, S., Kato, S., Suzuki, T., Ishioka, C., et al. 2006. Synthesis and biological analysis of new curcumin analogues bearing an enhanced potential for the medicinal treatment of cancer. *Mol Cancer Ther* 5:2563-2571.
83. Ma, Z., Shayeganpour, A., Brocks, D.R., Lavasanifar, A., and Samuel, J. 2007. High-performance liquid chromatography analysis of curcumin in rat plasma: application to pharmacokinetics of polymeric micellar formulation of curcumin. *Biomed Chromatogr* 21:546-552.
84. Anand, P., Nair, H.B., Sung, B., Kunnumakkara, A.B., Yadav, V.R., Tekmal, R.R., and Aggarwal, B.B. Design of curcumin-loaded PLGA nanoparticles

formulation with enhanced cellular uptake, and increased bioactivity in vitro and superior bioavailability in vivo. *Biochem Pharmacol* 79:330-338.
85. Freiberg, S., and Zhu, X.X. 2004. Polymer microspheres for controlled drug release. *Int J Pharm* 282:1-18.
86. Wischke, C., and Schwendeman, S.P. 2008. Principles of encapsulating hydrophobic drugs in PLA/PLGA microparticles. *Int J Pharm* 364:298-327.
87. Mittal, G., Sahana, D.K., Bhardwaj, V., and Ravi Kumar, M.N. 2007. Estradiol loaded PLGA nanoparticles for oral administration: effect of polymer molecular weight and copolymer composition on release behavior in vitro and in vivo. *J Control Release* 119:77-85.
88. Gopferich, A. 1996. Mechanisms of polymer degradation and erosion. *Biomaterials* 17:103-114.
89. Fournier, E., Passirani, C., Montero-Menei, C.N., and Benoit, J.P. 2003. Biocompatibility of implantable synthetic polymeric drug carriers: focus on brain biocompatibility. *Biomaterials* 24:3311-3331.
90. Klose, D., Siepmann, F., Elkharraz, K., Krenzlin, S., and Siepmann, J. 2006. How porosity and size affect the drug release mechanisms from PLGA-based microparticles. *Int J Pharm* 314:198-206.
91. Shive, M.S., and Anderson, J.M. 1997. Biodegradation and biocompatibility of PLA and PLGA microspheres. *Adv Drug Deliv Rev* 28:5-24.
92. Siepmann, J., and Gopferich, A. 2001. Mathematical modeling of bioerodible, polymeric drug delivery systems. *Adv Drug Deliv Rev* 48:229-247.
93. Pouton, C.W. 2006. Formulation of poorly water-soluble drugs for oral administration: physicochemical and physiological issues and the lipid formulation classification system. *Eur J Pharm Sci* 29:278-287.
94. Cui, J., Yu, B., Zhao, Y., Zhu, W., Li, H., Lou, H., and Zhai, G. 2009. Enhancement of oral absorption of curcumin by self-microemulsifying drug delivery systems. *Int J Pharm* 371:148-155.
95. Gursoy, R.N., and Benita, S. 2004. Self-emulsifying drug delivery systems (SEDDS) for improved oral delivery of lipophilic drugs. *Biomed Pharmacother* 58:173-182.
96. Constantinides, P.P. 1995. Lipid microemulsions for improving drug dissolution and oral absorption: physical and biopharmaceutical aspects. *Pharm Res* 12:1561-1572.
97. Dixit, A.R., Rajput, S.J., and Patel, S.G. Preparation and bioavailability assessment of SMEDDS containing valsartan. *AAPS PharmSciTech* 11:314-321.
98. Sha, X., Yan, G., Wu, Y., Li, J., and Fang, X. 2005. Effect of self-microemulsifying drug delivery systems containing Labrasol on tight junctions in Caco-2 cells. *Eur J Pharm Sci* 24:477-486.
99. Vonderscher, J., and Meinzer, A. 1994. Rationale for the development of Sandimmune Neoral. *Transplant Proc* 26:2925-2927.
100. Balakrishnan, P., Lee, B.J., Oh, D.H., Kim, J.O., Lee, Y.I., Kim, D.D., Jee, J.P., Lee, Y.B., Woo, J.S., Yong, C.S., et al. 2009. Enhanced oral bioavailability of Coenzyme Q10 by self-emulsifying drug delivery systems. *Int J Pharm* 374:66-72.

101. Buss, N., Snell, P., Bock, J., Hsu, A., and Jorga, K. 2001. Saquinavir and ritonavir pharmacokinetics following combined ritonavir and saquinavir (soft gelatin capsules) administration. *Br J Clin Pharmacol* 52:255-264.
102. Baselga, J., Perez, E.A., Pienkowski, T., and Bell, R. 2006. Adjuvant trastuzumab: a milestone in the treatment of HER-2-positive early breast cancer. *Oncologist* 11 Suppl 1:4-12.
103. 2012. American Cancer Society Breast Cancer Facts & Figures 2011-2012.
104. Ramsay, D.T., Kent, J.C., Hartmann, R.A., and Hartmann, P.E. 2005. Anatomy of the lactating human breast redefined with ultrasound imaging. *J Anat* 206:525-534.
105. Silverthorn, D.U. 2004. *Human Physiology Integrated Approach.* : Upper Saddle River: Pearson Benjamin Cummings.
106. Richert, M.M., Schwertfeger, K.L., Ryder, J.W., and Anderson, S.M. 2000. An atlas of mouse mammary gland development. *J Mammary Gland Biol Neoplasia* 5:227-241.
107. Piechocki, M.P., Dibbley, S.K., Lonardo, F., and Yoo, G.H. 2008. Gefitinib prevents cancer progression in mice expressing the activated rat HER2/neu. *Int J Cancer* 122:1722-1729.
108. Russo, J., Hu, Y.F., Yang, X., and Russo, I.H. 2000. Developmental, cellular, and molecular basis of human breast cancer. *J Natl Cancer Inst Monogr*:17-37.
109. Fischer, A. Biology of the mammary gland.
110. Sorlie, T. 2004. Molecular portraits of breast cancer: tumour subtypes as distinct disease entities. *Eur J Cancer* 40:2667-2675.
111. Bordeleau, L., Panchal, S., and Goodwin, P. Prognosis of BRCA-associated breast cancer: a summary of evidence. *Breast Cancer Res Treat* 119:13-24.
112. Carter, C.L., Allen, C., and Henson, D.E. 1989. Relation of tumor size, lymph node status, and survival in 24,740 breast cancer cases. *Cancer* 63:181-187.
113. Jemal, A., Siegel, R., Ward, E., Hao, Y., Xu, J., Murray, T., and Thun, M.J. 2008. Cancer statistics, 2008. *CA Cancer J Clin* 58:71-96.
114. Wilcken, N., and Dear, R. 2008. Chemotherapy in metastatic breast cancer: A summary of all randomised trials reported 2000-2007. *Eur J Cancer* 44:2218-2225.
115. Ursini-Siegel, J., Schade, B., Cardiff, R.D., and Muller, W.J. 2007. Insights from transgenic mouse models of ERBB2-induced breast cancer. *Nat Rev Cancer* 7:389-397.
116. Fossati, R., Confalonieri, C., Torri, V., Ghislandi, E., Penna, A., Pistotti, V., Tinazzi, A., and Liberati, A. 1998. Cytotoxic and hormonal treatment for metastatic breast cancer: a systematic review of published randomized trials involving 31,510 women. *J Clin Oncol* 16:3439-3460.
117. She, Q.B., Chandarlapaty, S., Ye, Q., Lobo, J., Haskell, K.M., Leander, K.R., DeFeo-Jones, D., Huber, H.E., and Rosen, N. 2008. Breast tumor cells with PI3K mutation or HER2 amplification are selectively addicted to Akt signaling. *PLoS One* 3:e3065.
118. Lucarelli, A.P., Martins, M.M., Montor, W., Oliveira, V., Galvao, M.A., and Piato, S. Cyclooxygenase-2 and human epidermal growth factor receptor type 2

(HER-2) expression simultaneously in invasive and in situ breast ductal carcinoma. *Sao Paulo Med J* 129:371-379.
119. Berghoff, A., Bago-Horvath, Z., De Vries, C., Dubsky, P., Pluschnig, U., Rudas, M., Rottenfusser, A., Knauer, M., Eiter, H., Fitzal, F., et al. Brain metastases free survival differs between breast cancer subtypes. *Br J Cancer* 106:440-446.
120. Kim, I.Y., Yong, H.Y., Kang, K.W., and Moon, A. 2009. Overexpression of ErbB2 induces invasion of MCF10A human breast epithelial cells via MMP-9. *Cancer Lett* 275:227-233.
121. Pellikainen, J.M., Ropponen, K.M., Kataja, V.V., Kellokoski, J.K., Eskelinen, M.J., and Kosma, V.M. 2004. Expression of matrix metalloproteinase (MMP)-2 and MMP-9 in breast cancer with a special reference to activator protein-2, HER2, and prognosis. *Clin Cancer Res* 10:7621-7628.
122. Loureiro, R.M., Maharaj, A.S., Dankort, D., Muller, W.J., and D'Amore, P.A. 2005. ErbB2 overexpression in mammary cells upregulates VEGF through the core promoter. *Biochem Biophys Res Commun* 326:455-465.
123. Vargo-Gogola, T., and Rosen, J.M. 2007. Modelling breast cancer: one size does not fit all. *Nat Rev Cancer* 7:659-672.
124. Ross, D.T., Scherf, U., Eisen, M.B., Perou, C.M., Rees, C., Spellman, P., Iyer, V., Jeffrey, S.S., Van de Rijn, M., Waltham, M., et al. 2000. Systematic variation in gene expression patterns in human cancer cell lines. *Nat Genet* 24:227-235.
125. Neve, R.M., Chin, K., Fridlyand, J., Yeh, J., Baehner, F.L., Fevr, T., Clark, L., Bayani, N., Coppe, J.P., Tong, F., et al. 2006. A collection of breast cancer cell lines for the study of functionally distinct cancer subtypes. *Cancer Cell* 10:515-527.
126. Edinger, M., Cao, Y.A., Hornig, Y.S., Jenkins, D.E., Verneris, M.R., Bachmann, M.H., Negrin, R.S., and Contag, C.H. 2002. Advancing animal models of neoplasia through in vivo bioluminescence imaging. *Eur J Cancer* 38:2128-2136.
127. Kavanaugh, C., and Green, J.E. 2003. The use of genetically altered mice for breast cancer prevention studies. *J Nutr* 133:2404S-2409S.
128. Sinn, E., Muller, W., Pattengale, P., Tepler, I., Wallace, R., and Leder, P. 1987. Coexpression of MMTV/v-Ha-ras and MMTV/c-myc genes in transgenic mice: synergistic action of oncogenes in vivo. *Cell* 49:465-475.
129. Sutherland, R.L., and Musgrove, E.A. 2002. Cyclin D1 and mammary carcinoma: new insights from transgenic mouse models. *Breast Cancer Res* 4:14-17.
130. Guy, C.T., Webster, M.A., Schaller, M., Parsons, T.J., Cardiff, R.D., and Muller, W.J. 1992. Expression of the neu protooncogene in the mammary epithelium of transgenic mice induces metastatic disease. *Proc Natl Acad Sci U S A* 89:10578-10582.
131. Saenz Robles, M.T., and Pipas, J.M. 2009. T antigen transgenic mouse models. *Semin Cancer Biol* 19:229-235.
132. Boggio, K., Nicoletti, G., Di Carlo, E., Cavallo, F., Landuzzi, L., Melani, C., Giovarelli, M., Rossi, I., Nanni, P., De Giovanni, C., et al. 1998. Interleukin 12-mediated prevention of spontaneous mammary adenocarcinomas in two lines of Her-2/neu transgenic mice. *J Exp Med* 188:589-596.

133. Quaglino, E., Mastini, C., Forni, G., and Cavallo, F. 2008. ErbB2 transgenic mice: a tool for investigation of the immune prevention and treatment of mammary carcinomas. *Curr Protoc Immunol* Chapter 20:Unit 20 29 21-20 29-10.
134. Di Carlo, E., Diodoro, M.G., Boggio, K., Modesti, A., Modesti, M., Nanni, P., Forni, G., and Musiani, P. 1999. Analysis of mammary carcinoma onset and progression in HER-2/neu oncogene transgenic mice reveals a lobular origin. *Lab Invest* 79:1261-1269.
135. Calogero, R.A., Cordero, F., Forni, G., and Cavallo, F. 2007. Inflammation and breast cancer. Inflammatory component of mammary carcinogenesis in ErbB2 transgenic mice. *Breast Cancer Res* 9:211.
136. Grange, C., Lanzardo, S., Cavallo, F., Camussi, G., and Bussolati, B. 2008. Sca-1 identifies the tumor-initiating cells in mammary tumors of BALB-neuT transgenic mice. *Neoplasia* 10:1433-1443.
137. Warin, R., Chambers, W.H., Potter, D.M., and Singh, S.V. 2009. Prevention of mammary carcinogenesis in MMTV-neu mice by cruciferous vegetable constituent benzyl isothiocyanate. *Cancer Res* 69:9473-9480.
138. Cipriani, B., Fridman, A., Bendtsen, C., Dharmapuri, S., Mennuni, C., Pak, I., Mesiti, G., Forni, G., Monaci, P., Bagchi, A., et al. 2008. Therapeutic vaccination halts disease progression in BALB-neuT mice: the amplitude of elicited immune response is predictive of vaccine efficacy. *Hum Gene Ther* 19:670-680.
139. Hynes, N.E., and MacDonald, G. 2009. ErbB receptors and signaling pathways in cancer. *Curr Opin Cell Biol* 21:177-184.
140. Tai, W., Mahato, R., and Cheng, K. The role of HER2 in cancer therapy and targeted drug delivery. *J Control Release* 146:264-275.
141. Korkaya, H., Paulson, A., Iovino, F., and Wicha, M.S. 2008. HER2 regulates the mammary stem/progenitor cell population driving tumorigenesis and invasion. *Oncogene* 27:6120-6130.
142. Geyer, C.E., Forster, J., Lindquist, D., Chan, S., Romieu, C.G., Pienkowski, T., Jagiello-Gruszfeld, A., Crown, J., Chan, A., Kaufman, B., et al. 2006. Lapatinib plus capecitabine for HER2-positive advanced breast cancer. *N Engl J Med* 355:2733-2743.
143. Ryan, Q., Ibrahim, A., Cohen, M.H., Johnson, J., Ko, C.W., Sridhara, R., Justice, R., and Pazdur, R. 2008. FDA drug approval summary: lapatinib in combination with capecitabine for previously treated metastatic breast cancer that overexpresses HER-2. *Oncologist* 13:1114-1119.
144. Bendell, J.C., Domchek, S.M., Burstein, H.J., Harris, L., Younger, J., Kuter, I., Bunnell, C., Rue, M., Gelman, R., and Winer, E. 2003. Central nervous system metastases in women who receive trastuzumab-based therapy for metastatic breast carcinoma. *Cancer* 97:2972-2977.
145. Polli, J.W., Olson, K.L., Chism, J.P., John-Williams, L.S., Yeager, R.L., Woodard, S.M., Otto, V., Castellino, S., and Demby, V.E. 2009. An unexpected synergist role of P-glycoprotein and breast cancer resistance protein on the central nervous system penetration of the tyrosine kinase inhibitor lapatinib (N-{3-chloro-4-[(3-fluorobenzyl)oxy]phenyl}-6-[5-({[2-(methylsulfonyl)ethyl]amino

}methyl)-2-furyl]-4-quinazolinamine; GW572016). *Drug Metab Dispos* 37:439-442.
146. Gonzalez-Angulo, A.M., Litton, J.K., Broglio, K.R., Meric-Bernstam, F., Rakkhit, R., Cardoso, F., Peintinger, F., Hanrahan, E.O., Sahin, A., Guray, M., et al. 2009. High risk of recurrence for patients with breast cancer who have human epidermal growth factor receptor 2-positive, node-negative tumors 1 cm or smaller. *J Clin Oncol* 27:5700-5706.
147. Anand, P., Kunnumakkara, A.B., Newman, R.A., and Aggarwal, B.B. 2007. Bioavailability of curcumin: problems and promises. *Mol Pharm* 4:807-818.
148. Benny, O., Menon, L.G., Ariel, G., Goren, E., Kim, S.K., Stewman, C., Black, P.M., Carroll, R.S., and Machluf, M. 2009. Local delivery of poly lactic-co-glycolic acid microspheres containing imatinib mesylate inhibits intracranial xenograft glioma growth. *Clin Cancer Res* 15:1222-1231.
149. Mundargi, R.C., Babu, V.R., Rangaswamy, V., Patel, P., and Aminabhavi, T.M. 2008. Nano/micro technologies for delivering macromolecular therapeutics using poly(D,L-lactide-co-glycolide) and its derivatives. *J Control Release* 125:193-209.
150. Shahani, K., and Panyam, J. Highly loaded, sustained-release microparticles of curcumin for chemoprevention. *J Pharm Sci*.
151. Shahani, K., Swaminathan, S.K., Freeman, D., Blum, A., Ma, L., and Panyam, J. Injectable sustained release microparticles of curcumin: a new concept for cancer chemoprevention. *Cancer Res* 70:4443-4452.
152. Boggio, K., Di Carlo, E., Rovero, S., Cavallo, F., Quaglino, E., Lollini, P.L., Nanni, P., Nicoletti, G., Wolf, S., Musiani, P., et al. 2000. Ability of systemic interleukin-12 to hamper progressive stages of mammary carcinogenesis in HER2/neu transgenic mice. *Cancer Res* 60:359-364.
153. Schaefers, M.M., Breshears, L.M., Anderson, M.J., Lin, Y.C., Grill, A.E., Panyam, J., Southern, P.J., Schlievert, P.M., and Peterson, M.L. Epithelial proinflammatory response and curcumin-mediated protection from staphylococcal toxic shock syndrome toxin-1. *PLoS One* 7:e32813.
154. Mei, M., Zhao, L., Li, Q., Chen, Y., Huang, A., Varghese, Z., Moorhead, J.F., Zhang, S., Powis, S.H., and Ruan, X.Z. Inflammatory stress exacerbates ectopic lipid deposition in C57BL/6J mice. *Lipids Health Dis* 10:110.
155. Rowe, D.L., Ozbay, T., O'Regan, R.M., and Nahta, R. 2009. Modulation of the BRCA1 Protein and Induction of Apoptosis in Triple Negative Breast Cancer Cell Lines by the Polyphenolic Compound Curcumin. *Breast Cancer (Auckl)* 3:61-75.
156. Sharma, R.A., Steward, W.P., and Gescher, A.J. 2007. Pharmacokinetics and pharmacodynamics of curcumin. *Adv Exp Med Biol* 595:453-470.
157. Beutler, B. 2000. Tlr4: central component of the sole mammalian LPS sensor. *Curr Opin Immunol* 12:20-26.
158. Draoui, N., and Feron, O. Lactate shuttles at a glance: from physiological paradigms to anti-cancer treatments. *Dis Model Mech* 4:727-732.
159. Semenza, G.L. 2008. Tumor metabolism: cancer cells give and take lactate. *J Clin Invest* 118:3835-3837.

160. Vegran, F., Boidot, R., Michiels, C., Sonveaux, P., and Feron, O. Lactate influx through the endothelial cell monocarboxylate transporter MCT1 supports an NF-kappaB/IL-8 pathway that drives tumor angiogenesis. *Cancer Res* 71:2550-2560.
161. Sonveaux, P., Copetti, T., De Saedeleer, C.J., Vegran, F., Verrax, J., Kennedy, K.M., Moon, E.J., Dhup, S., Danhier, P., Frerart, F., et al. Targeting the lactate transporter MCT1 in endothelial cells inhibits lactate-induced HIF-1 activation and tumor angiogenesis. *PLoS One* 7:e33418.
162. Moiseeva, E.P., Almeida, G.M., Jones, G.D., and Manson, M.M. 2007. Extended treatment with physiologic concentrations of dietary phytochemicals results in altered gene expression, reduced growth, and apoptosis of cancer cells. *Mol Cancer Ther* 6:3071-3079.
163. Aggarwal, B.B., Kumar, A., and Bharti, A.C. 2003. Anticancer potential of curcumin: preclinical and clinical studies. *Anticancer Res* 23:363-398.
164. Spernath, A., and Aserin, A. 2006. Microemulsions as carriers for drugs and nutraceuticals. *Adv Colloid Interface Sci* 128-130:47-64.
165. Zhongfa, L., Chiu, M., Wang, J., Chen, W., Yen, W., Fan-Havard, P., Yee, L.D., and Chan, K.K. Enhancement of curcumin oral absorption and pharmacokinetics of curcuminoids and curcumin metabolites in mice. *Cancer Chemother Pharmacol* 69:679-689.
166. Birt, D.F., Hendrich, S., and Wang, W. 2001. Dietary agents in cancer prevention: flavonoids and isoflavonoids. *Pharmacol Ther* 90:157-177.
167. Kakarala, M., Brenner, D.E., Korkaya, H., Cheng, C., Tazi, K., Ginestier, C., Liu, S., Dontu, G., and Wicha, M.S. Targeting breast stem cells with the cancer preventive compounds curcumin and piperine. *Breast Cancer Res Treat* 122:777-785.
168. Reen, R.K., Jamwal, D.S., Taneja, S.C., Koul, J.L., Dubey, R.K., Wiebel, F.J., and Singh, J. 1993. Impairment of UDP-glucose dehydrogenase and glucuronidation activities in liver and small intestine of rat and guinea pig in vitro by piperine. *Biochem Pharmacol* 46:229-238.
169. Li, L., Gao, Y., Zhang, L., Zeng, J., He, D., and Sun, Y. 2008. Silibinin inhibits cell growth and induces apoptosis by caspase activation, down-regulating survivin and blocking EGFR-ERK activation in renal cell carcinoma. *Cancer Lett* 272:61-69.
170. Wu, X., Xu, J., Huang, X., and Wen, C. Self-microemulsifying drug delivery system improves curcumin dissolution and bioavailability. *Drug Dev Ind Pharm* 37:15-23.
171. Setthacheewakul, S., Mahattanadul, S., Phadoongsombut, N., Pichayakorn, W., and Wiwattanapatapee, R. Development and evaluation of self-microemulsifying liquid and pellet formulations of curcumin, and absorption studies in rats. *Eur J Pharm Biopharm* 76:475-485.
172. Shiratani, H., Katoh, M., Nakajima, M., and Yokoi, T. 2008. Species differences in UDP-glucuronosyltransferase activities in mice and rats. *Drug Metab Dispos* 36:1745-1752.

173. Zhang, L., Zhu, W., Yang, C., Guo, H., Yu, A., Ji, J., Gao, Y., Sun, M., and Zhai, G. A novel folate-modified self-microemulsifying drug delivery system of curcumin for colon targeting. *Int J Nanomedicine* 7:151-162.
174. Roger, E., Kalscheuer, S., Kirtane, A., Guru, B.R., Grill, A.E., Whittum-Hudson, J., and Panyam, J. Folic Acid Functionalized Nanoparticles for Enhanced Oral Drug Delivery. *Mol Pharm*.
175. Gardiner, P.S., and Gilmer, J.F. 2003. The medicinal chemistry implications of the anticancer effects of aspirin and other NSAIDs. *Mini Rev Med Chem* 3:461-470.
176. Khajuria, A., Thusu, N., and Zutshi, U. 2002. Piperine modulates permeability characteristics of intestine by inducing alterations in membrane dynamics: influence on brush border membrane fluidity, ultrastructure and enzyme kinetics. *Phytomedicine* 9:224-231.
177. Qi, L., Singh, R.P., Lu, Y., Agarwal, R., Harrison, G.S., Franzusoff, A., and Glode, L.M. 2003. Epidermal growth factor receptor mediates silibinin-induced cytotoxicity in a rat glioma cell line. *Cancer Biol Ther* 2:526-531.
178. Kim, S., Han, J., Kim, J.S., Kim, J.H., Choe, J.H., Yang, J.H., Nam, S.J., and Lee, J.E. Silibinin suppresses EGFR ligand-induced CD44 expression through inhibition of EGFR activity in breast cancer cells. *Anticancer Res* 31:3767-3773.
179. Kim, S., Choi, J.H., Lim, H.I., Lee, S.K., Kim, W.W., Kim, J.S., Kim, J.H., Choe, J.H., Yang, J.H., Nam, S.J., et al. 2009. Silibinin prevents TPA-induced MMP-9 expression and VEGF secretion by inactivation of the Raf/MEK/ERK pathway in MCF-7 human breast cancer cells. *Phytomedicine* 16:573-580.
180. Deep, G., Gangar, S.C., Rajamanickam, S., Raina, K., Gu, M., Agarwal, C., Oberlies, N.H., and Agarwal, R. Angiopreventive efficacy of pure flavonolignans from milk thistle extract against prostate cancer: targeting VEGF-VEGFR signaling. *PLoS One* 7:e34630.
181. Deep, G., Gangar, S.C., Agarwal, C., and Agarwal, R. Role of E-cadherin in antimigratory and antiinvasive efficacy of silibinin in prostate cancer cells. *Cancer Prev Res (Phila)* 4:1222-1232.
182. Dastpeyman, M., Motamed, N., Azadmanesh, K., Mostafavi, E., Kia, V., Jahanian-Najafabadi, A., and Shokrgozar, M.A. Inhibition of silibinin on migration and adhesion capacity of human highly metastatic breast cancer cell line, MDA-MB-231, by evaluation of beta1-integrin and downstream molecules, Cdc42, Raf-1 and D4GDI. *Med Oncol*.
183. Pesakhov, S., Khanin, M., Studzinski, G.P., and Danilenko, M. Distinct combinatorial effects of the plant polyphenols curcumin, carnosic acid, and silibinin on proliferation and apoptosis in acute myeloid leukemia cells. *Nutr Cancer* 62:811-824.